ACTOMYOSIN TENSION GENERATION ON THE NUCLEAR SURFACE

By

THOMAS F. CHANCELLOR JR.

A DISSERTATION PRESENTED TO THE GRADUATE SCHOOL
OF THE UNIVERSITY OF FLORIDA IN PARTIAL FULFILLMENT
OF THE REQUIREMENTS FOR THE DEGREE OF
DOCTOR OF PHILOSOPHY

UNIVERSITY OF FLORIDA

2012

To my Parents

ACKNOWLEDGMENTS

I would like to acknowledge the people who supported me during my time at the University of Florida. First I would like to thank my advisor Dr. Tanmay Lele. Dr. Tanmay Lele was very supportive and patient throughout my time here. He has created an environment in his lab in which lab members work together with each other on genuinely interesting projects. As my advisor he has provided me with opportunities to learn how to conduct research, design experiments and improve my knowledge of chemical engineering and biophysics.

I would also like to thank the other members of my committee. Dr. Tseng has always provided good advice and a new perspective on research and career goals. He has always allowed me full use of his lab and has been very supportful. Dr. Dickinson was a regular at our lab meetings and has helped to guide my research to answer relevant questions. Dr. Keselowsky has been helpful and I have enjoyed working with members of his research group.

I would also like to thank my coworkers in the Lele Lab. First I would like to thank Dr. Hengyi Xiao who taught me the necessary biological techniques and skills to start my research. Dr. Robert Russell joined the lab with me as the first two members. I am grateful for his advice and his friendship. Jiyeon Lee was very helpful with developing substrate rigidity assays. I have enjoyed working with Jun Wu. He has always provided enthusiasm and help whenever I asked and was also a fun weightlifting partner. David Lovett has been supportive and helpful during my time here. I also would like to thank the master students and undergraduates who worked with me over the years, most specifically Agnes Mendonca, Nandini Shekhar, Rachel Sammons, Steve Winter, and Brittany Hicks.

I would like to thank Monica Sanders and Joleen Cacciatore for being great friends since my first days in Gainesville.

I would like to support the members of the Gainesville Hogs Rugby club for helping me to alleviate stress and providing me with countless good times and stories I will tell for the rest of my life. Some of the most enjoyable times I've had here have been on the pitch with these mates. Specifically I'd also like to thank Kerri O'malley for her kindness and generosity.

Finally I would like to thank my family. My cousin's Brian and Mark have been my best friends since birth. My grandparents Clifford and Mary Chancellor, and John and Wilma Searles have always been extremely caring. My sister Kelli Blake has always been there for me and helps keep my ego in check. My brother-in-law Brice Blake has been a welcome addition to our family. My parents Tom and Karen Chancellor have supported me throughout my life and education. I'd like to thank my dad for taking me to the football games and the track meets he coached and for being an example of what a man should be. I'd like to thank my mother for always supporting me and reminding me of life's true priorities. I truly believe all of my success is due to their love and guidance

TABLE OF CONTENTS

page

LIST OF TABLES

LIST OF FIGURES

Abstract of Dissertation Presented to the Graduate School
of the University of Florida in Partial Fulfillment of the
Requirements for the Degree of Doctor of Philosophy

ACTOMYOSIN TENSION GENERATION ON THE NUCLEAR SURFACE

By

Thomas F. Chancellor Jr.

August 2012

Chair: Tanmay Lele
Major: Chemical Engineering

The nucleus is positioned through physical interactions with the actomyosin, microtubule and intermediate filament cytoskeleton. Abnormalities in nuclear positioning result in disease. Cytoskeletal force transfer to the nucleus is hypothesized to be mediated by bonds between the cytoskeleton and proteins embedded in the nuclear envelope called the LINC complex. We determined the role of nesprin-1, a LINC complex protein in mediating nuclear force transfer and cell mechanosensing. Our results suggest a model in which the nucleus balances a part of the actomyosin tension in the cell. In the absence of nesprin-1, actomyosin tension is balanced entirely by the substrate, increasing nuclear heights, causing increased cell-substrate traction, decreased cell migration and abnormal cell mechanosensing.

The basic question of whether the nucleus is primarily “pushed” into position by compressive cytoskeletal forces, or “pulled” by tensile cytoskeletal forces is unresolved. Two methods were used to try and answer this fundamental question: Rac1 photoactivation and local tension relaxation through local blebbistatin treatment or

micromanipulation Our results suggest that the nucleus is pulled on both sides, resulting in a tug-of-war between actomyosin forces.

To further investigate the nuclear-cytoskeletal force balance we developed a novel method to perturb nuclei within living cells. This method is capable of detecting changes in nuclear cytoskeletal coupling. This method allows for the translation of the nucleus under a known external force. Preliminary results reveal that the nucleus resists translation and that the actin cytoskeleton deforms as the nucleus is translated.

We also investigated the effects of substrate rigidity on collective cell migration using a modified scratch wound assay. We found that wound healing rates were faster than the migration speeds of isolated cells on soft substrates. On these substrates, cell-cell pulling resulted in flattened cell morphologies with clear stress fibers. On more rigid substrates, isolated cells were able to spread and therefore migrate better, but the wound healed more slowly because individual cells could not migrate easily due to cell crowding

CHAPTER 1
INTRODUCTION

The LINC Complex is Required for Normal Cell Function

The formation of new blood capillaries, or angiogenesis, involves the polarization and directed migration of endothelial cells(1, 2). Research on angiogenesis has primarily focused on biochemical pathways that participate in directed endothelial cell motility(3). However, motility and polarization also require the coordinated motion of intracellular organelles. In particular, positioning of the nucleus is an important part of any dynamic changes in cell morphology(4), given that it is the largest and stiffest organelle in the cell. Yet, the physiological significance of nuclear positioning in the endothelial cell has remained unexplored.

The nucleus is positioned through physical interactions with the actomyosin, microtubule and intermediate filament cytoskeleton(4). This force transfer is hypothesized to be mediated by bonds between the cytoskeleton and proteins embedded in the nuclear envelope. Recent studies suggest that lamin(5-7), SUN proteins(4, 8-11),emerin(12) and nesprins(11, 13-16) are key components of the mechanical linkage between the nucleus and the cytoskeleton. There is increasing evidence that these LINC (for Linker of Nucleus and Cytoskeleton) complex proteins are required for normal cell function. Lamin A/C deficient mouse embryonic fibroblasts have reduced migration speeds and are unable to polarize in wound healing assays(7). Lamin A/C deficient fibroblasts have altered mechanotransduction as measured by abnormal NF-κB –mediated, strain-induced transcription(6). Interestingly, these cells also have a softer peri-nuclear cytoskeleton suggesting that lamin A/C is necessary for physically connecting F-actin to the nucleus(17, 18). Similarly, emerin-deficient

fibroblasts have irregular nuclear shape and respond abnormally to mechanical forces(12).

Nesprin-1 and nesprin-2 are nuclear membrane proteins that bind to F-actin (19) through the N-terminus and to transmembrane SUN proteins via the C terminus (8-11, 20). These proteins are hypothesized to be part of the LINC complex (11, 16, 21). The function of nesprin-1 in endothelial cells has received little attention. In Chapter 2 we show that nesprin-1 knockdown in endothelial cells by siRNA transfection causes a lack of cell reorientation under cyclic strain, increased cell traction and focal adhesion assembly, and decreased cell migration. An increase in nuclear height is observed in nesprin-1 depletion cells similar to blebbistatin treated, myosin II-inhibited cells. Our results suggest a model in which the nucleus balances a part of the actomyosin tension in the cell. In the absence of nesprin-1, actomyosin tension is balanced entirely by the substrate, causing increased cell traction, decreased migration and altered nuclear height.

Pushing Versus Pulling: The Dominant Forces That Position the Nucleus

An NIH 3T3 fibroblast crawling on a surface has a characteristic shape: a fan-like leading lamella containing actively protruding lamellipodia and filopodia from the leading edge, the centrosome located roughly near the cell centroid, the nucleus normally positioned behind the centrosome, and a typically long, thin trailing edge(2). The fibroblast advances persistently in a given direction by continuously forming new actin-rich protrusions from the stable leading lamella while using actomyosin tension to detach and retract its trailing edge. During crawling, the fibroblast moves the nucleus and maintains its position close to the cell center. On the cellular length scales, the nucleus is massive (~10-15 microns in diameter) and stiff relative to the cytoplasm(22).

Motion of such a large object in the crowded intracellular space requires a significant expenditure of energy and is an important task for the motile cell.

The cell accomplishes nuclear motion by transferring active cytoskeletal forces onto the nuclear surface through molecular connections between the nuclear lamina and the cytoskeleton established by LINC complex proteins (for linker of nucleoskeleton to cytoskeleton(20, 23). The main source of the active forces are non-muscle myosin II (NMMII) based contraction of F-actin filaments and the processive motion of nucleus-linked microtubule motors on microtubules(24). Microtubule motors such as dynein pull the nuclear surface in NIH 3T3 fibroblasts and cause nuclear rotations(25, 26) and nuclear translations in other cell types (10, 15, 27). For actomyosin-based nuclear force generation, much of the research has focused on initial polarization mechanisms in a wounded cell monolayer where the nucleus is observed to move away from the leading edge due to pushing by actomyosin retrograde flow within the first few hours after wounding(28-30).

The basic question of whether the nucleus is primarily “pushed” into position by compressive cytoskeletal forces, or “pulled” by tensile cytoskeletal forces is unresolved because the literature is contradictory on this point. In crawling cells at the edge of a freshly created wound, retrograde flow of actomyosin may push the nucleus toward the trailing edge(29), while a squeezing (pushing) force due to actomyosin contraction in the trailing edge(31) may move the nucleus toward the leading edge. Conversely, other studies suggest that the nucleus is normally under a state of tension(24, 32-35). Both pushing and pulling forces may simultaneously operate on the nucleus, but of interest in

this paper is the net direction of the force balance (i.e. pushing versus pulling) and the dominant cytoskeleton origin of these forces in a single, crawling NIH 3T3 fibroblast.

In Chapter 3, we used two approaches to perturb the force balance on the nucleus. First we used the Rac1 photoactivation assay to trigger the formation of new lamellipodia(36); the nucleus was observed to move in the direction of newly formed lamellipodia in a myosin and LINC complex dependent but microtubule independent manner. Next, we inhibited myosin activity in the trailing edge locally; interestingly, we observed the nucleus to move toward the leading edge in a LINC complex dependent fashion. We detached the trailing edge of fibroblasts and recorded nuclear motion and deformation in response to detachment as well as subsequent pulling of the trailing edge. We found that the nucleus underwent elastic deformations on manipulation of the trailing edge in a myosin dependent and LINC complex dependent fashion. Collectively, these experiments suggest the presence of pulling forces on the nucleus from the trailing edge.We also found that forward nuclear motion preceded trailing edge detachment, and cells with disrupted LINC complexes were unable to detach their trailing edges. Taken together, our results suggest that the nucleus is pulled on both sides, resulting in a tug-of-war between actomyosin forces. The nucleus acts as an integrator of tensile actomyosin forces in a motile cell, and the integration is necessary for detachment of the trailing edge.

Manipulating the Nucleus Inside a Living Cell

The relative magnitude of cytoskeletal forces on the nucleus is difficult to determine owing to the lack of suitable methods to quantitatively measure these forces in living cells. We explored the use of techniques that can apply known forces to the nucleus, cause a measureable displacement and quantify the response in living cells.

One technique used by researchers is straining cells attached to flexible silicon membranes by applying strain to the membrane. This technique has been employed to examine the role of lamin A/C in maintaining nuclear integrity in response to mechanical strain(37). An advantage of this technique is that multiple cells or even monolayers of cells can be stretched simultaneously in a manner that may be physiologically relevant. This technique can be further refined through the use of micro-patterned substrates so that cells are stretched in a particular orientation(38). One limitation of applying strain through the substrate is that force cannot be directly applied to nucleus and requires well- attached cells with an intact cytoskeleton that is integrated with the nucleus.

Magnetic beads or nano-rods can be injected into living cells and nuclei and then manipulated using an external magnetic field to produce local forces. The external force can be applied to pull the beads in a uniform direction(39) or rotate them(40). This method has been used to study the elastic modulus of nuclear structures like chromatin(41). Celedon et al used nanorods injected into the nucleus to find that the viscosity of lamin A null nuclei was 7 times less then control cells and that the shear modulus of the null nuclei was also 3 times lower(42). Although magnetic probes can be used to apply a torque on small localized areas within the nucleus, it is not possible to apply enough force to translate the entire nucleus.

Other methods include micromanipulation with glass needles attached to a micromanipulator (these can be made sensitive enough to measure pN scale forces like the elasticity of actin filaments(43)). Microneedles have been used to measure the forces being exerted by the lamellipodia of migrating fibroblasts(44). Glass needles can also be coated with ECM proteins to form adhesions with integrin receptors on cells that

allow them the user to “pull” on a selected part of the cell. Maniotis et al first demonstrated that the nucleus was physically linked to the actin cytoskeleton with such a method (45). In chapter 4, a new technique will be described that allows us to qualitatively measure nuclear-cytoskeletal interactions. This technique allows us to translate the nucleus in order to detect changes in nuclear-cytoskeletal binding, to perturb the nucleus to study restoration forces, and to visualize how the cytoskeleton and nucleus are physically connected.

Does Collective Cell Migration Depend on Substrate Rigidity

Cells *in vitro* appear to function optimally when cultured on substrates that have physiologically relevant rigidities (46, 47). Neurons will form longer branches on substrates with soft rigidities similar to those measured of brain tissue (48). Similarly myoblasts differentiate on substrates with rigidities like that of muscle and osteoblasts function optimally on hard bone-like substrates (49). In addition the recent finding that stem cell differentiation can be guided by substrate rigidity (50)reveals that substrate rigidity might be a vital parameter for the design of biomedical implants and the engineering of tissues(51).

Single cell motility rates have been shown to vary widely in response to changes in substrate rigidity. Motility rates in smooth muscle cells (52), neutrophils (53), NIH 3T3 fibroblasts (54), tumor cells (55, 56) and human dermal fibroblasts cells (57) have all been shown to have a substrate dependence. The accepted explanation for the dependence of migration speed on substrate rigidity is that cells on soft substrates are not able to generate substantial forces due to reduced actomyosin tension and cell-substrate adhesion.

Unlike isolated cells, cells in contact with other cells exert tension on each other as well as the underlying substrate (58, 59). Cell-cell adherence, which is primarily due to cadherin proteins, provides cells an additional location to generate tension forces. Traction forces of cells seeded on cadherin coated substrates have been shown to be comparable to those observed when cells are seeded on fibronectin coated surfaces which bind with focal adhesions (60). As this cell-cell tension is not present in isolated cells, substrate rigidity may affect collective cell migration differently than isolated cells(61). A popular method to quantify collective cell migration is the scratch wound assay (30, 62-64). An advantage of this technique is that collective cell migration rates can be repeatedly measured in order to compare different conditions. Typically the scratch wound assay is done by wounding a cell monolayer cultured on glass or polystyrene with the tip of a syringe and observing the migration of the monolayer into the wound. This technique cannot be used when studying cells cultured on soft substrates such as polyacrylamide because the wounding of the cell with a syringe would also damage the underlying substrate.

In Chapter 5 we used a micromanipulator to precisely translate the vertical position of a micropipette tip and removed cells without contacting the underlying gel surface. We observed a clear but modest variation in the rates of wound closure created by this method as a function of rigidity. The rates of closure were high on soft and very rigid substrates (Young's modulus (E) of 0.4 and 308 kPa) compared to intermediate moduli (E=24 and 39 kPa), but the mode of closure appeared different on the soft and rigid substrates. On soft substrates, cells leading the wound closure appeared to pull trailing cells through cell-cell contacts, whereas on rigid substrates, cells moved more

independently. In contrast to these collective migration results, motility of isolated NIH 3T3 fibroblasts was lowest on the soft substrates and increased with rigidity. We also developed and applied a novel assay to qualitatively compare relative magnitudes of cell-cell pulling forces relative to cell-substrate adhesion forces on different substrates. These results show that cell-cell adhesion forces dominate cell-substrate adhesion forces on soft substrates, and that cell-cell pulling forces contribute significantly to wound healing on soft substrates.

Table 1-1 Diseases associated with LINC complex proteins

Disease/Disorder	LINC complex protein
Partial Lipodystrophy	Lamin A(65)
Peripheral Neuropathy	Lamin A(65)
Hutchison Gilford Progeria Syndrome	Lamin(66)
Atypical Werners Syndrome	Lamin(65)
Mandibulocaral Dysplasia	Lamin(25)
Emery Dreifuss Muscular Dystrophy	Nesprin-1 and 2, Lamin(13)
Cardiomyopathy	Nesprin 1 and 2, Lamin(13)
Skeletal Myopathy	Nesprin 1 and 2, Lamin(13)

CHAPTER 2
NUCLEAR TENSION IS REQUIRED FOR NORMAL CELL MECHANOSENSING AND CELL FUNCTION

The function of nesprin-1 in endothelial cells has received little attention. Here we show that nesprin-1 knockdown in endothelial cells by siRNA transfection causes a lack of cell reorientation under cyclic strain, increased cell traction and focal adhesion assembly, and decreased cell migration. An increase in nuclear height is observed in nesprin-1 depletion cells similar to blebbistatin treated, myosin II-inhibited cells. Our results suggest a model in which the nucleus balances a part of the actomyosin tension in the cell. In the absence of nesprin-1, actomyosin tension is balanced entirely by the substrate, causing increased cell traction, decreased migration and altered nuclear height.

Materials and Methods

Cell Culture

Human umbilical vascular endothelial cells (HUVECs) were maintained in DMEM-high glucose (Cellgro) supplemented with 10% donor bovine serum (Cellgro, Manassas, VA**)** and maintained at 37^{o} C in a humidified 5% CO_2 environment. HUVECs were tested for their endothelial function with an in vitro 3D angiogenesis assay and were found to form typical tube-like structures characteristic of endothelial cells (Figure 2-1). In wounding experiments, cells were seeded at 80% confluence on fibronectin-coated (5 μg/ml) glass bottomed dishes (MatTek, Ashland, MA) cultured to confluence.

siRNA Knock Down of Nesprin-1

Cells were transfected with 100 nM of SMARTpool siRNAs (Dharmacon, Lafayette, CO) against human nesprin-1 using siLentFect lipid transfection reagent (BioRad, Hercules, CA). The siRNA oligonucleotide target sequences used were as

follows: GAAAUUGUCCCUAUUGAUU, GCAAAGCCCUGGAUGAUAG, GAAGAGACGUGGCGAUUGU and CCAAACGGCUGGUGUGAUU. Non-targeting SMARTpool siRNAs served as controls.

Western Blotting

Cells cultured in regular growth media were washed with cold PBS and lysed with cell lysis buffer (Cell Signal, Boston, MA) for 10 minutes on ice. Cells were scraped, collected and centrifuged at 10,000 rpm for 10 minutes at 4^{o}C. The supernatant was collected and SDS-sample buffer was added and stored at -20^{o}C until use. The samples were separated on 10% SDS polyacrylamide gels and then transferred onto a PVDF membrane. The membranes were treated with anti-nesprin-1 mouse monoclonal antibody (Abcam,Cambridge, MA) at 1:200 dilutions in 5% milk overnight at 4^{o}C. Phosphorylated myosin levels were measured by treating membranes with a phospho-myosin antibody (Cell Signal, Boston MA) which recognizes myosin light chain 2 only when dually phosphorylated at Thr18 and Ser19. The membranes were then washed three times in TBST and treated with peroxidase conjugated secondary antibody at 1:10000 in 5 % milk in TBST. Blots were developed using SuperSignal West Pico Chemiluminescent reagent (Pierce, Rockford, IL) and exposed to X-OMAT film (Kodak).

Immunostaining

Cells were fixed with 4% paraformaldehyde (Electron Microscopy Sciences, Morris Road Fort Washington, Pa) for 20 minutes, washed with PBS (Cellgro, Manassas, VA) and then permeabilized with 0.1 % Triton X-100 in 1% BSA solution. Cells were next incubated with nesprin-1 primary monoclonal mouse antibody (Abcam, Cambridge, MA) or vinculin monoclonal mouse antibody (Sigma, St. Louis, MO) at a 1:100 dilution overnight at 4^{o}C. Samples were washed and treated with goat-anti-mouse 488nm

fluorescent secondary antibody (Calbiochem, San Diego, CA) for 1 hour at room temperature. For actin staining, cells were incubated with Alexa Fluor 594 phalloidin (Invitrogen, Carlsbad, CA) for 1 hour. Nuclear staining was done using Hoechst33342 diluted at 1:100 for 30 min. The samples were imaged on a Leica SP5 confocal microscope equipped with a 63X objective.

Application of Mechanical Strain and Measurement of Cell Reorientation

Cells were cultured on fibronectin (5 µg/ml) coated 6 well Uniflex plates (Flexcell, Hillsborough, NC) and exposed to 10 % uniaxial strain with a frequency of 0.5 Hz for 18 hrs using the Flexcell-4000 system (67). Cells were then fixed and stained with phalloidin (Sigma, St. Louis MO) for imaging F-actin. Images of cells were acquired as described above and the cell angle relative to the strain direction was quantified using ImageJ software. Approximately 300 cells were evaluated for each condition corresponding to 6 fields; 50 cells from each field.

Cell Motility Assay

To assess cell motility, cells were cultured on fibronectin treated glass bottomed dishes for 6 hrs. The dishes were transferred onto the microscope stage and imaged with a 10X phase contrast lens inside an environmental chamber maintained at 37^{o}C and with 5% CO2. Images were taken every 10 minutes for 10 hours and analyzed using a Matlab program that tracked the position of the centroid of cells in (x,y) coordinates vs. time. The mean squared displacement was calculated from the data using non-overlapping time intervals (68). The speed of each cell was determined from the measured displacement of the centroid at 10 minutes. The persistence time of each cell was calculated by fitting the mean-square displacement to the persistent random walk model using nonlinear least-square regression as reported elsewhere (69). A

minimum of 17 cells were measured for each condition. Images taken 8 hours after passage were also used to measure cell spreading area of cells transfected with control and nesprin-1 targeting siRNA. The area of at least 12 cells was measured for each condition using Nikon Elements software (Figure 2-2).

Scratch-Wound Assay

Confluent cells were washed and serum starved for 24 hours after which a wound was created by scraping across the surface of each monolayer using a 20 gauge needle. After wounding, the cells were washed with PBS and cultured in full growth medium while images of the cells were taken simultaneously every 30 minutes for 18 hours on a Nikon TE2000 microscope equipped with an environmental chamber. Nikon Elements software was used to measure the area of the wound at each time interval. Only wounds with original widths between 175μm and 225μm were measured. To measure cell polarization, cells were serum starved for 12 hours, wounded and treated with 2-μM lysophosphatidic acid for 4 hrs, fixed and stained with rabbit anti-γ-tubulin antibody (Sigma) and mouse monoclonal α-tubulin antibody (Sigma). Cells with centrosomes located within 30 degrees of a line perpendicular to the wound were considered polarized similar to the approach in (7). Angles were measured with Nikon Elements software. At least 30 cells per condition were measured.

Traction Force Microscopy

Fibronectin coated polyacrylamide gels (Young's modulus of 45 kPa) for traction force microscopy were prepared on glass bottomed dishes (MatTek, Ashland MA) as previously described in(70). Red fluorescent microspheres (0.5μm diameter, Invitrogen, Carlsbad,CA) were suspended in the polyacrylamide gel prior to gel formation and used as fiduciary markers. Cells were plated at low concentrations (5% confluence) and

incubated for 24 hours at 37 ºC with 5% CO2 in full growth media. DIC and fluorescent images of isolated cells were then taken simultaneously before and after treatment with 5% SDS (Sigma, St. Louis MO) solution. Traction force analysis was performed using the Matlab software and methods described in(71). A minimum of 8 cells were measured for each condition.

Confocal Imaging to Determine Nuclear Height

Cells were fixed with 4% paraformaldehyde and nuclei and the F-actin cytoskeleton stained as described above. The samples were imaged on a Leica SP5 confocal microscope equipped with a 63X objective. Z-stacks were acquired and Leica application suite software used to measure the height of the nucleus. Each experiment was repeated 3 times (n>15). Similar procedures were used for cells treated with blebbistatin (n>15).

3D-In Vitro Angiogenesis Assay

A 1:20 dilution of HUVECs was taken from an 80% confluent 12 well dish and mixed with 300 µl of Matrigel® using cold glass pipettes. The Matrigel solution was then placed on a glass bottomed dish (MatTek, Ashland, MA) and kept in a 37ºC incubator for 1 hr. After 1 hr, 2 ml of growth media was added. The growth media was changed every 2 days for 2 weeks. At the end of the experiments, the gel was imaged on on a Nikon TE2000 microscope equipped with a 20X lens to analyze tube formation.

Results

siRNA Knock Down of Nesprin-1 in HUVECs

Nesprin-1 has been shown to localize to the nuclear envelope in fibroblasts, vascular smooth muscle cells and cardiac muscle cells(11, 21, 72, 73). Immunostaining with a specific antibody against nesprin-1 revealed a similar localization to the nuclear

envelope in HUVECs (Figure 2-3A). Western blotting analysis (Figure 2-3B) showed a major band at a molecular weight of approximately 110 kDa, with additional bands at around 75 kDa and 40 kDa, consistent with previous studies(13, 21, 72). Treatment with specific siRNA against nesprin-1 significantly reduced all bands in Western blots (Figure 2-3B and C). However, nesprin-1 knockdown did not alter the expression levels (Figure 2-4) or the localization (Figure 2-5) of a closely related member of the nesprin family, nesprin-2, confirming the specificity of nesprin-1 knockdown by the siRNA transfection. Cells transfected with nesprin-1 targeting and control siRNA were next immunostained for nesprin-1. Confocal fluorescent imaging (Figure 2-3D) also showed that nesprin-1 expression in siRNA transfected cells was reduced significantly compared to cells expressing control siRNA and non-transfected cells. Quantification of pixel intensity of these images further confirmed that the majority of individual cells had reduced nesprin-1 expression (Figure 2-6). Taken, together, these results clearly demonstrate that the siRNA transfection specifically knocked down nesprin-1 in HUVECs.

Nesprin-1 Knockdown Abolishes Cyclic Strain-Induced HUVEC Reorientation, and Increases Focal Adhesion Assembly and Cell Traction

Next, we investigated if nesprin-1 knockdown affected endothelial cell physiology. HUVEC reorientation in response to applied uniaxial cyclic strain was examined. Control and nesprin-1 deficient HUVECs were exposed to cyclic mechanical strain (10%, 0.5 Hz) for 18 hours using the FlexCell 4000 device (67). Non-transfected HUVECs oriented predominantly along a direction perpendicular to the direction of mechanical strain (Figure 2-7). F-actin staining showed that stress fibers also aligned perpendicular to the direction of the strain. In contrast, knockdown of nesprin-1 abolished HUVEC reorientation in response to cyclic strain. Further, we found that cells transfected with

control siRNA responded similarly to the untreated cells, establishing the specificity of the effect of nesprin-1 knockdown on strain-induced cell reorientation.

Cell reorientation under cyclic strain requires disassembly of existing focal adhesions, and the preferential stabilization of newly formed adhesions in a direction perpendicular to applied strain (74). We therefore explored if focal adhesion assembly was altered in nesprin-1 depleted cells. Cells were immunostained for vinculin and focal adhesions were imaged on a confocal fluorescence microscope. Nesprin-1 deficient cells assembled a significantly larger number of focal adhesions compared to control cells (Figure 2-8 A and B ,Figure 2-9). F-actin was also more concentrated toward the base of the cell in nesprin-1 deficient cells (Figure 2-10). The increased focal adhesion number suggested a potential increase in cell traction in nesprin-1 depleted cells. Using traction force microscopy, we found that nesprin-1 depletion indeed significantly increased traction stresses on the substrate (Figure 2-8 C and D). Nesprin-1 deficient cells were also observed to spread more than control cells (Figure 2-11).

Transient Disassembly of Focal Adhesions Restores Reorientation Under Strain in Nesprin-1 Depleted Cells

The above experiments motivated the hypothesis that cells were unable to reorient in response to cyclic strain owing to increased focal adhesion assembly and traction. Therefore, we reasoned that transiently causing the disassembly of focal adhesions could allow the nesprin-1 depleted cell to reorient under applied strain. To do this, we used a previously published approach to cause the time-dependent disassembly of focal adhesions by treatment with the Rho-kinase inhibitor Y27632(75). To only cause a transient disassembly of focal adhesions, we treated the drug for a short time (30 minutes) after which the drug was washed off and cyclic strain was applied. Drug

washout permits the reassembly of focal adhesions(76). Interestingly, cells treated in this manner were able to reorient under cyclic strain (Figure 2-12). This confirms our hypothesis that nesprin-1 depleted cells are unable to reorient due to increased adhesion to the substrate.

Altered Actomyosin Forces on the Nucleus

Actomyosin tension has been shown previously to control nuclear shape (33). The extent to which nesprin-1 mediates this force transfer to the nuclear shape is unclear. We performed z-stack imaging with a laser scanning confocal microscope of the stained nucleus in nesprin-1 deficient cells. Reconstructed three-dimensional images were used to quantify nuclear heights. Nesprin-1 deficient cells showed a significant increase in nuclear height (7.1±.8 μm) as opposed to control cells which had nuclear heights of 5.0 ±.0.4μm (Figure 2-13 A and B). This suggests that nesprin-1 mediated pulling forces on the nucleus flatten the nucleus into a disk-like shape in endothelial cells. We next asked if inhibiting actomyosin forces could similarly change nuclear height. The nuclear heights of non-transfected cells were measured after treatment with the non-muscle myosin II inhibitor blebbistatin (100μM) for 1 hour. A significant increase in nuclear height (6.2 ±0.4 μm) was observed in the blebbistatin treated cells (Figure 2-13 A and B). These results, support previous observations by Ingber and coworkers (33, 34) and Wang and coworkers (77) that the nucleus balances actomyosin tension. Finally, we used the initial cell polarization assay (Figure 2-14) in which rearward actomyosin motion from the leading edge of the wounded cell pushes the nucleus in a manner that gives the cell a polarized appearance (30). The nuclear-centrosomal-leading edge axis was significantly disrupted in cells, which provides further support to the conclusion that

actomyosin forces are significantly decreased on the nucleus in the absence of nesprin-1.

The increase in nuclear height in nesprin-1 depleted cells observed above could be attributed potentially to differences in non-muscle myosin II activity. However, Western Blotting revealed that the levels of phophorylated non-muscle myosin II are unchanged in nesprin-1 depleted cells compared to control (Fig. 13 C and D).

Nesprin-1 Deficiency Causes Abnormal HUVEC Migration

Increased traction and focal adhesions typically correlate with a decrease in cell migration speed(78),(54). We therefore tested whether nesprin-1 depletion alters cell migration in a scratch-wound assay. Time lapse imaging over the course of 12 hours was performed on wounded monolayers of nesprin-1 depleted and control cells. Cells transfected with control siRNA completely closed the scratched wound in around 8 hours (Fig 4-15). In contrast, cells transfected with nesprin-1 targeting siRNA failed to close the wound at 8 hours (Figure 2-15).

To examine if nesprin-1 deficiency also affects individual cell motility, migrating cells were imaged with phase contrast microscopy, and the time-dependent position of the nuclear centroid was quantified. Mean square displacement (MSD) data was calculated with non-overlapping intervals and fit to a model for cell migration. We found that the speed of single cells was significantly decreased in nesprin-1 deficient cells compared to control (Figure 2-15 D).

Discussion

The mechanical linkage between the nucleus and the actomyosin cytoskeleton was demonstrated several years ago by showing that applied force to transmembrane integrins at the endothelial cell membrane caused deformation of the nucleus (34).

Actomyosin tension exerted on the nucleus has been shown to stabilize its shape(33). This linkage is also crucial for the cell's ability to position the nucleus in the cell(4). The recent discovery of LINC complex proteins has triggered interest in the function of specific molecular linkers in nucleo-cytoskeletal force transfer. In this paper, we provide evidence for new functions of nesprin-1, a nuclear membrane protein that links the nucleus to the F-actin cytoskeleton. Nesprin-1 depletion causes abnormal cell reorientation under cyclic strain, increased nuclear height, decreased cell migration and increased adhesion assembly and traction in endothelial cells.

In the absence of nesprin-1, we found that cells are unable to reorient in response to uniaxial cyclic strain; however, transient disassembly of adhesions restores HUVEC reorientation. It is known that elevation of actomyosin tension causes increased cell-substrate adhesion that interferes with cellular reorientation under applied strain(76). However, we did not find any differences in myosin phosphorylation (which typically correlates with actomyosin tension(70)) in nesprin-1 deficient cells or in microtubule and intermediate filament organization (Figure-2-16). Yet, we found that nesprin-1 deficient cells assemble more focal adhesions, have more concentrated F-actin toward the base of the cell and exert more traction on the substrate compared to control cells. Nesprin-1 deficient cells also had increased nuclear heights similar to cells with inhibited myosin activity suggesting that nesprin-1 may decouple tensile actomyosin forces from the nucleus.

To explain these findings, we propose a model (Figure 2-17) in which part of the actomyosin tension is exerted on (and balanced by) the nucleus through connections mediated by nesprin-1. In the absence of these connections, the actomyosin forces are

assumed to be balanced at an additional number of focal adhesions, which will result in greater traction stresses on the substrate. A key feature of the model is that increased substrate deformation can result even though myosin activity is unchanged. Increased focal adhesion assembly and traction stresses would then prevent cell reorientation under cyclic strain, in a similar manner to cells with increased actomyosin tension(76). Additionally, as actomyosin forces are redirected from the nucleus to the substrate due to the lack of nesprin-1 mediated binding, less actomyosin tension is exerted on the nucleus. This tension (which would normally balance osmotic pressure(33)) is decreased, resulting in increased nuclear height.

The observed decrease in cell migration speed is consistent with increased adhesion assembly and traction. This is because cell speed is low at low and high adhesive strengths, and is maximum at an intermediate value(52, 78, 79). As the nesprin-1 depleted cells form more focal adhesions than normal cells(Figure 2-8 A and B), cell migration speed is expected to decrease (Figure 2-15 D).

While the model in Figure 2-17 is consistent with our observations, it is a static model that does not offer an explanation of how more focal adhesions are formed when actomyosin is disconnected from the nuclear surface. Future studies that investigate the dynamic assembly and disassembly of adhesions, and the fate of rearward actomyosin flow from the membrane in nesprin-1 deficient cells could help better answer this question. Other nesprin isoforms such as nesprin-2 also link the nuclear surface to the actomyosin cytoskeleton (13, 16, 20, 80) and could possibly compensate for nesprin-1 (16). However, the fact that nesprin-2 expression (Figure 2-4 A and B) and localization (Figure 2-5) was not altered by nesprin-1 knockdown, and yet F-actin distribution was

perturbed (Figure 2-10) suggests that nesprin-1 may play an essential role in linking the nucleus and F-actin.

In summary, our results suggest an important role for nesprin-1 in endothelial cell function. In the absence of nesprin-1, endothelial cells assemble more adhesions, exert greater traction on the surface, have increased nuclear heights and have decreased migration speeds. Non-muscle myosin II phosphorylation is unchanged in nesprin-1 depleted cells. These results support a model in which actomyosin tension normally balanced by the nucleus is balanced in nesprin-1 deficient cells by the substrate. Our findings with nesprin-1 depleted cells show a remarkable similarity with other recent studies that have demonstrated decreased speeds of wound healing and defective nuclear positioning in lamin A/C and emerin deficient cells(5, 7). Given that lamin A/C and emerin are structurally and functionally different from nesprin-1, this raises the possibility that other LINC complex proteins may also influence cell behavior in a manner similar to the proposed model.

Erratum

We recently discovered a contamination in our HUVEC cell line. The HUVEC cells used in our original study may have been contaminated. We repeated the key result in our paper using primary HUVECs and the results matched those previously reported (Figure 2-7). We note that many other studies with different cell types have shown that nuclear-cytoskeletal linkages are critical for mechanosensing (for a review see (81)). Also a recent paper reported a role for nesprin-3 in flow-induced polarization and migration by human aortic endothelial cells(82) . We would like to thank Jason M Haugh for his advice on this matter.

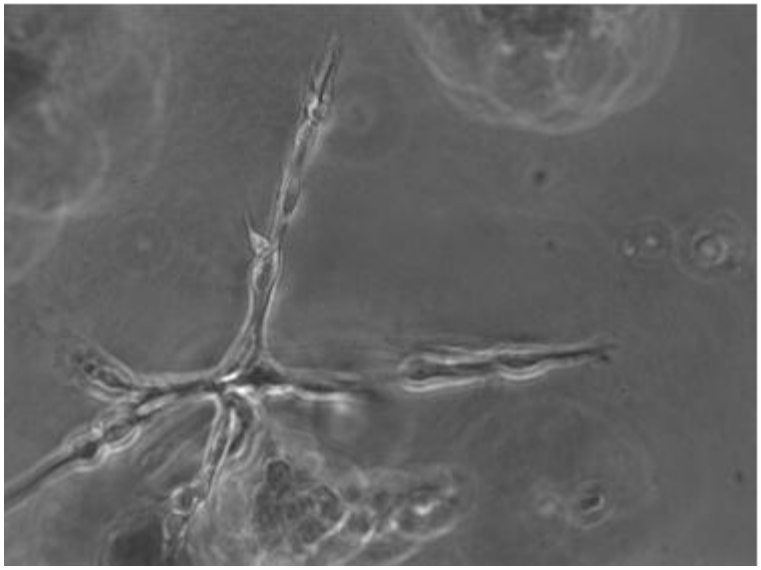

Figure 2-1. In vitro 3D Angiogenesis assay of HUVEC cells HUVECs were mixed with Matrigel and monitored for their ability make tubular structures (angiogenesis) for 2 weeks as described in Materials and Methods. The representative image shows tube formation by HUVECs in 3D matrigel confirming that these cells are functional endothelial cells.

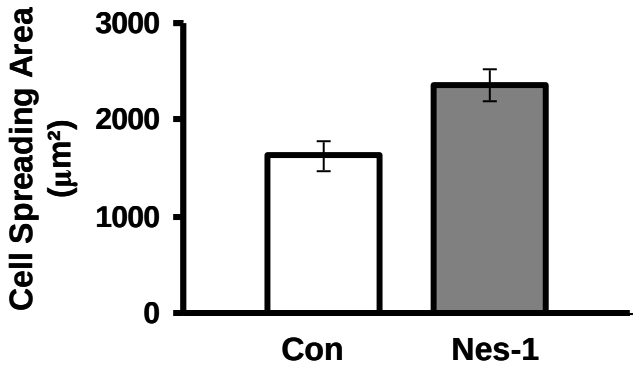

Figure 2-2. Cell spreading area increases in nesprin deficient cells. HUVECs were cultured on fibronectin coated glass bottomed dishes for 8 hrs and were then imaged on a Nikon E2000 microscope equipped with a 10X planar objective. Nikon Elements software was used to measure 15 cells in each condition. * Indicates $p<0.05$.

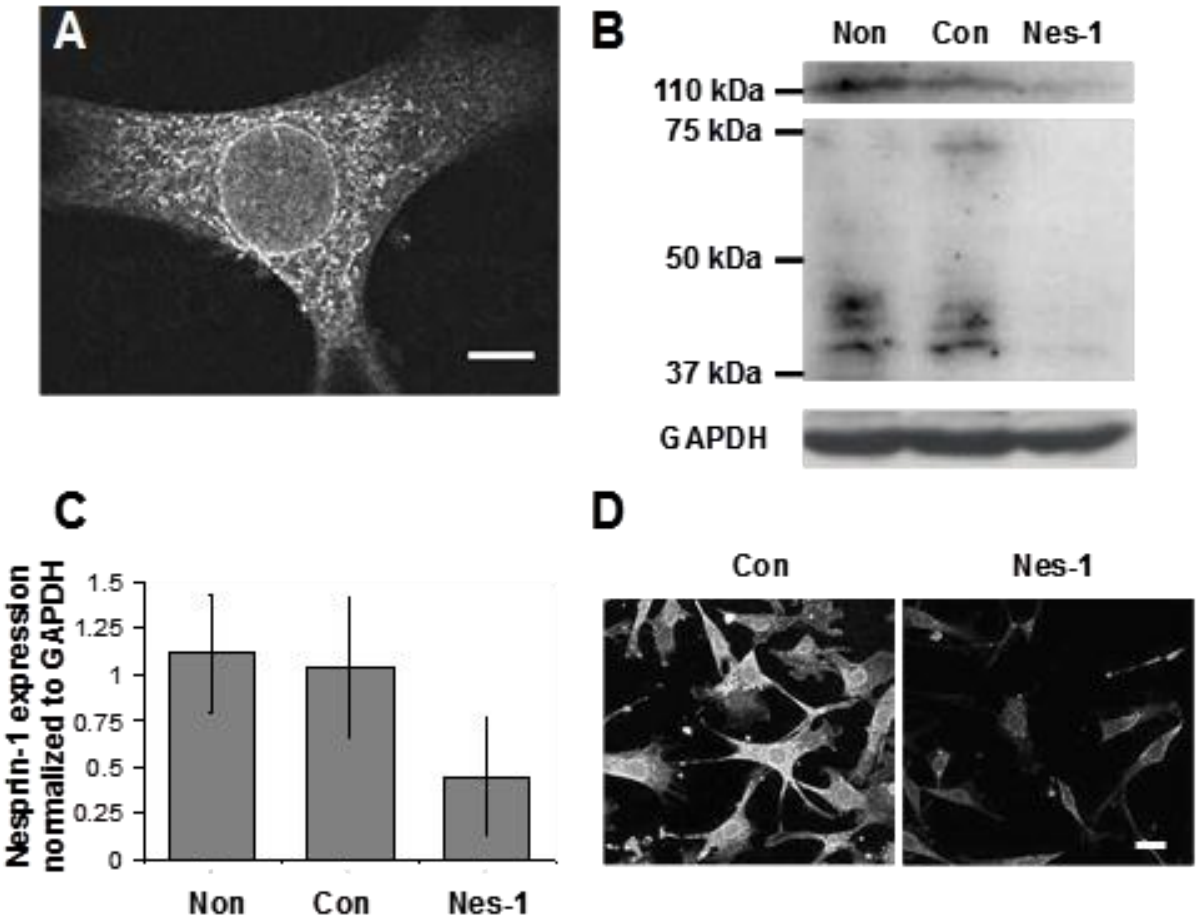

Figure 2-3. Transfection of HUVECs with siRNA targeting nesprin-1 results in a significant reduction in nesprin-1 expression. A) Confocal fluorescence image of HUVEC immunostained for nesprin-1. Nesprin-1 localizes to the nuclear membrane (Scale bar = 5 μm). B) Western blot analysis of nesprin-1 expression in HUVECs. HUVECs transfected with siRNA targeting nesprin-1 (Nes-1) show a significant reduction in nesprin-1 expression as compared to non-transfected cells (Non) and cells transfected with control siRNA (Con). C) Quantification of nesprin-1 expression relative to GAPDH expression demonstrating a significant decrease in siRNA transfected cells. Error bars represent SEM from three different experiments. *p <0.05 D) Low magnification confocal fluorescence images of HUVECs immunostained for nesprin-1. A significant reduction in nesprin-1 expression is observed in cells transfected with nesprin-1 targeting siRNA (images were acquired at the same laser power, photomultiplier gain and magnification). Scale bar is 25 μm.

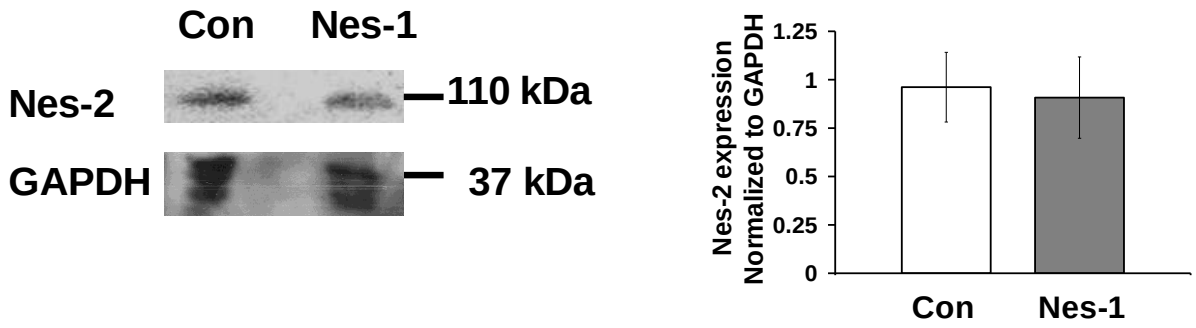

Figure. 2-4. Nesprin 2 expression is unchanged by unchanged by siRNA targeting nesprin-1. Western blots (A) and their quantification (B) showing that Nesprin-2 (Nes-2) expression is unchanged in cells depleted of Nes-1. Error bars represent SEM; differences are not statistically significant.

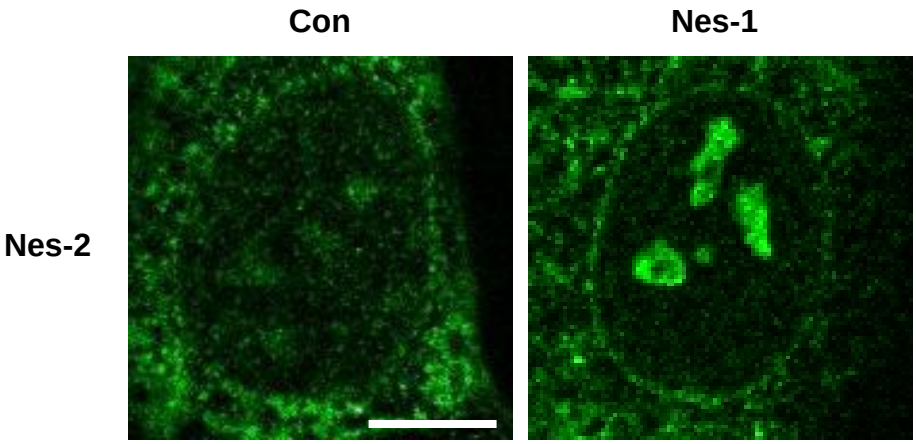

Figure 2-5. Nesprin-2 is present in the nuclear envelope in nesprin-1 deficient cells. Cells were transfected with control and nesprin-1 targeting siRNA and cultured for 72 hours and then fixed as described in the methods section. Cells were imaged using a Leica confocal microscope equipped with a 63X objective.

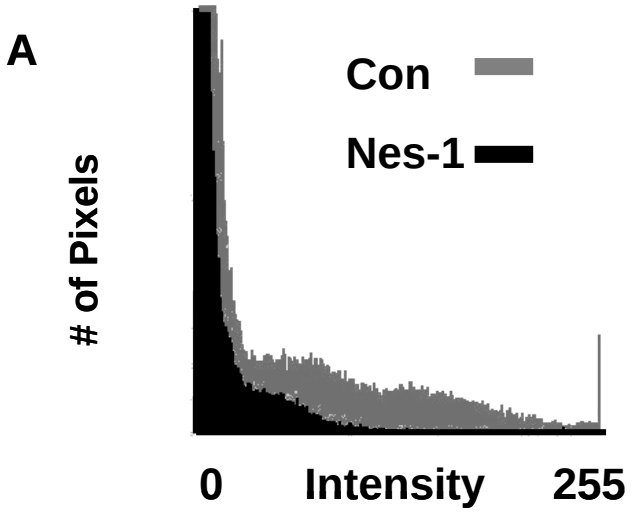

B

	Mean	Stdev
Con	50.1	59.3
Nes-1	15.3	20.1

Figure 2-6. Quantification of Nesprin-1 expression.A) Histogram comparison of pixel intensity of cells transfected with control and nesprin-1 siRNA immuostained for nesprin-1. B) Quantification of the pixel intensity shows a significant decrease in nesprin-1 expression in nes-1 siRNA treated cells compared to control siRNA treated cells.

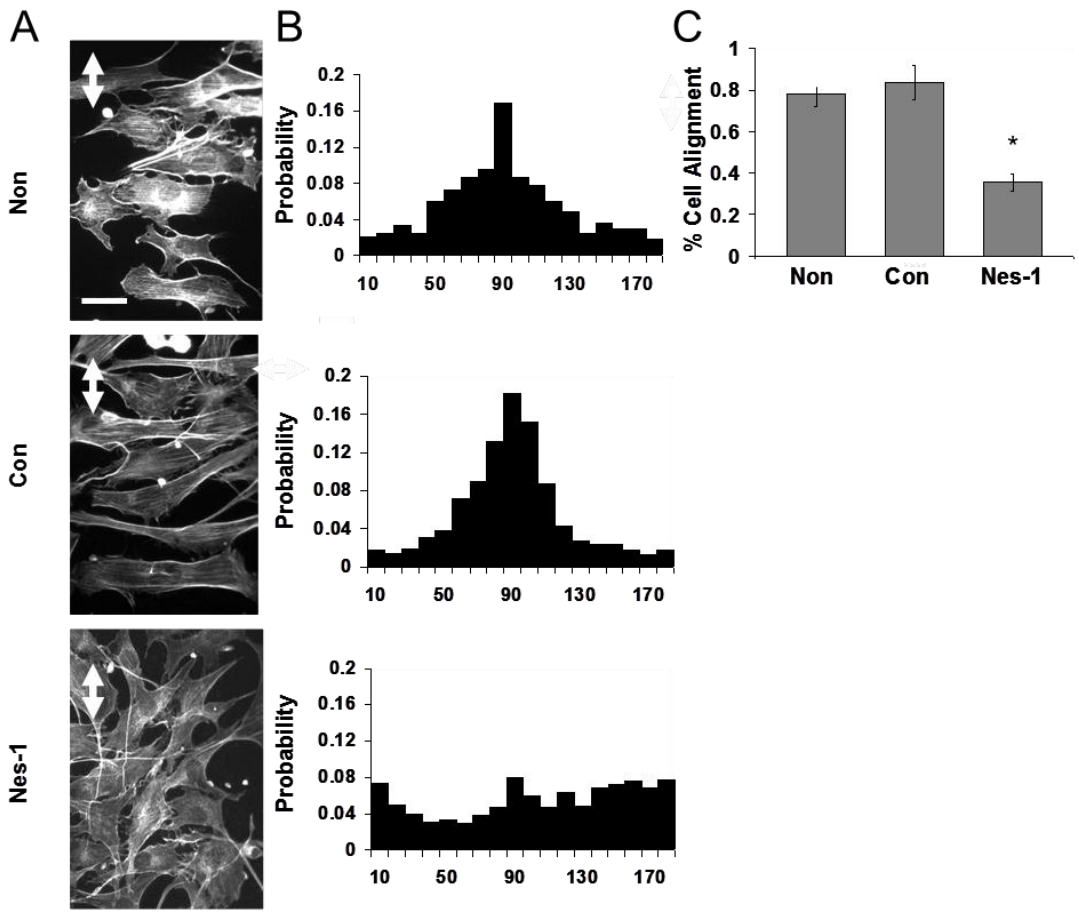

Figure 2-7. A) HUVECs cultured on flexible silicon membranes coated with fibronectin were exposed to 10 % cyclic, uniaxial strain at 0.5 Hz, fixed and stained with Alexa-phalloidin to visualize F-actin stress fibers. Non-transfected HUVECs and cells expressing control siRNA oriented perpendicular to the strain direction (strain direction is marked by white double arrow) while cells transfected with nesprin-1 targeting siRNA did not align in any preferred direction. Stress fibers were observed predominantly perpendicular to the strain direction except in nesprin-1 deficient cells. Scale bar is 50 □m. B) Probability distributions of cell angle measured relative to strain axis. A clear preference for a direction perpendicular to the strain axis is observed in the distribution for non-transfected and control siRNA transfected cells; the distribution is random for nesprin-1 siRNA transfected cells. The distribution was quantified from pooled data from three independent experiments corresponding to 300 cells per condition. C) Quantification of the reorientation response. The data is presented as percentage of cells that reoriented 90o ± 30o relative to the strain direction similar to the approach in (76). Error bars represent SEM from three different experiments and * indicates $p<0.01$.

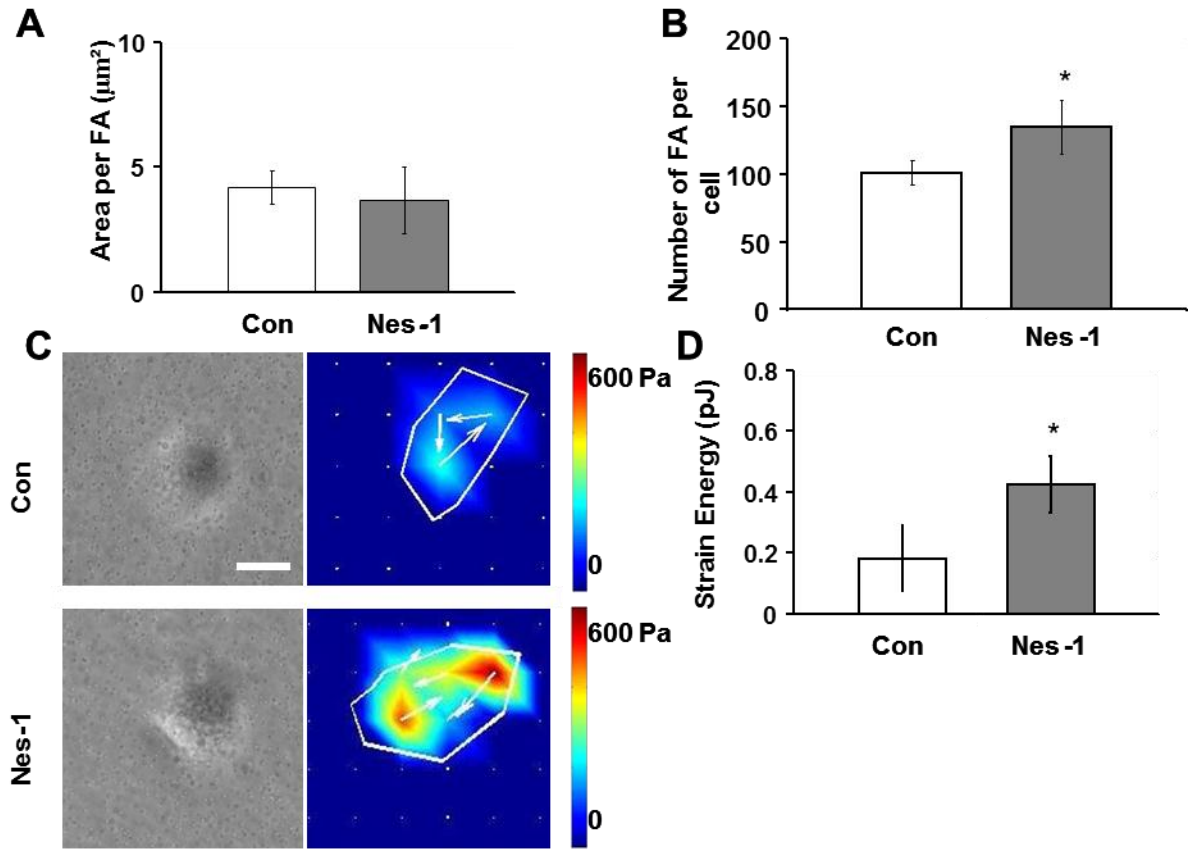

Figure 2-8. Nesprin-1 depletion results in increased cell traction and focal adhesions. A) The area per FA was unchanged between cells transfected with control and nesprin-1 targeting siRNA, while the number of FAs (B) increased in nesprin-1 deficient cells ($p<0.05$). C) Representative phase contrast images and traction stress maps of cells transfected with nesprin-1 targeting and control siRNA. Scale bar is 200 μm. D) Surface strain energy is increased in nesprin-1 deficient cells compared to control cells ($p<0.05$). Error bars represent SEM from three different experiments and * indicates $p<0.01$. A minimum of 8 cells were measured for each condition.

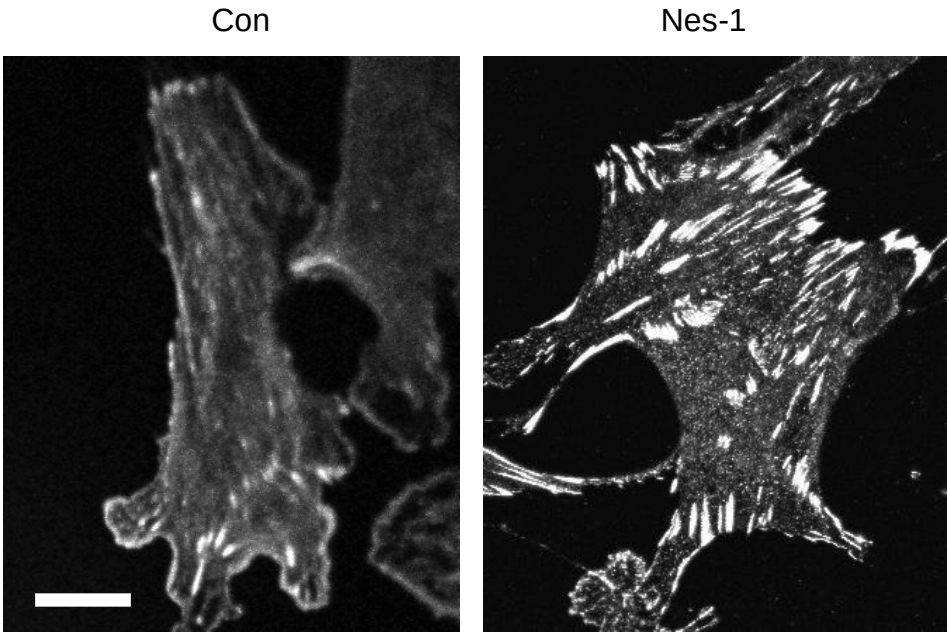

Figure 2-9. Nesprin-1 deficient cells have an increased number of focal adhesions. Cells were cultured on fibronectin coated glass bottomed dishes (MatTek) for 24 hours then fixed and stained for vinculin. Confocal images at the base of each cell were taken to focal adhesion number and area. Scale bar is 15 um

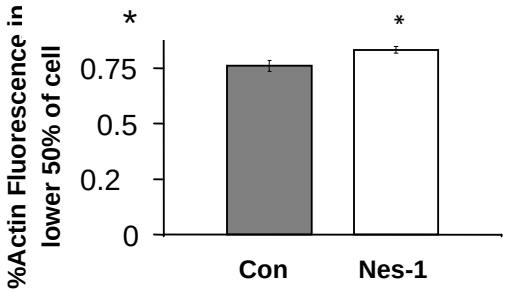

Figure 2-10. Reduction of nesprin-1 expression shifts the distribution of F-actin toward the base of the cell. Cells transfected with control siRNA and siRNA targeting nesprin-1 were stained for F-actin and z-stack images were collected. The distribution of F-actin was measured along a single line through the highest point of the cell. The distribution was normalized and the sum of the fluorescent intensity was compared for the lower 50% of the cell.

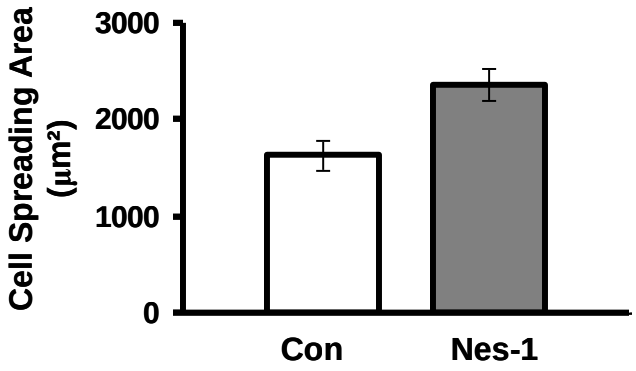

Figure 2-11. Cell spreading area increases in nesprin deficient cells. HUVECs were cultured on fibronectin coated glass bottomed dishes for 8 hrs and were then imaged on a Nikon E2000 microscope equipped with a 10X planar objective. Nikon Elements software was used to measure 15 cells in each condition. * Indicates $p<0.05$.

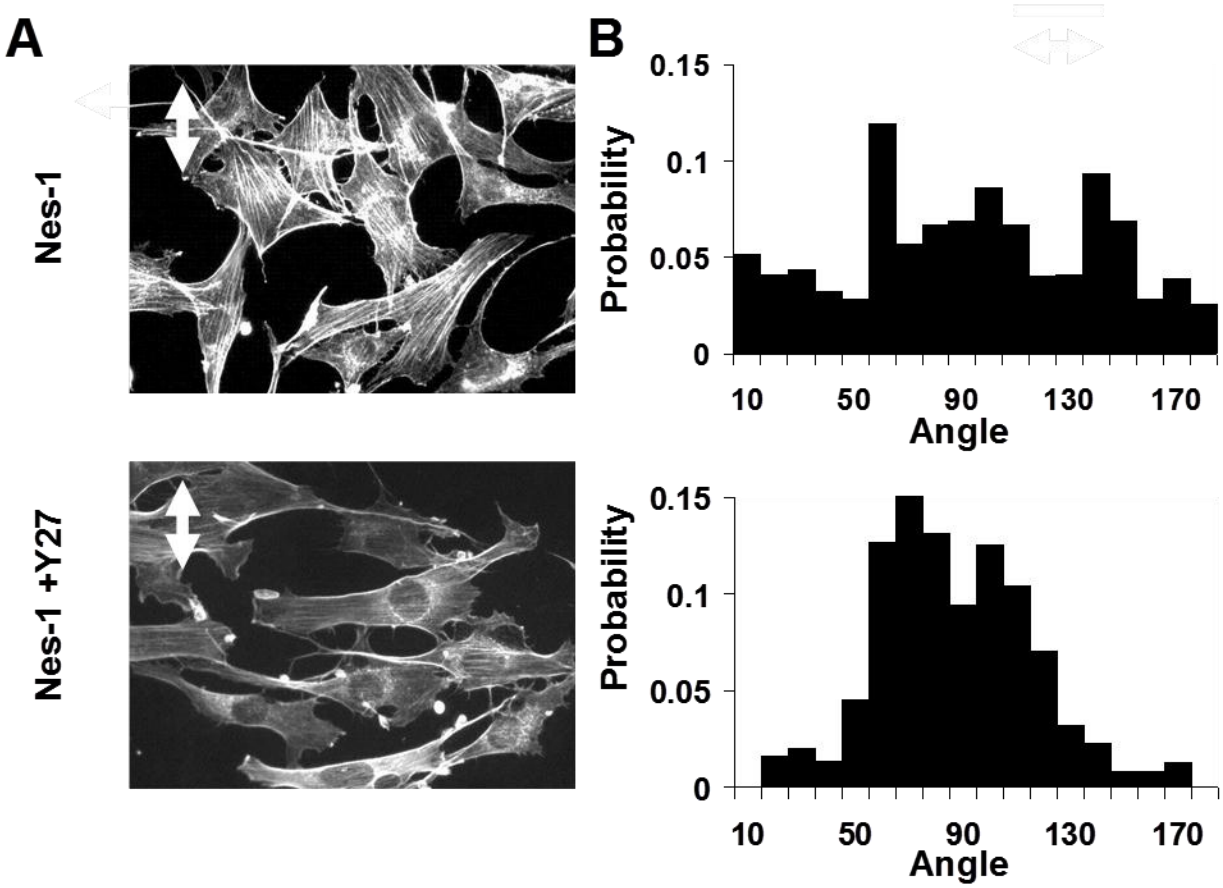

Figure 2-12. Rho kinase inhibition restores the reorientation response in nesprin-1 deficient cells. A) After 18 hours of 10 % cyclic, uniaxial strain at 0.5 Hz (strain direction is marked by white double arrow), cells transfected with nesprin-1 targeting siRNA did not align in any preferred direction. Pre-treatment of cells with Y27632 for 30 minutes followed by washout and cyclic stretching restored the reorientation response of nesprin-1 deficient cells. Scale bar is 50 μm. B) Probability distributions of cell angle measured relative to strain axis. Y27632 treated nesprin-1 deficient cells have a much higher probability of reorienting perpendicular to the applied strain. The distribution was quantified from pooled data from 2 independent experiments corresponding to 150 cells per condition.

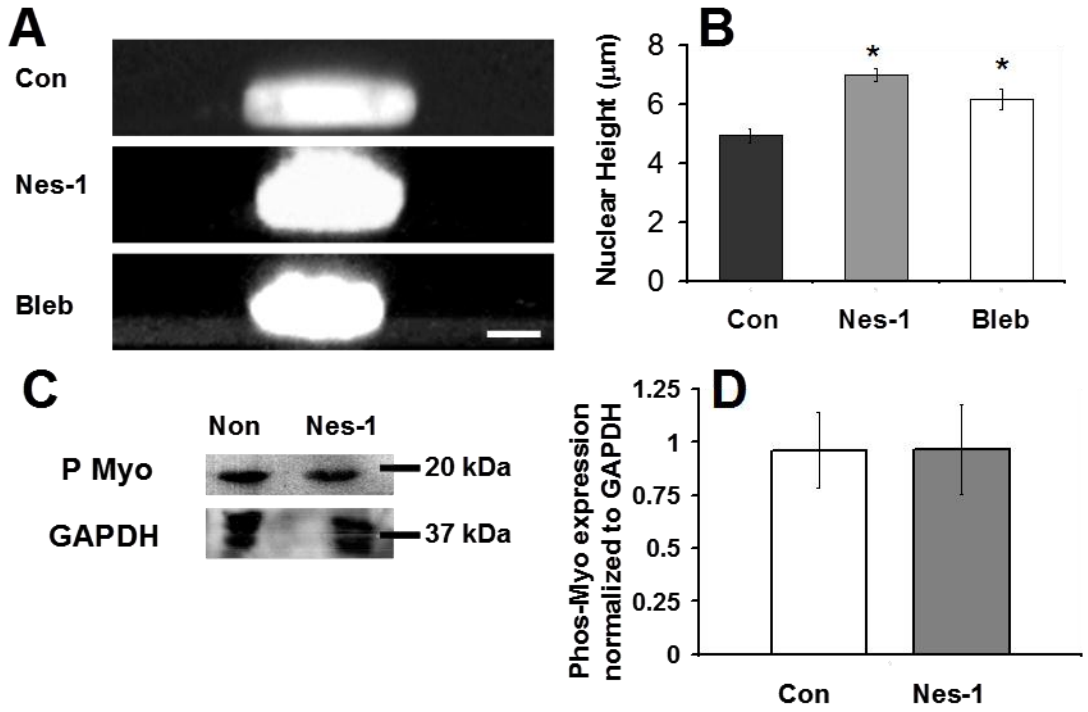

Figure 2-13. Nuclear height increases in nesprin-1 deficient HUVECs . A) Representative Z-stack images generated with confocal microscopy show an increase in nuclear height in nesprin-1 deficient and blebbistatin (bleb) treated cells. Hoechst33342 was used to stain the nucleus. Scale bar is 5 µm. B) Plot quantifies the increase in nuclear height of nesprin-1 deficient HUVECs and HUVECs treated with blebbistatin. Error bars represent SEM and both * indicate $p<0.05$ (each statistical comparison is with Con). A minimum of 15 cells were measured for each condition. C) Western blot of phosphorylated myosin (P Myo) in non-transfected and siRNA transfected cells. D) Quantification shows no difference in myosin II light chain phosphorylation. Error bars represent SEM from three different experiments.

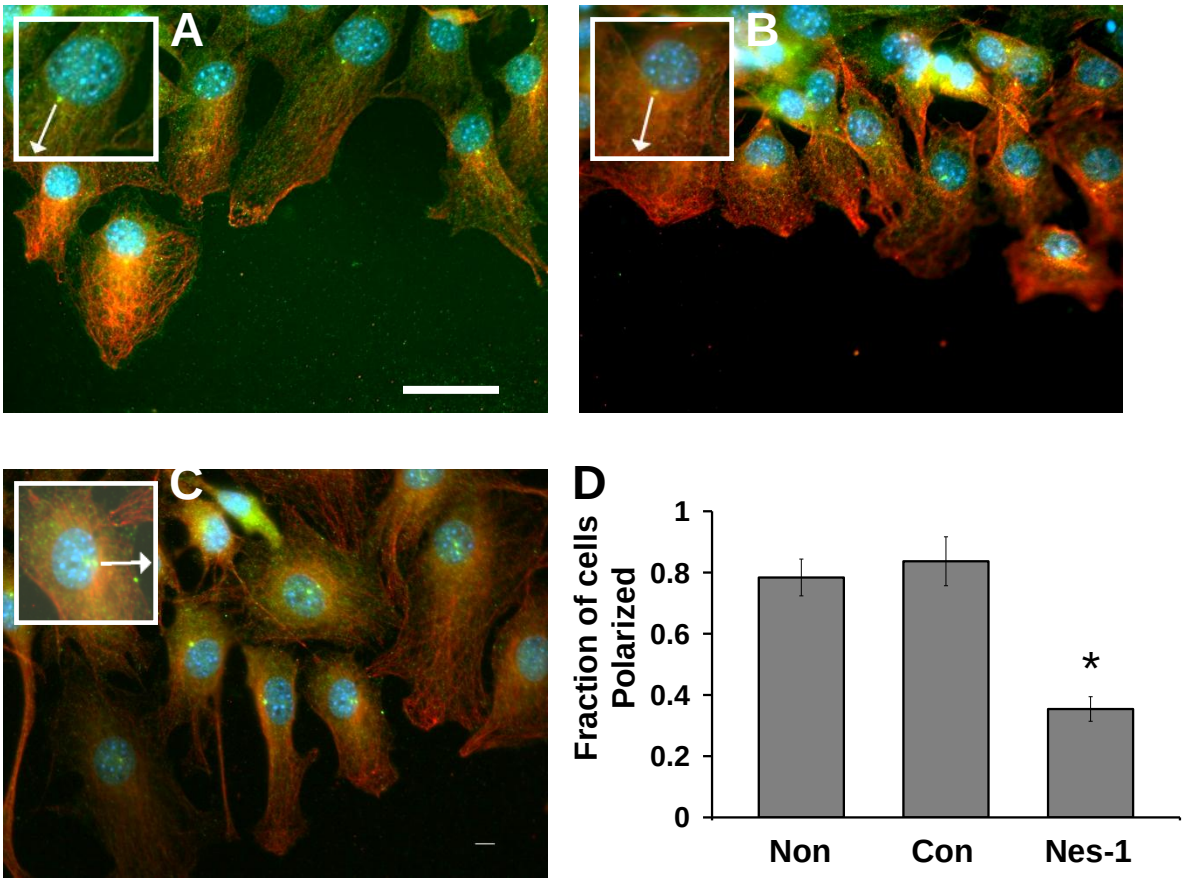

Figure 2-14. Actomyosin forces are decoupled from the nucleus in the absence of nesprin-1. HUVEC cells serum-starved overnight were wounded and treated with LPA. LPA treatment triggers rearward actomyosin flow that moves the nucleus away from the wounded edge(30). To quantify this, the cell polarization vector in non-transfected HUVECs (A) and cells transfected with control siRNA(B) was measured and found to be approximately perpendicular to the wounded edge. White arrows indicate the direction of polarization of each cell calculated by drawing a vector from the nuclear centroid to the □-tubulin stained centrosome . C) Nesprin-1 deficent cells are unable to polarize as is clear from the random directions of the cell polarization vector with respect to the wounded edge. Scale bar is 50 □m. All cells were stained for □-tubulin (green) , F-actin (red) and for chromatin (blue). D) Quantification of cell polarization. Cells which were oriented within 30 degrees of a line perpendicular to the leading edge were quantified as polarized cells according to the approach in (7). The polarization defects in nesprin-1 deficient cells are statistically significant (*p< 0.01).

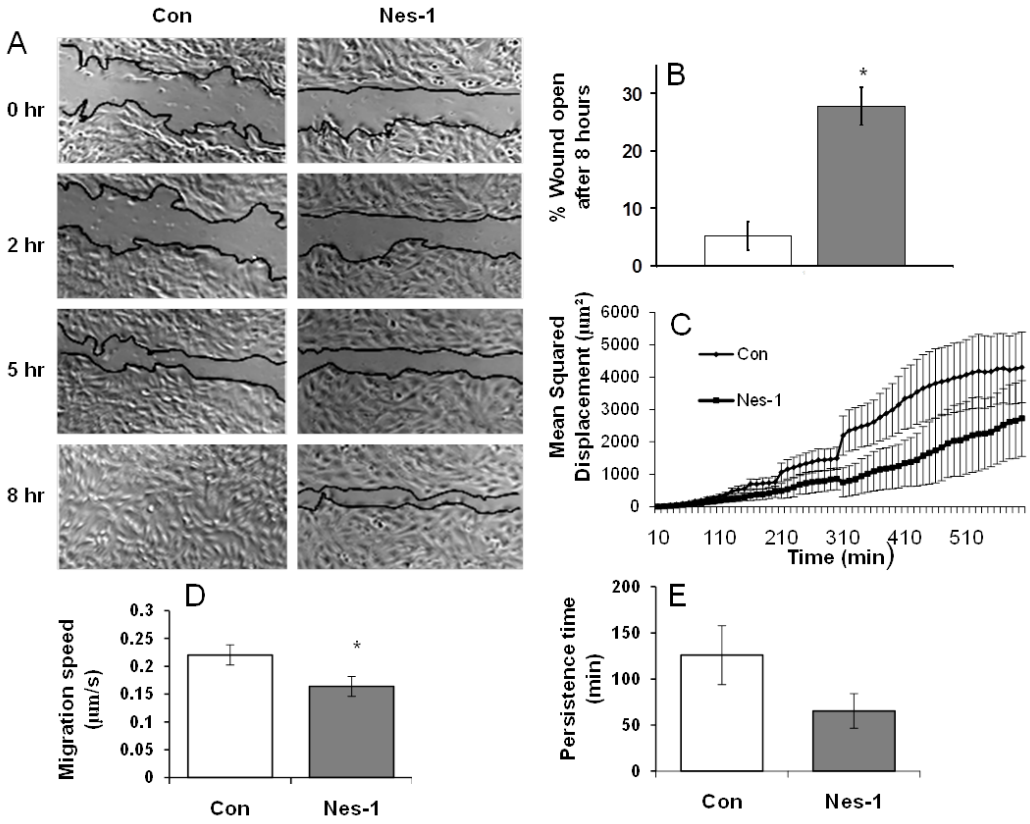

Figure 2-15. Nesprin-1 deficient HUVECs have decreased wound healing rates, single-cell speed and persistence times. A) Phase contrast images of HUVECs at 0, 2, 5 and 8 hours after wounding are shown. Wound edges are marked in black; scale bar is 200 μm. B) Plot shows the unhealed percentage of the original wound for HUVECs transfected with control and nesprin-1 siRNA at 8 hours. Error bars represent SEM from three different experiments and * indicates a $p < 0.01$. C) Plot shows MSD calculated using single-cell trajectories and pooled together from at least ten different cells. Error bars represent SEM. MSD is significantly decreased in nesprin-1 deficient cells. D) Individual cell migration speed, and E) persistence time is decreased in nesprin-1 deficient cells; the decrease in persistence time is not statistically significant. At least 17 cells were analyzed for each condition in the motility experiments;* indicates $p<0.05$.

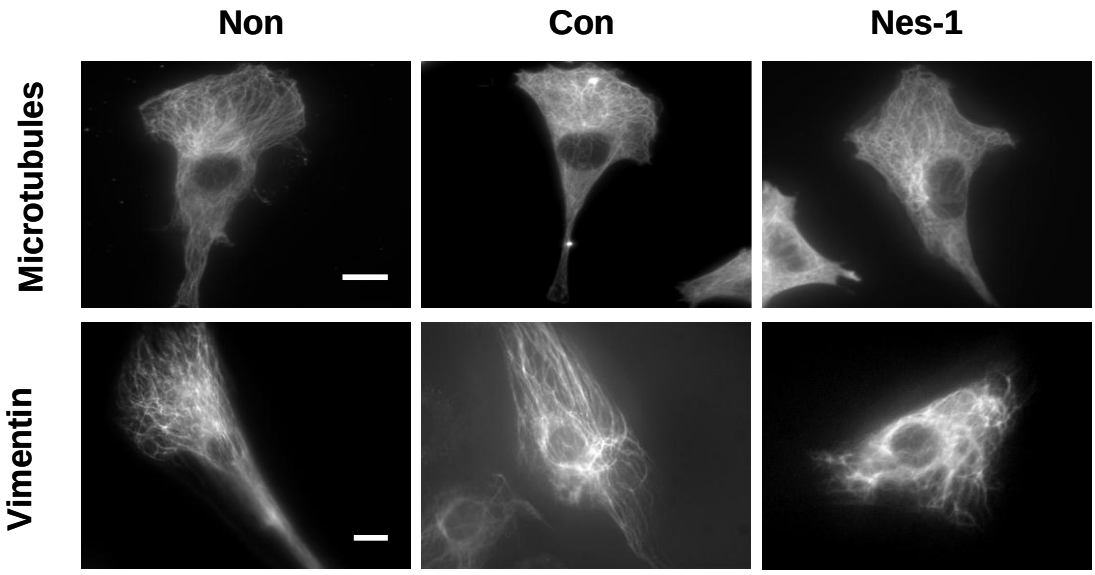

Figure 2-16. Cytoskeletal organization in nes-1 deficient cells. There were no visible differences in microtubule and intermediate filament assembly in nes-1 deficient cells. Scale bars for both sets of images are 10 μm.

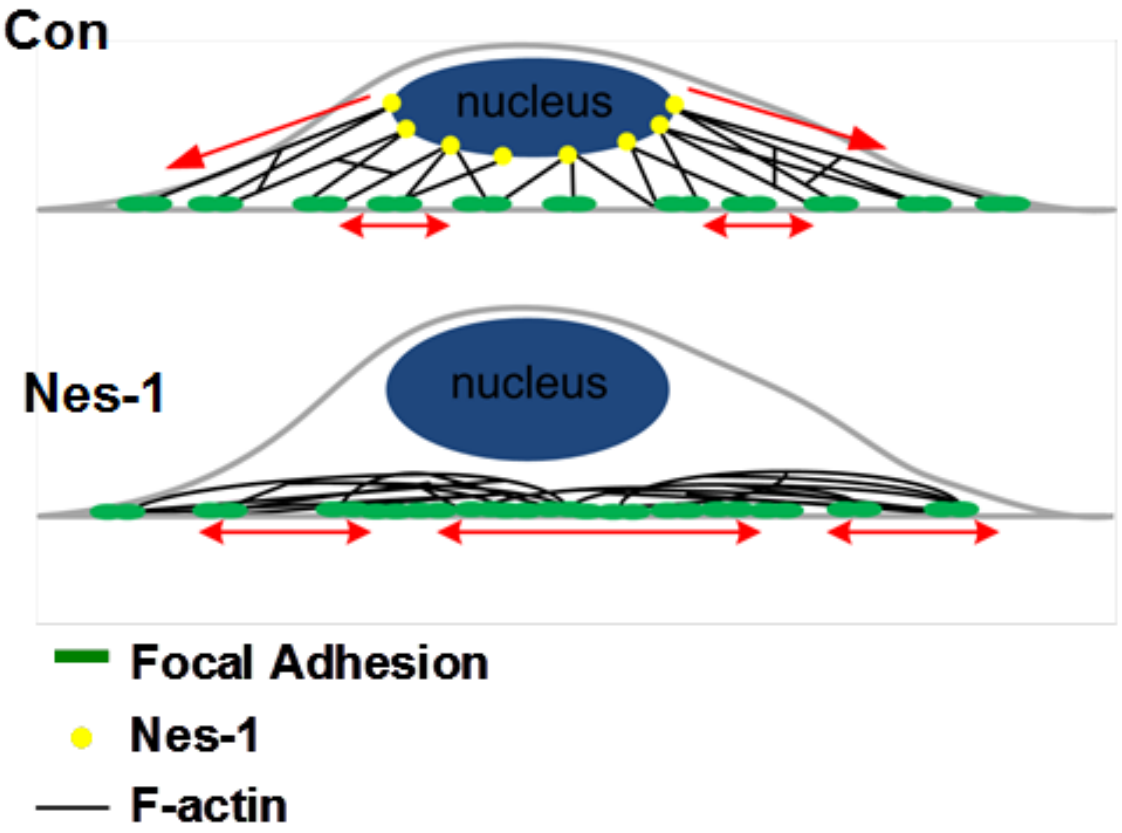

Figure 2-17. Physical model for nuclear-actomyosin force balance. In control cells (top) the actomyosin tension is balanced in part by the nucleus due to mechanical links mediated by nesprin-1. In the absence of nesprin-1 (bottom), the forces are balanced by the substrate at an increased number of focal adhesions even though myosin II activity is unchanged.

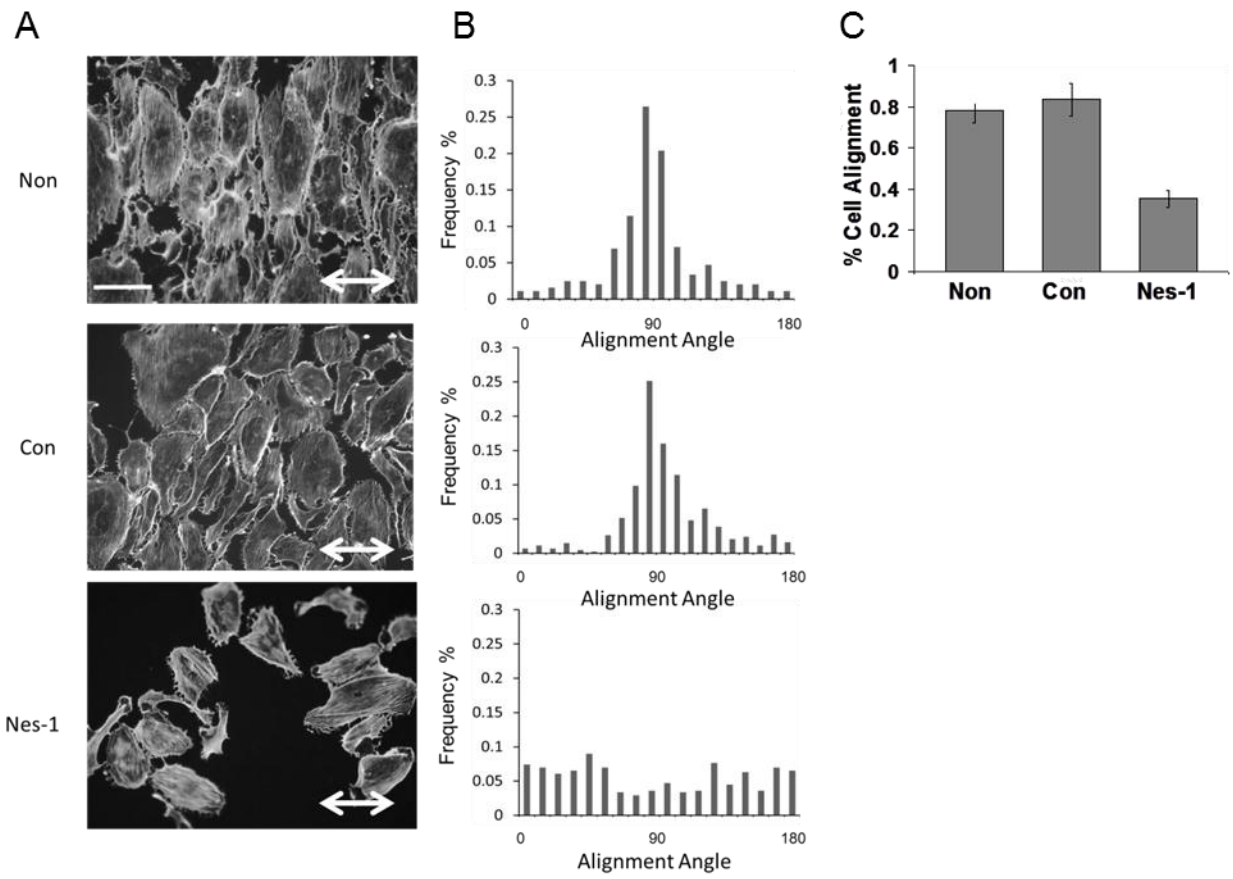

Figure 2-18. Nesprin-1 deficient HUVECs are unable to align in response to uniaxial cyclic strain. A) HUVECs cultured on flexible silicon membranes coated with fibronectin were exposed to 10 % cyclic, uniaxial strain at 0.5 Hz, fixed and stained with Alexa-phalloidin to visualize F-actin stress fibers. Non-transfected HUVECs and cells expressing control siRNA oriented perpendicular to the strain direction (strain direction is marked by white double arrow) while cells transfected with nesprin-1 targeting siRNA did not align in any preferred direction. Stress fibers were observed predominantly perpendicular to the strain direction except in nesprin-1 deficient cells. Scale bar is 50 µm. B) Probability distributions of cell angle measured relative to strain axis. A clear preference for a direction perpendicular to the strain axis is observed in the distribution for non-transfected and control siRNA transfected cells; the distribution is random for nesprin-1 siRNA transfected cells. The distribution was quantified from pooled data from three independent experiments corresponding to 300 cells per condition. C) Quantification of the reorientation response. The data is presented as percentage of cells that reoriented 90o ± 30o relative to the strain direction similar to the approach in (76). Error bars represent SEM from three different experiments and * indicates $p<0.01$.

CHAPTER 3
THE NUCLEUS IS IN A TUG-OF-WAR BETWEEN ACTOMYOSIN PULLING FORCES IN A CRAWLING FIBROBLAST

The basic question of whether the nucleus is primarily “pushed” into position by compressive cytoskeletal forces, or “pulled” by tensile cytoskeletal forces is unresolved because the literature is contradictory on this point. In crawling cells at the edge of a freshly created wound, retrograde flow of actomyosin may push the nucleus toward the trailing edge(29), while a squeezing (pushing) force due to actomyosin contraction in the trailing edge(31) may move the nucleus toward the leading edge. Conversely, other studies suggest that the nucleus is normally under a state of tension(24, 32-35). Both pushing and pulling forces may simultaneously operate on the nucleus, but of interest in this paper is the net direction of the force balance (i.e. pushing versus pulling) and the dominant cytoskeleton origin of these forces in a single, crawling NIH 3T3 fibroblast.

Materials and Methods

Cell Culture, Plasmids and Transfection, Drug Treatment

NIH 3T3 fibroblasts were cultured in DMEM (Mediatech, Manassas, VA) with 10% donor bovine serum (Gibco, Grand Island, NY). For microscopy, cells were cultured on glass-bottomed dishes (MatTek Corp, Ashland, TX) coated with 5μg/ml fibronectin (BD Biocoat^{TM}, Franklin Lakes, NJ) at 4˚C overnight. For photoactivation experiments, cells were serum-starved for two days in DMEM with 1% BSA (Sigma-Aldrich, St. Louis, MO).

YFP-γ-tubulin was prepared from the MBA-91 AfCS Set of Subcellular Localization Markers (ATCC, Manassas, VA). GFP-actin was provided by Dr. Donald E. Ingber in Harvard University. mCherry-PA-Rac1 (Addgene plasmid 22027). DsRed-CC1was kindly provided by Prof. Trina A. Schroer from Johns Hopkins University. EGFP-KASH4

was previously described in (15) . Transient transfection of plasmids into NIH 3T3 fibroblasts was performed with Lipofactamine^{TM} 2000 transfection reagent (Life Technologies, Invitrogen, Carlsbad, CA).

For microtubule disruption experiment, cells were treated with nocodazole (Sigma-Aldrich, St. Louis, MO) at the final concentration of 1.6 μM for over one hour prior to the experiment. For myosin inhibition, cells were treated with blebbistatin (EMD, Gibbstown, NJ) at the final concentration of 50 μM for over one hour prior to the experiment.

Time-Lapse Imaging and Analysis

Time-lapse imaging was performed on a Nikon TE2000 inverted fluorescent microscope with a 40X/1.45NA oil immersion objective and CCD camera (CoolSNAP, HQ^2, Photometrics, Tucson, AZ). During microscopy, cells were maintained at 37 ˚C in a temperature, CO_2 and humidity controlled environmental chamber.

Confocal Microscopy and Photoactivation

The samples were imaged on a Leica SP5 DM6000 confocal microscope equipped with a 63X oil immersion objective. For photoactivation, a region in between the nucleus and the edge of a cell, which is approximately the size of the nucleus, was chosen using the ROI (region of interests) function. 488 Argon laser was applied at 1% power to activate Rac1. Images were taken every 10 seconds. During microscopy, cells were maintained at 37 ˚C in a temperature, CO_2 and humidity controlled environmental chamber.

Image Analysis

Image series from cell migration experiments were processed in ImageJ (NIH). Then they were imported into Matlab (MathWorks, Natick, MA). Programs were developed to track the nuclear centroid and the contour of cells.

Image series from the photoactivation experiment were imported into Matlab (MathWorks, Natick, MA), and a program was developed for nuclear position tracking. After the positions of nuclei in different experiments were obtained, the coordinates were rotated as shown in Figure S1. The vector pointing from nuclear centroid at time=0 to the activation center was used as the θ=0 axis in the polar coordinate. All the trajectories were rotated following this rule. The directional movements then were calculated as the projecting distance of the trajectories on the θ=0 axis.

Micromanipulation by Microinjector

Eppendorf Femtojet® microinjection system (Eppendorf North America, Hauppauge, NY)was used. The microneedle was lowered to the surface of the dish 250 μm from the cell. The needle was then lowered slowly, bending the main shaft of the needle and translating the tip across the surface of the glass bottomed dish until the neelde slid underneath the cell. The needle was then translated towards the end of the cell which was targeted for release. After a slight translation the needle would be raised. This was repeated until the trailing edge or lamellipodia had been removed. For pulling experiments the tipoff the needle was carefully lowered on top of the previously released trailing edge and pressed against the glass surface. The tip was then translated away to reapply tension to the cell.

Results

Forward Motion of the Nucleus Occurs Due to Actomyosin Contraction Between the Leading Edge and the Nucleus

It is known that trailing edge detachment can cause forward motion of the nucleus in crawling NIH 3T3 fibroblasts. We examined the correlation between nuclear motion and trailing edge motion. Forward motion of the nucleus toward the leading edge did not necessarily require the detachment of the trailing edge (Figure 3-1A, B and C). As seen in Figure 3-1B, the forward motion of the nucleus correlated with forward motion of the cell centroid, but not with motion of the trailing edge. The extent of trailing edge motion was minimal compared to nuclear displacement and cell-centroid displacement (Figure 3-1C). Thus significant forward motion of the nucleus can occur without large changes in the shape of the trailing edge. We also observed many examples where nuclear motion does occur when the trailing edge detached (an example is in Figure 3-8).

What causes forward nuclear motion in the absence of significant trailing edge detachment? One hypothesis (originally proposed by Lauffenburger and Horwitz(2) is that the nucleus is pulled forward by actomyosin contraction occurring in the leading edge. To test this, we adapted the Rac1 photoactivation assay recently introduced by Hahn and coworkers (36, 83, 84). The approach is to trigger local polymerization of F-actin; this newly created F-actin is expected to combine with myosin and result in increased local contraction.

On creation of local lamellipodium with Rac1 photoactivation (Figure 2-1A ,the bright circle indicates the photoactivated spot), the nucleus was observed to move persistently toward the direction of the newly formed lamellipodium (outline in Figure 3-

2A,Figure 3-1A). Figure3 1B shows nuclear trajectory plots pooled from several experiments; all trajectories are oriented such that the line joining the initial position of the nuclear centroid and the photoactivated spot is oriented along the positive x-axis. All photoactivation experiments were performed for 30 minutes. As seen, the fluctuating trajectories of the nucleus have a drift bias toward the positive x-axis. The trajectories of the nucleus did correlate with centrosomal trajectories (both moved in the general direction of the newly created lamellipodium, Figure 3-2C). However, depolymerization of microtubules with nocodazole did not eliminate the directional motion of the nucleus (Figure 3-2D,E, Figure 3-3A). Inhibition of myosin activity by blebbistatin treatment, or disruption of the LINC complex with KASH4 domain over-expression eliminated the directional motion of the nucleus toward the photoactivated spot (Figure 3-2E, Figure 3-3B and 3-3C,). As evident from the mean projection of trajectories along the x-axis (Figure 3-2G), only control and nocodazole treated cells showed significant nuclear displacement toward the photoactivated spot, KASH4 over-expressing and blebbistatin treated cells showed essentially zero mean displacements. Interestingly, when the variance of the trajectories about the mean positions was computed (Figure 3-2H), nocodazole treated cells had significantly higher variance in nuclear position than control cells, suggesting that microtubule disruption increases fluctuations in nuclear position as it moves toward the photoactivated spot.

The results above suggest that fluctuations in motion of the nucleus are damped because the nucleus is bound to microtubules (for example through nuclear envelope-embedded motors such as dynein and/or kinesin). But the directional motion of the nucleus on the formation of new lamellipodia does not depend on microtubule motor

activity. Consistent with this picture, we found that the nucleus can move forward without requiring trailing edge detachment in dynein inhibited cells; the motion is similar to that in control cells because the nucleus tracks the cell centroid (Figure 3-4A and B). On inhibition of myosin activity through blebbistatin treatment, the nucleus did not move directionally in the photoactivation experiment; nor did it move when KASH4 was overexpressed in the cells. Taken together with the microtubule disruption experiments, the results point to actomyosin contraction as the dominant pulling force on the nucleus which moves it forward during motility of NIH 3T3 fibroblasts. Consistent with this picture, when the lamella was severed with a micropipette, the nucleus was observed to move back; this motion was reduced significantly on over-expression of GFP-KASH in the cell (Figure 3-3).

Myosin Inhibition in the Trailing Edge Causes Nuclear Motion Toward the Leading Edge Without Change in Cell Shape.

The nucleus is under a net pulling force toward the leading edge, what balances the forward pulling force such that nuclear centrality is maintained? To answer this question, we locally inhibited myosin activity using a micropipette to introduce a flow of blebbistatin at high concentrations (500 μM) over the trailing edge (Figure 3-5A, also see Figure 3-6). Traction force measurements (Figure 3-5 F) confirmed that the actomyosin forces were locally reduced.In less than five minutes of local introduction of blebbistatin, the nucleus moved toward the leading edge and away from the trailing edge (Figure 3-5B and D). This occurred without any appreciable change in trailing edge shape, and without any noticeable forward motion of the cell body (Figure 3-5B). Nuclear movement toward the leading edge on myosin inhibition in the trailing edge was

considerably decreased when KASH4 domains were over expressed in cells to disrupt the LINC complex (Figure3-5 C, E and Figure 3-6).

Solid-like Coupling Between the Nucleus and the Trailing Edge

We next detached the trailing edge by introducing a micropipette tip under the trailing edge and snapping it (Figure 3-7A). Trailing edge detachment resulted in movement of the nucleus toward the leading edge (Figure 3-7A). The forward motion of the nucleus on detachment of the trailing edge could be interpreted as due to either pushing forces generated by forward motion of the trailing edge contents, or due to a dissipation of tensile forces on the trailing surface of the nucleus, resulting in a net forward force on the nucleus. Because forward nuclear motion was also accompanied by a change in the shape of the nucleus (as discussed in pulling experiments in Figure 3-7B), we quantified the movement of the leading and trailing edge of the nucleus on trailing edge detachment. Both nuclear leading and trailing edges moved forward on trailing edge detachment in control cells, but this motion was significantly decreased in blebbistatin treated and KASH4 expressing cells. (Figure 3-7 B, C).

We next examined nuclear shape changes on trailing edge detachment. The ratio of the major to minor axis consistently decreased on trailing edge detachment suggesting that the nucleus changes from an elongated cross-section to a rounded shape with time (Figure 3-7 D). In KASH4 overexpressing cells and in blebbistatin treated cells, the nucleus did not change shape significantly on trailing edge detachment (Figure 3-7 D). The shape change in control cells again could occur either due to pushing forces as the trailing edge retracts or a dissipation of pulling forces; but these forces were clearly absent in blebbistatin treated and KASH4 expressing cells. More interestingly, when a detached trailing edge was again pulled on and extended (Figure

3-7 E), the nucleus was observed to almost instantaneously elongate again to nearly its original shape in a myosin dependent manner (Figure 3-7 E,F,G). This experiment suggests that the nucleus is hardwired with actomyosin tensile structures, because while pushing forces can move the nucleus forward on detachment, elongation of the nucleus due to trailing edge extension cannot be explained by pushing forces in the reverse direction. The solid like coupling is clearly apparent in the near instantaneous response of nuclear position to pulling. Figure 3-7 F shows that the motion of the nucleus correlates closely with the motion of the micropipette that is attached to the trailing edge. Shown in Figure 3-7 G is pooled data demonstrating the correlation between motion of the microneedle tip and the nucleus; this correlation is absent in blebbistatin treated cells.

The forward motion of the nucleus on local myosin inhibition in the trailing edge and the myosin-dependent solid-like coupling between the nucleus and the trailing edge suggest strongly that the nucleus is pulled toward the trailing edge by actomyosin forces. The transfer of the pulling forces to the nuclear surface occurs through molecular linkages with the cytoskeleton as suggested by the lack of nuclear motion or deformation in KASH4 expressing cells.

Effect of LINC Complex Disruption on Trailing Edge Detachment

Several recent papers have shown that LINC complex disruption reduces the persistence of cell motility. While in control cells, the trailing edge detached in crawling fibroblasts resulting in forward cell motion, in KASH4 over expressing cells the trailing edge was observed not to detach but rather slip along the surface without large changes in shape (Figure 3-8A, B and E). The speed of forward cell and nuclear motion was greatly reduced. The movement of the nucleus correlated both with cell centroid

motion and trailing edge motion, which again indicates that the cell moves without sudden detachments of the trailing edge (Figure 3-8C, D, E). Interestingly we observed that trailing edge detachment was typically preceded by forward nuclear and cell motion in control cells. Shown in Figure 3-8 F are nuclear displacements in the direction of the leading edge, versus time to detachment. As seen, the nucleus starts to move along with the cell body in a persistent fashion over several microns, while the trailing edge remains fixed in place and gets longer and thinner(not shown). In KASH4 expressing cells, the trailing edge rarely detaches, and when it does so, the nucleus along with the cell has moved large distances (Figure 3-8G).

Discussion

Our results suggest that there is a tug of war between forward pulling and rearward pulling forces on the nuclear surface. The dominant contribution to these pulling forces is from actomyosin contraction. Given that F-actin continuously polymerizes at the leading edge, there is a continuous source of newly polymerizing actin that can contract to pull on the nucleus. The trailing edge is relatively stable in shape (until it detaches), and hence it is reasonable to surmise that the tensile pulling forces in the trailing edge are relatively constant in magnitude. Net forward motion of the nucleus would be predicted to occur when pulling forces at the front exceed those at the back. An actomyosin tug-of-war is thus a simple positioning mechanism for the nucleus in a crawling cell.

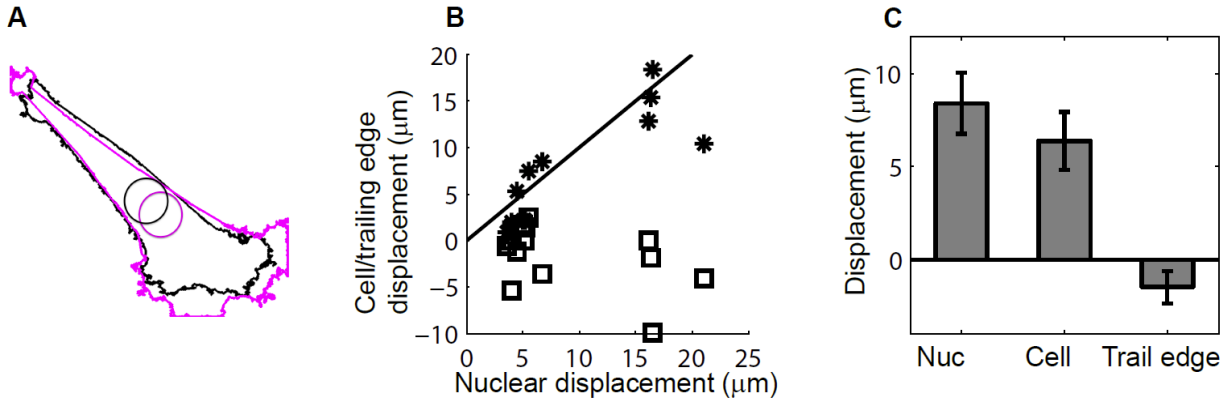

Figure 3-1. Nuclear movement in motile fibroblasts does not required detachment of the trailing edge. (A) The trailing edge retraction is not necessary for moving the nucleus. Superposition of cell outline at zero minute (black) and 30 minute (pink). The nucleus moved forward upon the formation of lamellipodia, while the trailing edge did not retract. (B) Nuclear movement is highly correlated with cell centroid movement (*), but not correlated with trail edge movement (squares) in control (n=14) cells. The solid line is y=x line. (C) Comparison of mean movement of the nucleus and cell centroid and the trailing edge in 30 minutes shows that the nucleus and cell centroid move similar distances, while the trailing edge did not move appreciably. Error bars indicate standard error of the mean (SEM), '*', $p < 0.01$.

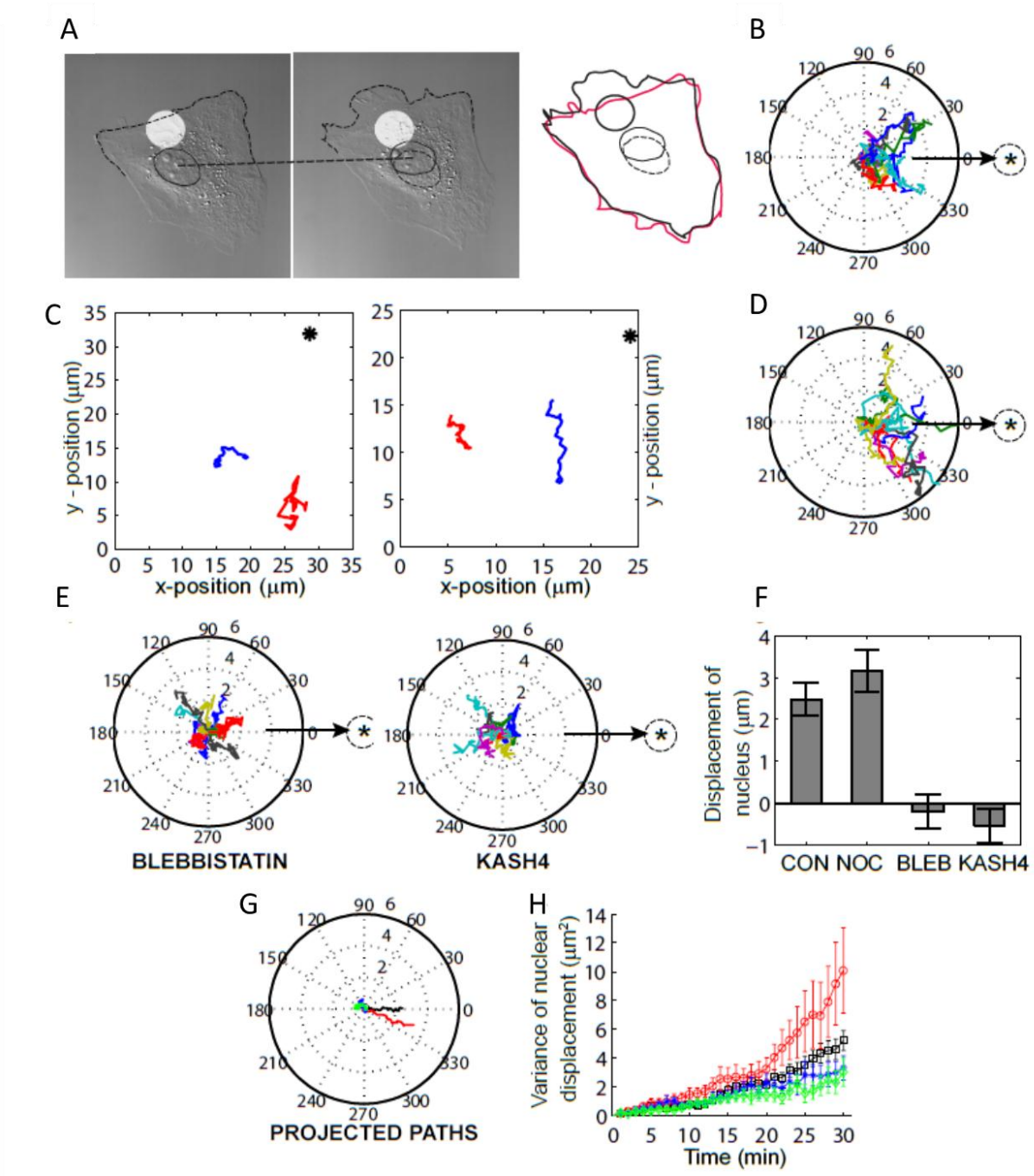

Figure 3-2. Directional nuclear translation upon Rac-1 photo-activation. (A)Frames of a time-lapse recording of a nucleus (dark eclipse) moving towards the photo-activation site (bright circles), and Superposition of cell outline at zero minute (red) and 30 minute (black). Scale bar, 10 µm. (B) Trajectories of nuclear movement upon photo-activation were overlaid with a common starting point. The zero degree is the direction of activation. The unit is micron. The nucleus moved towards the activation site in control cells (N=11). (C) Examples of trajectories of the nucleus (blue) and the centrosome (red) in photoactivation

experiments. (D) Trajectories of nuclear movement upon photo-activation in nocodazole treated cells (N=11). (E) Trajectories of nuclear movement upon photo-activation in blebbistatin treated (N=10) or KASH4 transfected cells (N=10). (F) Average directional displacement of the nucleus towards the activation site. Positive value means the nucleus moved towards the activation site. (G) Average trajectories of the nucleus and (H) variance of the nuclear displacment in control photoactivation (black, N=11), nocodazole treated cells (red, N=11), blebbistatin treated cells (blue, N=10) and KASH4 transfected cells (green, N=10) show that there is larger fluctuation in nocodazole treated cells.

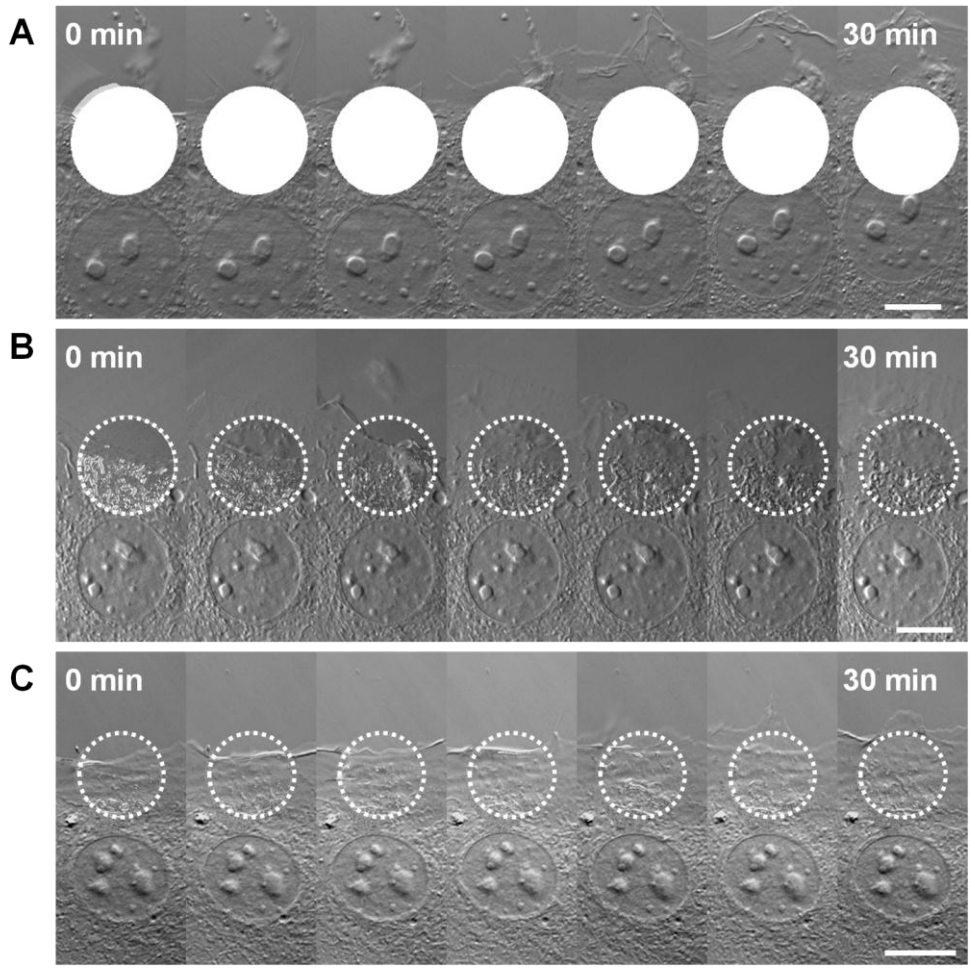

Figure 3-3. Effects cytoskeletal disruption on nuclear movement in response to Rac photoactivation. Kymograph of images corresponding to nuclear movement upon photoactivation in (A) nocodazole treated cells, (B) blebbistatin treated cells and (C) KASH4 over-expressed cells. Disruption of microtubules by nocodazole treatments does not affect the forward motion of the nucleus, while blebbistatin treatment and KASH4 over-expression eliminate the forward motion of the nucleus. Scale bar, 10 μm.

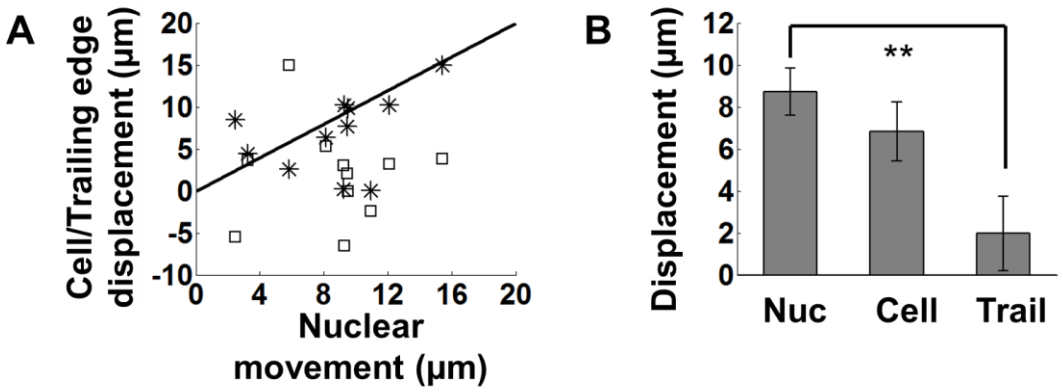

Figure 3-4. Nucleus capable of translation without trailing edge movement in dynein inhibited cells. A) Nuclear movement is still highly correlated with cell centroid movement i (*), but not correlated with trail edge movement (squares) in dynein inhibited cells (*) B) Quantification of nuclear and cell and trailing edge displacement.

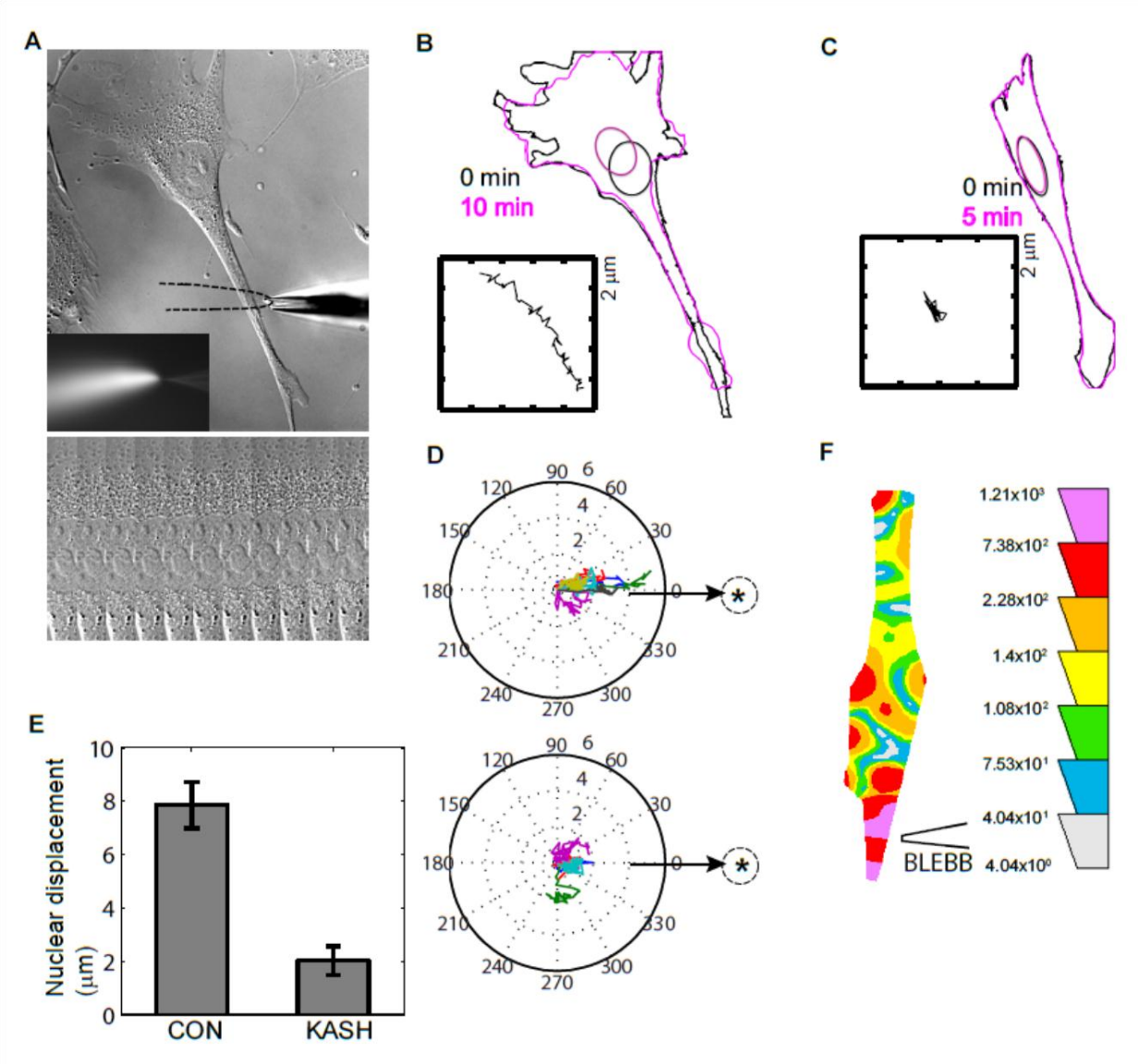

Figure 3-5. Nuclear movement upon local introduction of blebbistatin. (A) Top, blebbistatin was introduced by microneedle at the trailing edge of the cell. The nucleus moved towards the leading edge, this motion was abolished in cells over-expressing GFP-KASH. Inset, Epi-flourescent image of blebbistatin spray with 4 kDa FITC Dextran. The micro-pippette tip was used to localize blebbistatin to the tail region of the cell. Bottom, kymograph of images corresponding to the box in top picture. (B) Superposition of cell and nuclear outlines at different time points in control cell. There was no appreciable change in trailing edge shape and forward motion of the cell body. Inset, trajectory of the nucleus. (C) Superposition of cell and nuclear outlines at different time points in KASH4 transfected cells. Inset, trajectory of the nucleus. (D) Trajectories of nuclear movement in blebbistatin spray experiment (Top, control cells, n=6: bottom, KASH4 transfected cells, n=5) were overlaid with a common starting point. The zero degree is the direction

from the trailing edge to nuclear centroid at time = 0. The unit is micron. (E) Average displacement of nuclear trailing edge upon local introduction of blebbistatin (control, N=6; KASH, N=7, $p < 0.01$). Scale bars: 10 μm. (F) Traction stress of a cell 5 min after local introduction of blebbistatin, which shows larger force change at the tail region where blebbistatin was introduced.

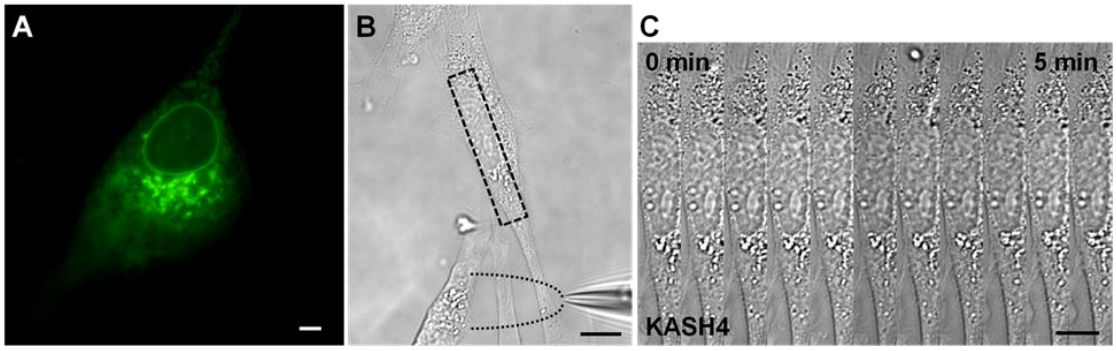

Figure 3-6. Nuclear movement upon local introduction of blebbistatin in GFP-KASH4 cells. (A) A NIH 3T3 cell transfected with EGFP-KASH4. (B) Cells were transfected with GFP-KASH4. Blebbistatin was introduced by microneedle at the trailing edge of the cell. The nucleus did not move. (C) Kymograph images corresponding to the box in (B). Forward motion of the nucleus was inhibited by KASH4 over-expression. Scale bars: 5 µm.

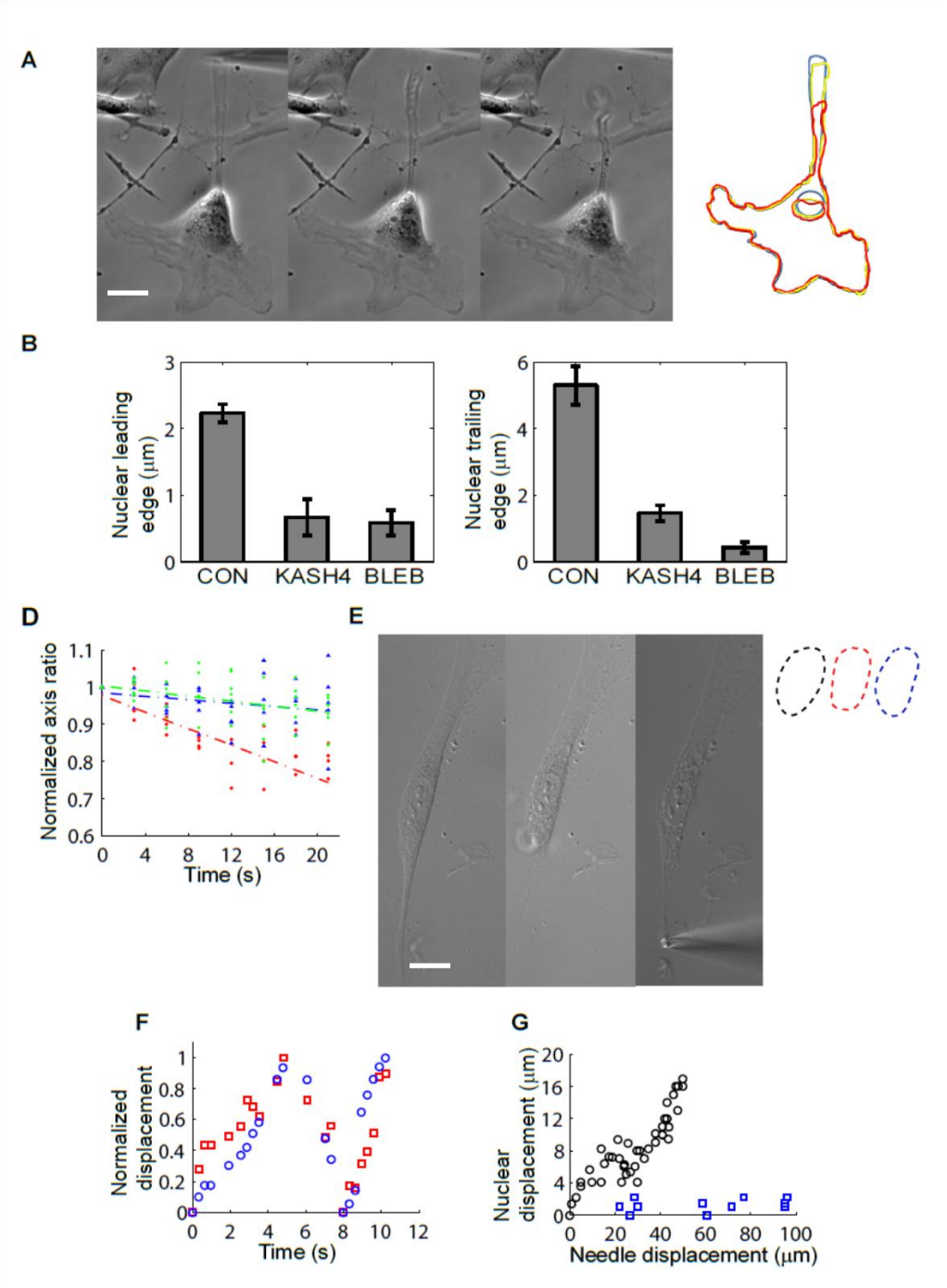

Figure 3-7. Micromanipulation reveals that the nucleus is under tension between the leading edge and trailing edge. (A) Captured images of a cell whose tail was released by a micropipette. Removal of cell trailing edge results in forward nuclear movement in control cells. Superposition of cell and nuclear outlines at zero second (blue), 5 second (yellow) and 10 second (red) show the forward motion and deformation of the nucleus. (B and C) Quantification of the forward movement reveals that both the leadling (B) and trailing (C) edges of the nucleus traveled further in control cells than in KASH cells. Error bars

indicate SEM,. (D) Nuclear Deformation in response to tail release. The nucleus deformed in control cells (red, N=5), while remained the same shape in KASH4 transfected cells (blue, N=5) and blebbistatin treated cells (green, N=6). (E) Pulling on the released section of the cell results in nuclear movement in the direction of the pull. (F) Normalized displacements of the nucleus and micro-needle show that they are highly correlated. (G) Example plot of nuclear displacement versus micro-needle displacement. There is no correlation between nuclear displacement and the micro-needle movement in blebbistatin treated cells (blue squares), while it is highly correlated in control cells.

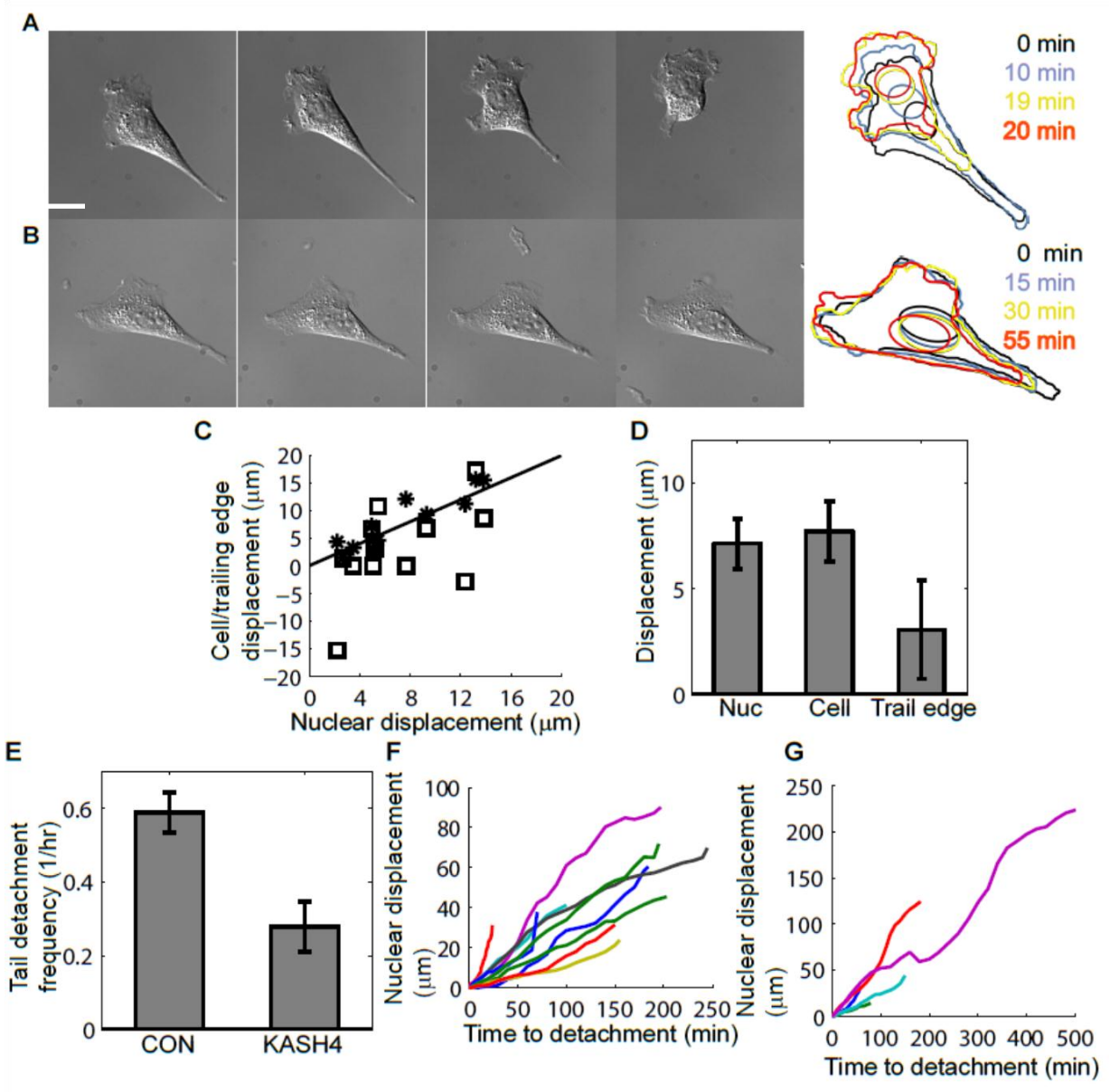

Figure 3-8. Effect of KASH on trailing edge detachment. (A) Captured images of the trailing edge detachment during forward protrusion of an NIH 3T3 fibroblast and superposition of cell outline at different time points. The nucleus kept moving towards the leading edge. (B) Captured images of the trailing edge movement during forward protrusion of an KASH4 transfected cell and superposition of cell outline at different time points. The trailing edge slides forward other than detached from the substrate. (C) Nuclear movement is highly correlated with cell centroid movement (*) in KASH4 (N=11) transfected cells, as well as with the trailing edge movement (squares) in some cases. Most nuclei moved similar distance as or less than the cell centroid did. The solid line is y=x line. (D) Average movement of the nucleus and cell centroid in KASH4 (N=11) transfected cells in 30 minutes also show that they moved similar distances.The trailing edge move forward, while it was much less than

the nucleus did. Error bars indicate standard error of the mean (SEM), '*, **', $p < 0.01$. (E) Trailing edge detachment frequency is much higher in control (N=24) cells than in KASH4 transfected cells (N=20). (F and G) Trajectories of the nuclear displacement during cell tail stretching and trailing edge detachment in control (F, N=10) and KASH4 transfected (G, N=5) cells. The nucleus keeps moving forward during this period.

CHAPTER 4
A NOVEL MICROPIPETTE ASPIRATION TECHNIQUE TO APPLY FORCES TO THE NUCLEUS

Micropipette aspiration is a popular method for measuring cell-cell and cell-substrate adhesion forces. An approach to measuring cell adhesion forces involves repeatedly bring a micropipette tip (radius of 4-8μm) to the edge of the cell surface and applying a known suction pressure to the cell. Next the micropipette tip is pulled away at a constant velocity; if the cell does not detach the suction pressure is increased. The procedure is repeated until the cell finally detaches, allowing an estimate of the forces between cells from different origins. We have adapted this method for pulling on the nucleus in the cell with known forces. We show preliminary results with the method, and discuss applications of the technique for studying nuclear mechanics.

Materials and Methods

Cell Culture

Experiments were conducted on NIH 3T3 fibroblast cells which were used at passages of 10-11 and maintained at low confluence. Cells were grown in a medium of Dulbecco's Modified Eagle's Medium (DMEM, Mediatech, Manassas, VA) supplemented with 10% Donor Bovine Serum (DBS, Gibco, Grand Island, NY) and 1% antibiotics.

Cells were passed on sparsely at a 1:10 dilution on a 3.5 cm glass bottom dishes. The dishes were then filled with 3 ml media to avoid image defects due to reflection caused by entry of the needle. Transfections were performed using 1.5-2μg GFP-KASH4 plasmid DNA and 4 μl of the transfection agent lipofectamine 2000. Cells were transfected in a 12 well cell culture dish overnight and were then plated at dilutions of 1:20 on a glass bottom dish (MatTek, Ashland, Texas).

Treatment with 50 µM blebbistatin was used for nuclear aspiration experiments. A lower blebbistatin concentration of 12.5 µM was used for nuclear perturbation experiments. The cells were incubated for half an hour before experiments were performed. Experiments on blebbistatin cells were conducted within 90 minutes of treatment.

In the nuclear perturbation experiments cells were treated with the live cell nuclear stain Cyto 59 at a 1:1000 dilution for 30 minutes and washed with fresh growth media immediately before the experiment.

Imaging and Micromanipulation

Cells were imaged on a Nikon TE 2000-E microscope on a 20X objective in Phase mode. The microscope was equipped with a covered glass chamber used to maintain the temperature at 37.0C. A CO_2 tank was used to supply CO_2 to a small chamber covering the cells that maintained CO_2 levels at 5%. Results were recorded and analyzed using the NIS Elements software and image J.

An Eppendorf InjectMan® NI 2 micromanipulator system was used for applying forces to the cell. The micromanipulator arm was attached to an inbuilt module on the microscope. The flexible arm was maneuvered to reach the dish through the CO_2 chamber thus maintaining the CO_2 levels for the duration of the experiment. The arm of the needle was set to a constant of 45^o indicating the angle at which it approached the adherent cells. This system is equipped with a joystick that controls the position of the needle in the x-y plane by moving back and forth. It can also be twisted up and down to lower or raise the needle in the z direction. The InjectMan® system was coupled with a Femtojet® system for varying the aspiration pressure on the nucleus. The needles used

for aspiration procedure were the Femtotip II® microinjection needles with a tip diameter of 0.5 µm.

Description of the Nuclear Aspiration Experiments

The cells were imaged on 3.5 cm glass bottom dish within the CO2 chamber. The Femtotip® needle is controlled by the micromanipulator arm and has a capillary connecting it to the Femtojet® system which maintains a specified pressure. The capillary pressure within the needle can be adjusted by varying the capillary pressure knob on the controller®. The needle was then maneuvered until it was visually in line with the objective and lowered until it made contact with the cell growth medium.

Next a 20X phase or 40X DIC objective was used to focus on the cell monolayer first. The plane of focus was raised to focus above the cells and on the needle. The needle was then carefully lowered until it was 10-20 µm above the targeted cell. It must be noted here that the needle is very fragile since the diameter of the tip is very small. Under these conditions lowering the needle and scraping it on the dish surface in an incorrect manner can lead to breakage.

Once the micropipette was positioned above a targeted cell the needle was lowered slowly until it just made contact with the top of the nucleus. The desired pressure was set on the external pump and the capillary inside the needle was allowed to reach an equilibrium height. The needle was assumed to be in contact with the nucleus when slight deformations in nucleus were observed. Care was taken to not puncture the nucleus as this would lead to cell death. After establishing contact with the nucleus the capillary connected to the external pump was disconnected, instantaneously reducing the pressure inside the micropipette to 1 atm. The

micropipette was then translated towards the manipulator at a speed of 5µm/s until the nucleus was removed from the cell or had disconnected from the micropipette.

On an average 12 experiments were conducted at each external pump pressure and the behavior of the nucleus was noted visually. The external pump pressure ranged from 0-1700 hPa (170000 Pa) with increments of 100hPa.

Description of Nuclear Displacement Experiments

A micropipette was brought into contact with the nucleus of a cell as described above. The external pump pressure was set to a pressure between 75-200 hPa. The micropipette was then translated away from the nucleus at 2.5 µM until the stabilizing forces on the nucleus overcame the vacuum of the micropipette. The experiment was recorded at real-time speed with the AVI recorder module of the Nikon elements package.

Capillary Action of the Needle

As shown in Figure 4-1, the needle is immersed in the sample medium of h ~ 2 cm depth and aspirates a liquid column of length l, diameter d and angle α. The hydrostatic force balance requires that air pressure inside the capillary P_1 plus the fluid head in the column $l\rho g\cos\alpha$ balance the pressure at the capillary ρgh and the capillary pressure $p_c = 4\gamma\cos\theta/d$. Here θ is the wetting angle of water in the capillary and γ is the surface tension. That is

$$P_1 + l\rho g\cos a + 1atm = \rho gh + 4\gamma\cos\theta/a + 1atm \qquad (4\text{-}1)$$

The fluid heads can be assumed to be negligible relative to the capillary pressure, in which case pipette air pressure approximately balances the capillary pressure.

$$P_1 \approx 4\,\gamma\cos\theta/d \qquad (4\text{-}2)$$

In the experiment when P1 is reduced from the pump pressure to 0 Pa (gauge pressure), a pressure imbalance is near-instantaneously reached and the nucleus is exposed to a vacuum equal to that of the original pump pressure. Because the tip is tapered (d is variable), the suction pressure on the nucleus can be controlled by adjusting the initial pressure of the external pump.

Results

Capillary Pressure in the Micropipette is Capable of Aspirating the Nucleus From the Cell

To test if the capillary was strong enough to remove the nucleus from the cell,the pulls were done with a pump pressure of 1700 hPa. The resulting vacuum of 1700 hPa pulled the nucleus as the pipette was translated (Figure 4-2). The translation of the nucleus resulted in a deformation of the edges of the nucleus as they appeared to still be attached to elements of the cell (FIG 4-2). The degree of this deformation continued to increase until the nucleus was over 40 μm from its original location and the last connections were broken. The complete removal of the nucleus reveals that the micropipette is clearly capable of producing forces capable of overcoming those that hold the nucleus in the cell.

Nuclear Translation is Not Due to Nonspecific Binding Between Nucleus and Micropipette

To ensure that nonspecific binding between the micropipette and the nucleus (or the contents of the nucleus) were not causing the nucleus to become attached to the pipette, experiments were performed with an initial gauge pressure of 0 Pa. No movementof the nucleus was observed (FIG 4-3).

Nuclear Aspiration Experiments Can be Categorized Into 3 Distinct Cases

Three distinct cases were observed depending on the chosen capillary pressure. At low or zero suction pressures, there was no apparent movement of the nucleus. An illustration of this is in Figure 4-3 where the nucleus did not translate with the needle. This was treated as a null pull. At intermediate vacuum, the needle pulled the nucleus with sufficient suction force to dislodge within the cell body, as in Figure 4-4. However the nucleus could not be removed past the cortical membrane and emerge out of the cell completely. The nucleus detached from the capillary after translating at a certain distance- at the point of detachment, the force applied to the nucleus is equal to the capillary pressure x cross-sectional area of the capillary tip. At high enough vacuum shown in Figure 4-2, the aspiration pressure was large enough to pull the nucleus out of the cell completely past the cortical and stress fiber network.

KASH Transfection Increases Probability of Local Detachment of the Nucleus

The nucleus was detached from the cytoskeletal elements holding it in place without completely leaving the cell body. Cases of success and failure were scored as 1 and 0 which was then used to calculate the probability of detachment at each pressureThe net probability for pulling at each successive pressure was plotted against shown in Figure 4-5. The results of pulling in control and KASH cells fit well (Figure 4-5 solid line indicates fit) with a sigmoidal model (R2=0.91 and 0.84 respectively) represented by the following equation within the probability limits (0<P<1):

$$y = \frac{1}{(1+EXP(\frac{-(P-P_0)}{W})} \quad (4\text{-}1)$$

Where P is the applied pressure. The value of the characteristic pressure of detachment P0 was found to be 837 hPa representing the pressure at which 50%

success in aspiration was seen. The value of P0 in the case of GFP-KASH4 transfected cells was much lower at 472 hPa showing a significant departure from the value obtained for control cells. Control nuclei were aspirated with a probability of 0.92 at 1600 hPa while GFP-KASH4 expressing cells were aspirated with a probability of 1 at a pressure of 900 hPa (Figure 4-5). Thus there was a significant difference observed in probability of detachment at every pressure increment between control and KASH4 expressing cells.

. These results suggest that micropipette aspiration is capable of detecting changes in nucleo-cytoskeletal binding. The difference in detachment pressures between GFP-KASH4 and control cells also suggest that the cytoskeleton is responsible for resisting nuclear motion from external forces.

The Actin Cytoskeleton is Deformed by Nuclear Movement

Nuclear aspiration experiments were performed on NIH3T3 cells transfected with GFP-Actin. At pressures of 1700 hPa the nucleus was translated at 5 μm/s while simultaneously imaging the cell every 0.25s. Actin stress fibers were seen to translate as the nucleus was moved away from their location (Figure 4-6). Some but not all stress fibers appeared to be directly connected to the nucleus (Figure 4-7). Less movement was seen from stress fibers when the nucleus was moving towards them unless direct contact between the nucleus and a stress fiber occurred (Figure 4-8).

The Nucleus Returns to the Equilibrium Position After Small Perturbations

At lower aspiration pressures we perturbed the location of the nucleus between 2-5 μm. After release from the micropipette the nucleus quickly returned to the original locations (Figure 4-9). The nuclear shape (Figure 4-9b) was deformed during the perturbation but release of the nucleus restored its equilibrium shape.

Discussion

The nucleus is not free to drift, but is mechanically anchored to the cytoskeleton(15, 20, 24, 30, 85). Motion of the nucleus in a new direction requires the breakage and formation of new bonds between the nucleus and the cytoskeleton(24). In this work we have developed a novel technique to investigate nuclear cytoskeletal rupture and stabilization forces.

Using a micropipette we exerted measurable forces on the nucleus with a capillary under vacuum. As the pressure is known in the capillary, when the nucleus translates but ultimately detaches from the capillary tip, the force applied to the nucleus at the point of detachment is the capillary pressure x capillary tip area. In this way, the extent of nuclear translation can be varied by altering the suction pressure of the needle. By probing the nucleus in this manner, we expect that it will be possible to estimate the forces due to individual cytoskeletal elements that resist motion of the nucleus. This is supported by the observation that cells in which the KASH domain was over expressed showed less resistance to nuclear detachment (Figure 4-5). The highest probability of detachment in Control and KASH treated cells was observed at suction pressures of 1200, and 900 respectively.

Conducting nuclear aspiration experiments on cells expressing GFP-actin revealed that the actin cytoskeleton is perturbed by nuclear translation. Interestingly more deformation was observed in stress fibers located behind the translating nucleus compared to stress fibers located in front of it. Figure (4-6). Deformation of stress fibers in front the translating nucleus only occurred if the nucleus made direct contact with the fiber (Figure 4-8). Translation of the nucleus disclosed that some stress fibers may be directly bound to the nuclear envelope (Figure 4-7).

Mutations in LINC complex proteins have been associated with mis-positioned and irregularly shaped nuclei(5). One hypothesis for these irregularities is the absence of a centering forces on the nucleus. Small perturbations of nuclear position are possible by lowering the suction pressure in the micropipette as shown in Figure 4.9. After the perturbation the restoring forces quickly returned the nucleus to near its original equilibrium (Figure 4-9B). Combining this method with cytoskeleton altering drugs or treatments will allow the estimation of the contributions of intermediate, microfilament and actin cytoskeletons in restoring the nucleus to its central position.

In conclusion ,we have designed a new method to translate the nucleus with a measurable externally applied force. The flexibility of this technique will allow it to be of great use in future research on the nucleo-cytoskeleton force balance.

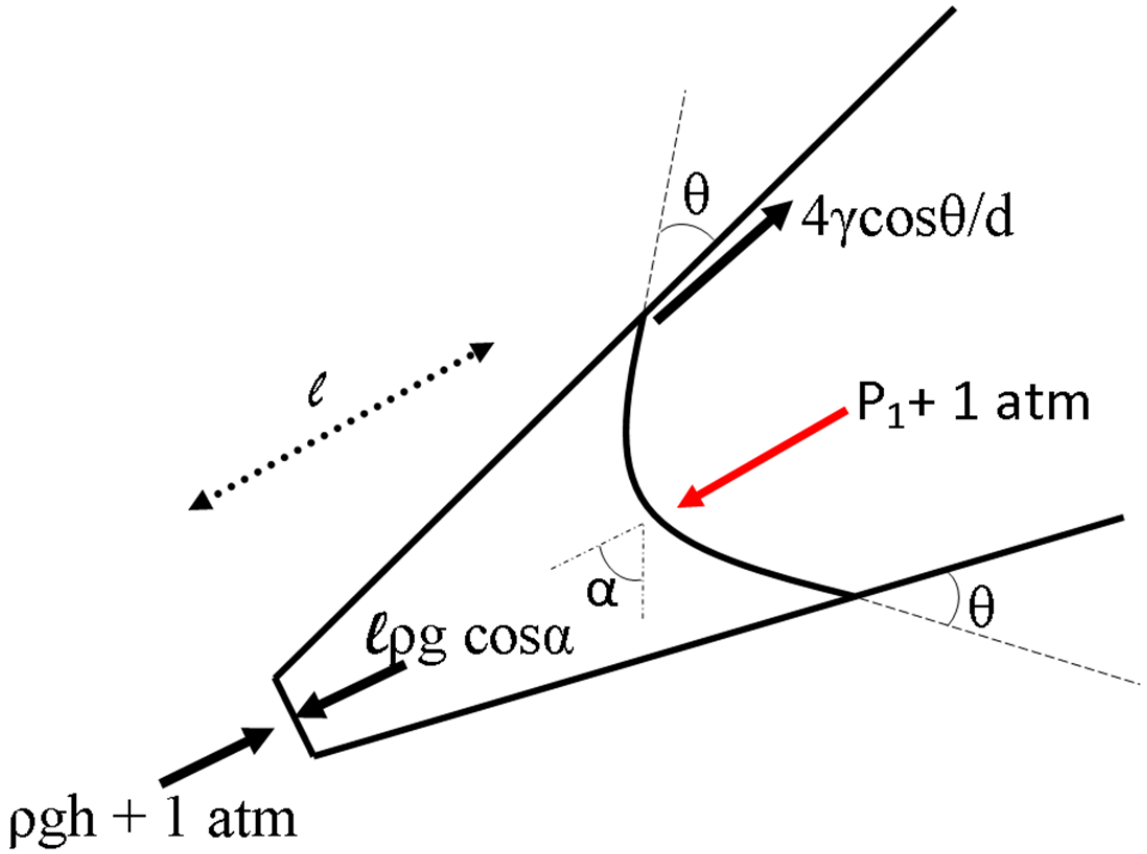

Figure 4-1. Free body diagram of pressures at the micropipette tip. The length of liquid in the column is l, the angle that the needle makes with the horizontal is α and the wetting angle of water and glass is θ. The needle used here is an Eppendorf Femtotip® which has a tapering diameter as shown in figure.

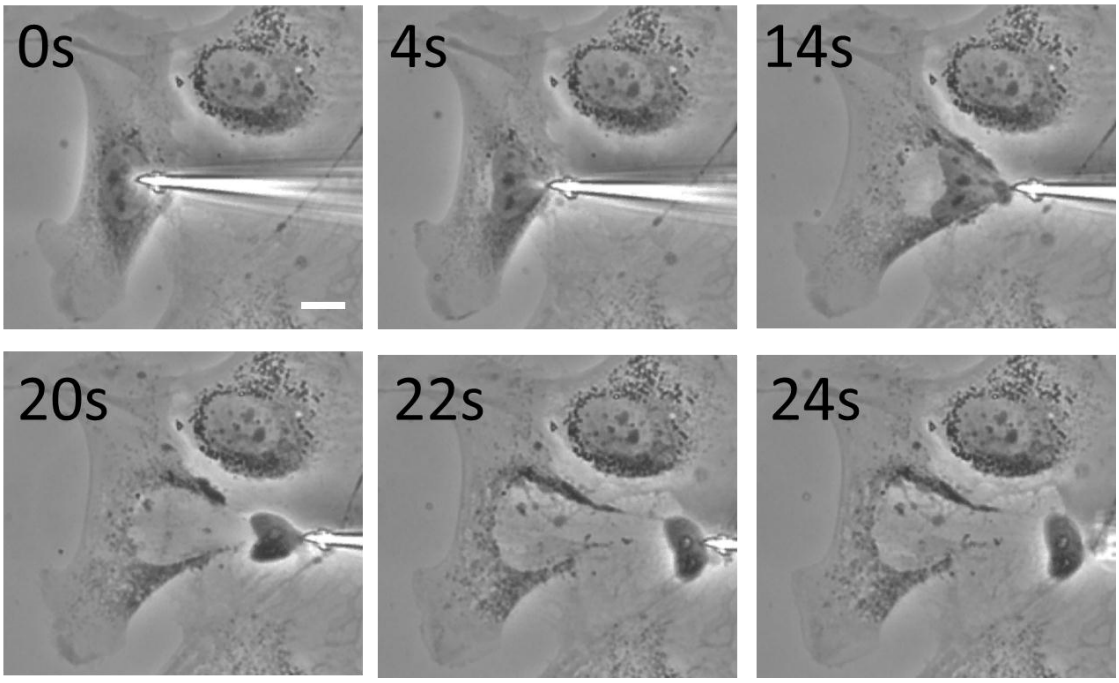

Figure 4-2. Capillary action can of produce forces capable of translating the nucleus in NIH 3T3 cells. Scale bar is 5 micronsThe needle was slowly pulled removing the the nucleus from the cell, the last frame shows the needle releasing the nucleus as the vacuum is released. Scale bar is 5 µm

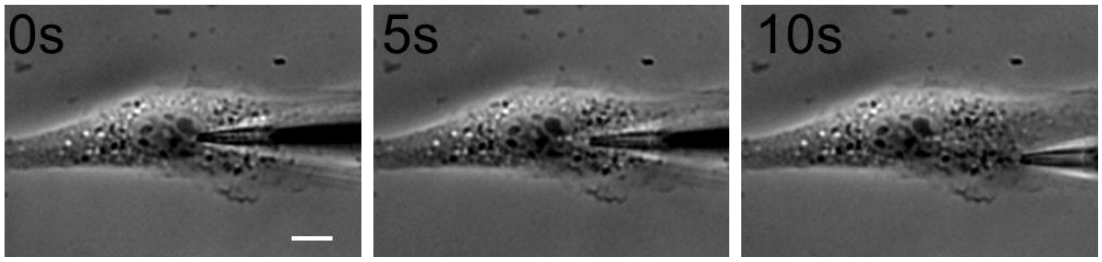

Figure 4-3. Non specific binding between nucleus and micropipette does not cause nuclear translation. When no suction pressure is applied no nuclear movement is observed. This confirms that nonspecific binding between the nucleus and needle is not sufficient to translate the nucleus. Scale bar is 5 µmµ

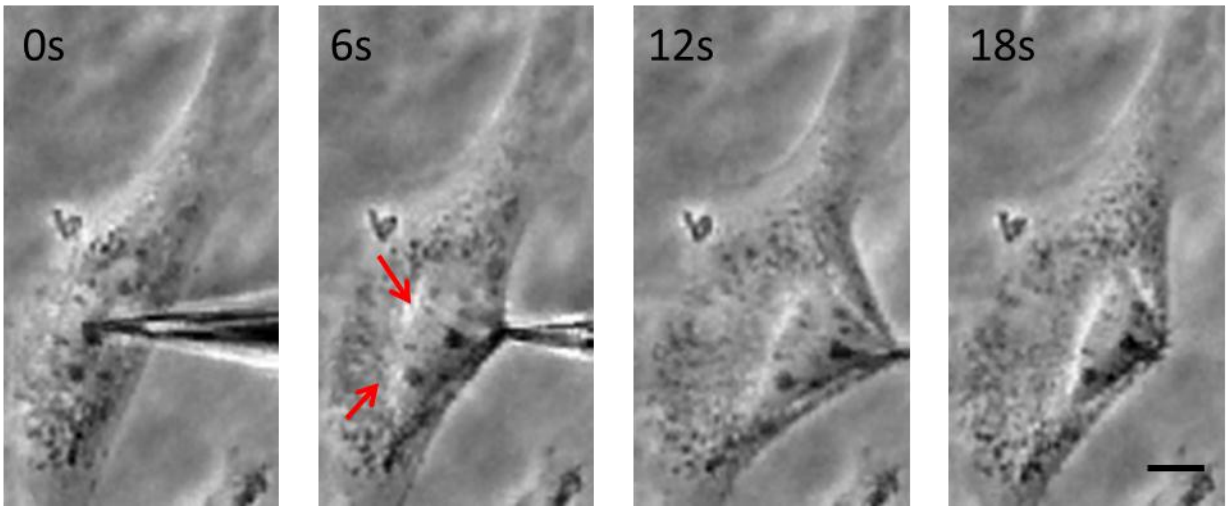

Figure 4-4. Local nuclear detachment within the cell body. At lower suction pressures (<1300 for controls) local nuclear detachment was often observed. The nucleus appears to break away from the trailing cytoskeleton (start of tear indicated by red arrows) but the suction pressure of the needle is not strong enough to completely remove the nucleus from the cell.

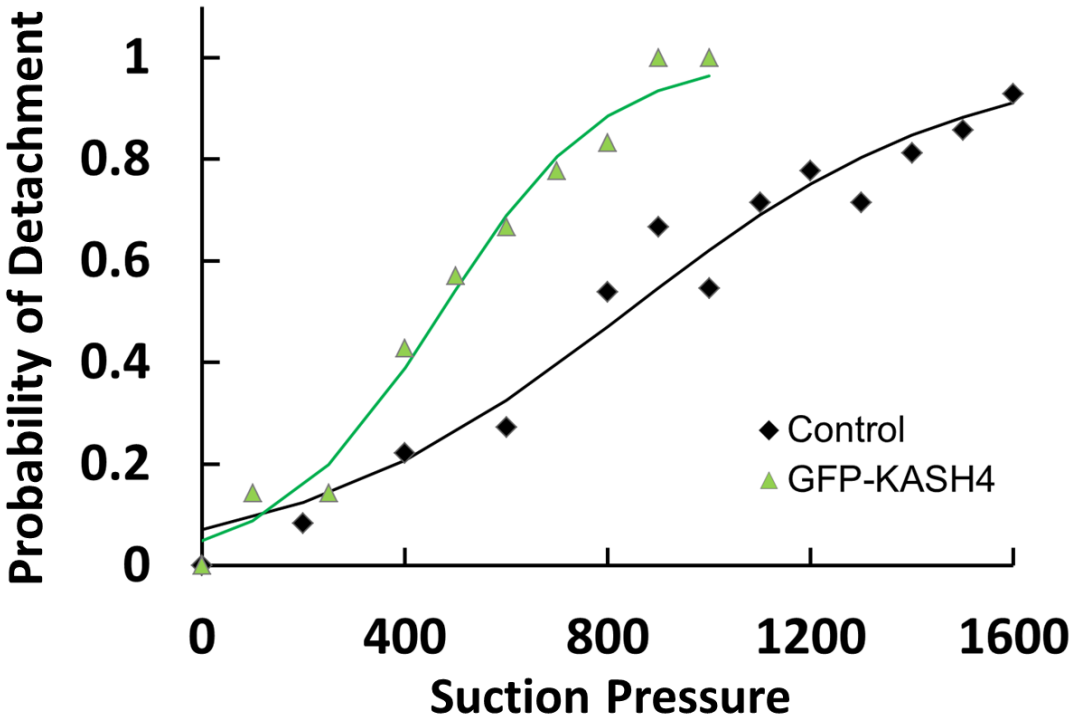

Figure 4-5. Pressure versus probability of detachment in control and KASH cells. Control cells have stronger nuclear cytoskeletal coupling as evident from the higher pressure needed detach the nucleus. The black dots represent control cells and the green triangles represent KASH cells. Both plots have been fit to a sigmoidal fit: $y = \frac{1}{(1+EXP(\frac{-(P-P_0)}{W})}$. The fit was found to be significantly different at pressures above 400 hPa.

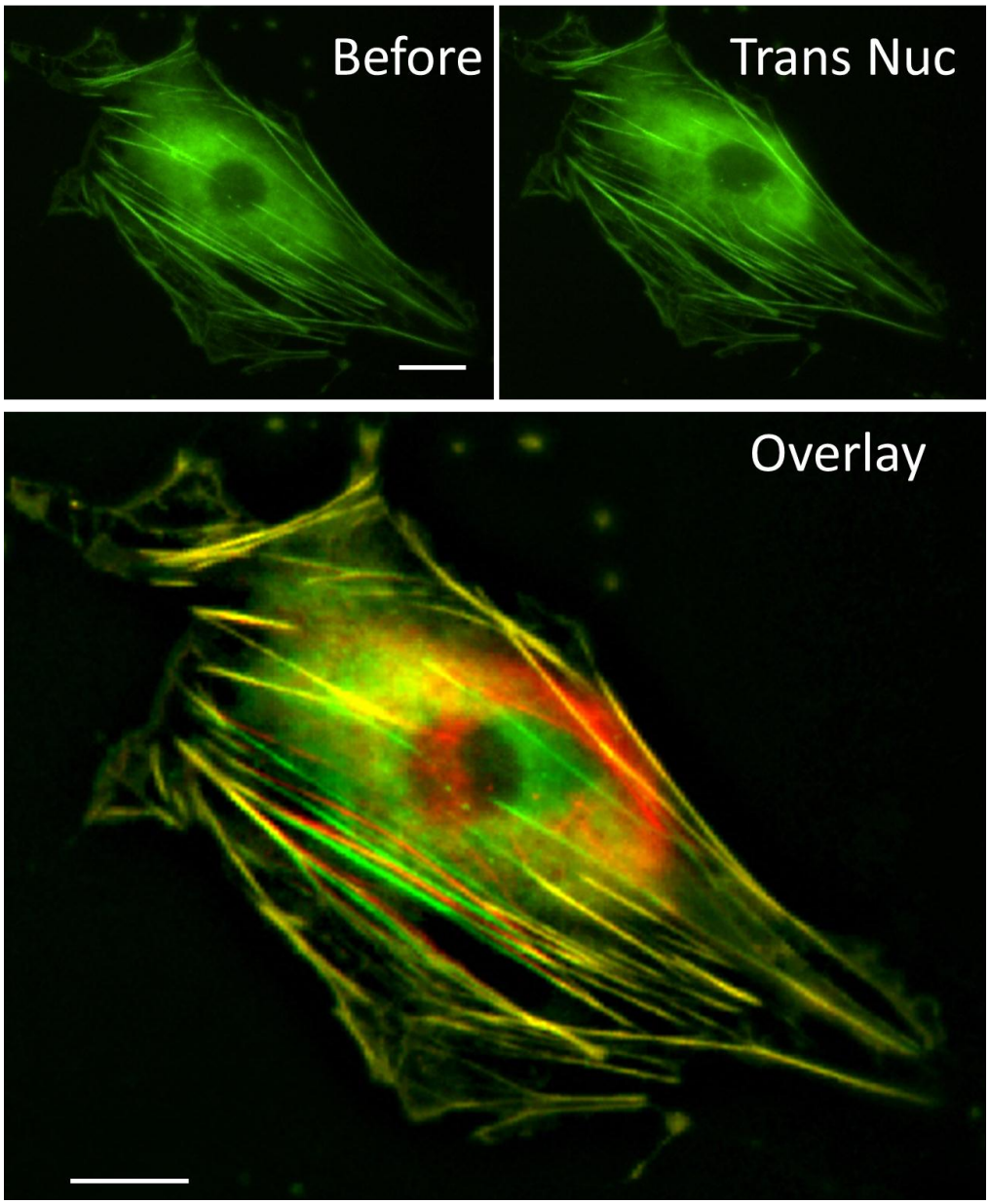

Figure 4-6. Examples of actin network deformation in response to nuclear translation. In the overlay green represents the original position and red represents the position after nuclear translation . Translation of the nucleus causes significant deformation of the nucleus, more deformation is seen from stress fibers located behind the translating nucleus. In the overlay green represents the cell before the nucleus is translated. Red represents the cells after nuclear translation. All scale bars are 10 μm

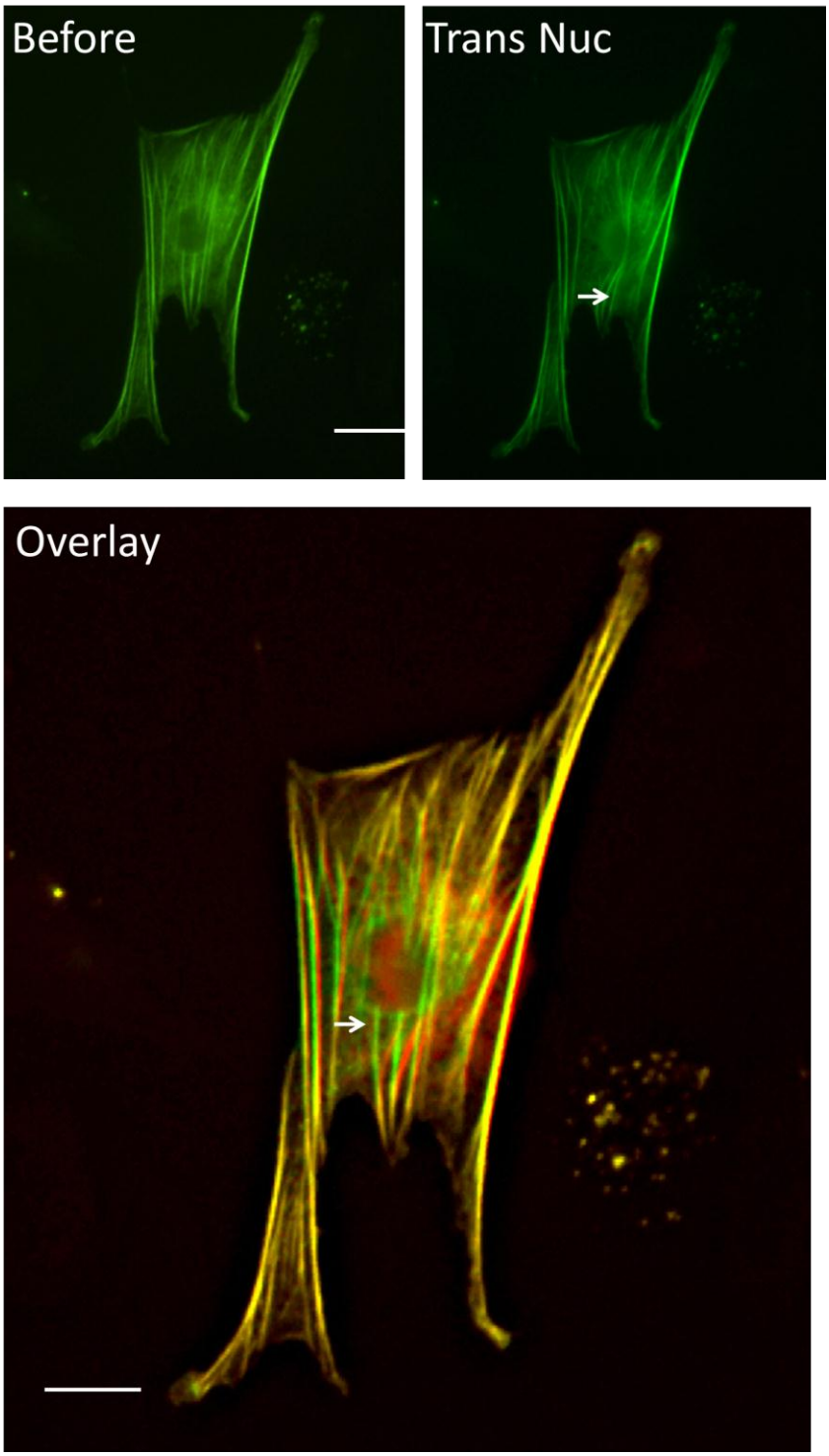

Figure 4-7. Evidence of stress fibers bound to the nuclear envelope. Some, but not all basil stress fibers appear to be directly connected to the nucleus as indicated by the arrow. In the overlay green represents the cell before the nucleus is translated. Red represents the cells after nuclear translation All scale bars are 10 µm

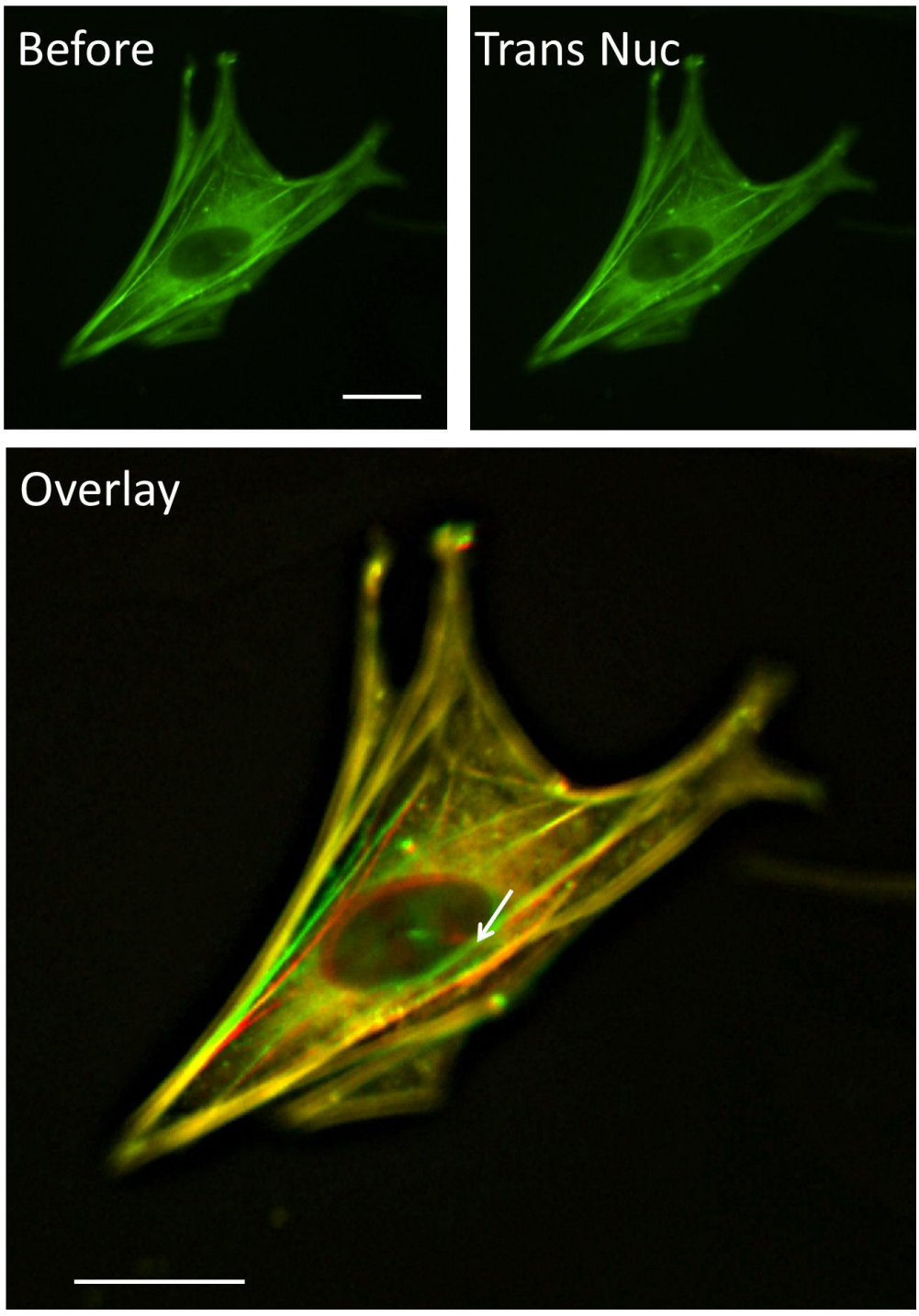

Figure 4-8. Translation of the nucleus appears to push stress fibers. Example of direct contact with the nucleus appearing to push a stress fiber (see arrow). In the overlay green represents the cell before the nucleus is translated. Red represents the cells after nuclear translation . All scale bars are 10 µm.

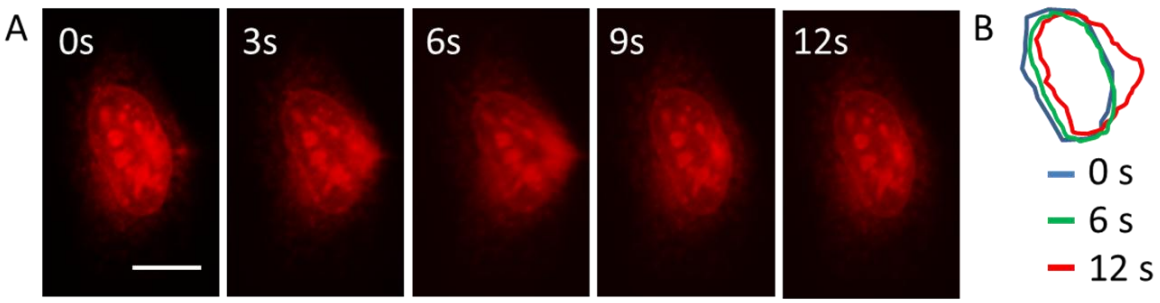

Figure 4-9. The nucleus returns to equilibrium position after perturbation. A) A micropipette was lowered until contact was made with the nucleus. A suction pressure of 200 hPa was then applied and the pipette was moved at 2.5 µm/s until the nucleus broke away from micropipette tip. The nucleus quickly recovered within 1 µm of the original equilibrium location) Overlays of nuclear shape and position at 0s 6s and 12 s. Scale bar is 5µm

CHAPTER 5
THE CONTROL OF WOUND HEALING BY MECHANICAL CUES: ROLE OF SUBSTRATE RIGIDITY

Here we used a micromanipulator to precisely translate the vertical position of a micropipette tip and removed cells without contacting the underlying gel surface. We observed a clear but modest variation in the rates of wound closure created by this method as a function of rigidity. On soft substrates, cells leading the wound closure appeared to pull trailing cells through cell-cell contacts, whereas on rigid substrates, cells moved more independently. In contrast to these collective migration results, motility of isolated NIH 3T3 fibroblasts was lowest on the soft substrates and increased with rigidity. We also developed and applied a novel assay to qualitatively compare relative magnitudes of cell-cell pulling forces relative to cell-substrate adhesion forces on different substrates. These results show that cell-cell adhesion forces dominate cell-substrate adhesion forces on soft substrates, and that cell-cell pulling forces contribute significantly to wound healing on soft substrates.

Materials and Methods

Cell Culture

NIH 3T3 fibroblasts (ATCC) were maintained in DMEM-high glucose (Cellgro) supplemented with 10% donor bovine serum (Cellgro, Manassas, VA) and maintained at 37^{o} C in a humidified 5% CO_2 environment. In wounding experiments, cells were seeded at 80% confluence on fibronectin-coated (5 µg/ml) polyacrylamide gels polymerized on glass bottomed dishes (MatTek, Ashland, MA) and were cultured to confluence. In myosin II inhibition experiments the cells were cultured for 30 minutes prior to wounding in media treated with 50 µM blebbistatin (EMD Biosciences, San Diego,Ca).

Fabrication of Polyacrylamide Gels

Polyacrylamide (PAAm) substrates were fabricated as reported elsewhere (54, 86). Four different ratios of acrylamide and bis-acrylamide (Fisher Scientific, Pittsburgh, PA), 50:1, 40:1, 20:1, and 12.5:1 were chosen to make gels with Young's modulus of 0.4 kPa, 24.5 kPa, 38.7 kPa and 308 kPa. The Young's modulus of the polyacrylamide (PAA) gels was measured with an AR-G2 rheometer (TA Instruments). Rheometer values were very close to those reported by Putnam and coworkers (52) for the 50:1, 40:1 and 20:1 crosslinked gels; the rheometer measurements were unreliable for the 12.5:1 gel. For this gel, we used a Young's modulus of 308 kPa based on experimental measurements by Putnam and coworkers(52) for the same crosslinking concentration. For bead tracking experiments, 0.5 µm FluoSpheres (Invitrogen, Eugene OR) were added in a 1:500 (vol/vol) ratio to the gel mixture prior to polymerization. For all gels, the surface was treated with 200 mM sulfo-SANPAH (Thermo Fisher Scientific, Waltham, MA) and then incubated with 5 µg/ml fibronectin (FN) overnight.

Time-Lapse Imaging of Wound Healing

After wounding, cells were imaged every 10 minutes for 12 hours on a Nikon TE2000 microscope equipped with an environmental chamber. Image J software was used to measure the area of the wound at each time interval. Average widths were calculated by measuring the area of the wound and dividing by the length of the image. Only wounds with original widths between 300µm and 600µm were measured.

Microwound Retraction Experiment

Cells monolayers were grown as described above. A femptotip needle was then lowered down to the monolayer until it made contact with the nucleus of an individual cell. The needle was then moved between 100-200 µm across the monolayer until the

targeted cell was peeled from the surface. Care was taken to ensure that no damage was done to the substrate. Once the cells were removed, the needle was quickly removed from the surface and the resulting wound was imaged every 60 seconds for 30 minutes. The area of the wound was measured using Image J software

Immunostaining

Cells were fixed with 4% paraformaldehyde (Electron Microscopy Sciences) for 20 minutes, washed with PBS (Cellgro) and then permeabilized with 0.1 % Triton X-100 in 1% BSA solution. For actin staining, cells were incubated with Alexa Fluor 594 phalloidin (Invitrogen) for 1 hour. The samples were imaged on a Nikon TE2000 epi-fluorescent microscope equipped with a 40X objective.

Cell Tracking

Individual cells were tracked using the open-source Matlab software *Time Lapse Analyzer* using the multi-target phase contrast module. To validate the results each track was visually inspected.

Results

Effect of Gel Rigidity on Wound Healing

Wounds were created using a microneedle with a 0.5 micron tip diameter mounted on a micromanipulator. The needle was lowered onto the cell monolayer until it made contact with the apical surface of a single cell. The needle was then moved across the monolayer peeling the cells off the surface but never making contact with the gel (Figure 5-1A). The needle was then repositioned to remove another strip and the process was repeated. Wound widths between 300-600 μm were created with lengths at least 5 times the width of the wound to ensure that the wound healing observed was uni-directional. To determine whether any surface patterning of ECM proteins due to the

direction of the tip motions had influenced cell migration, wounds were created using a diagonal pattern (Figure 5-2); no change in cell migration was observed.

Using the method described above, wounds were created in NIH 3T3 fibroblast monolayers cultured on polyacrylamide gels. Figure 5-1B shows representative time-lapse images of wound healing on different rigidities. On 0.4 kPa and 308 kPa substrates, the wound healing was faster than on the substrates of intermediate rigidity. Leader cells elongated (Figure 5-1B, Inset) as they crawled into the wound on the 0.4 kPa substrate resulting in 'sprouting' structures that emanated from the wound edge. During this sprouting elongation, the leading cells remained attached to trailing cells. On the most rigid material studied (308 kPa), the extent of elongation decreased compared to the 0.4 kPa substrate. Also, cells on rigid substrates appeared less attached to each other and more scattered, consistent with observations by others(87).

Analysis of Rigidity Dependent Wound Healing

To quantitatively analyze the wound healing process, we measured the time-dependent change in the width of the wound. Because the width varied along the wound front, we report an effective width, defined as the area unpopulated by cells per unit length of the wound. Shown in Figure 5-2 are representative plots of the time-dependent decrease in wound width on the different gels. There was a notable change in the initial kinetics of wound healing on the softest gel (0.4 kPa) compared to other gels (Figure 5-3 A-D). The kinetic profile on the 0.4 kPa gel appears to include an initial lag time(~2.5 hours) where there is little wound healing. On the other substrates, the lag time was absent. To compare rates across different conditions, we fit linear models to the linear region on all gels (the 0.4 kPa gel data was fit to a line after the initial lag time) to estimate the initial wound healing rate. The wound healing rate was found to be slightly

faster on the 0.4 kPa gel than on the 24 kPa gel, and was highest on the stiffest substrate. This result differed from the measured motility of isolated cells (Table 5-1) where the cell speed was clearly slowest on the soft gel and increased on more rigid substrates. Interestingly, the wound healing rate was significantly faster on the 0.4 kPa substrate than the migration speed of isolated cells on the same material (Table 5-1).

We next tracked individual cells in the monolayer. Shown in Figure 5-3C are trajectories on the different substrates. On the 0.4 kPa and 308 kPa substrates, cell trajectories appear more persistent as cells migrate into the wound. On intermediate stiffnesses, trajectories appear slightly less directionally persistent as the cells migrate into the wound. The small variations in the persistence of the trajectories may be the reason for the modest variation in wound closure rates with stiffness.

We examined the role of non-muscle myosin II in mediating the wound healing response. Blebbistatin treatment was used to specifically inhibit myosin activity. The morphologies of cells were dramatically altered in all cases on blebbistatin treatment, with cell-cell contacts decreasing significantly (Figure 5-4). On the 0.4 kPa substrate, myosin inhibition eliminated the lag time observed in the control experiment and the cells were observed to more immediately migrate into the wound (Figure 5-5). Blebbistatin treatment slowed the wound healing significantly on the softer (0.4kPa and 24 kPa) gels while leaving wound healing rates on the 39 and 308 kPa rigid substrates unchanged (Figure 5-6).

Cell-Cell forces Dominate Cell-Substrate Adhesion Forces on Soft Gels

The observation that the wounds healed faster on soft gels than single cells, and that myosin inhibition slowed wound healing on soft but not rigid gels suggested that cell-cell connections may allow cells at the edge of the monolayer to move faster on soft

materials than isolated cells. To quantify the relative magnitudes of cell-cell pulling forces versus cell-substrate adhesive forces, we removed a single cell from fibroblast monolayers and measured the effect on the monolayer. The cell was removed by contacting a nucleus within a monolayer with a micropipette tip, and moving the tip linearly between 100-200 μm(Figure 5-7A). When the cell was detached from the surface, the needle was quickly withdrawn from the monolayer. On single cell removal, the surrounding cells retracted radially from the 'microwound', with retraction reaching a steady state within 2-5 minutes on rigid substrates. Softer substrates took longer to reach a steady state (not shown).

We found a large retraction from the micro-wound on soft gels, and the extent of this initial retraction was less on more rigid substrates (Figure 5-7B). On gels with large retractions, the surrounding cell monolayer was observed to contract and move a substantial distance away from the tear location. Inhibiting myosin activity by treatment with blebbistatin eliminated this retraction(Figure 5-7B, Blebb). To determine whether the observed retraction was a retraction of the cell monolayer relative to the substrate, relaxation of the underlying substrate or a combination of both, we tracked the displacement of beads embedded in the underlying substrate following creation of the microwound., Although beads underwent displacements throughout the gel, as seen in Figure 5-7D, the individual bead displacements (<1 micron, Figure 5-7E) were much smaller than the overall retraction of the monolayer (~50 microns). We conclude that the observed retraction in the microwound was primarily due to contraction of the cell monolayer rather than relaxation of the substrate. The larger retraction on soft substrates compared to rigid substrates coupled with relatively small relaxation of the

substrate in the retraction zone again supports the conclusion that cell-cell adhesion forces dominate cell-substrate adhesive forces on soft substrates, compared to on stiff substrates.

We next examined the F-actin microstructures in NIH 3T3 fibroblast monolayers. On soft gels, isolated cells were less spread and lacked clear stress fibers, whereas cells at the edges of monolayer wounds displayed a more flattened morphology and assembled clear stress fibers (Figure 5-7F). A similar observation has been reported in (88) for clusters of two or three cells. Together, these results suggest that cells unable to transfer tension onto their substrates will instead form connections and pull on adjoining cells.

Discussion

In this paper, we modified the popular wound healing assay for studying collective cell migration on gels. We found that wound healing rates were faster than the speeds of isolated cells on the 0.4 kPa substrate. On the 0.4 kPa substrate, cell-cell pulling resulted in flattened cell morphologies with clear stress fibers (Figure 5-7F). On more rigid substrates, isolated cells were able to spread and therefore migrate better, but the wound healed more slowly because individual cells could not migrate easily due to cell crowding. This conclusion is supported by the observation that blebbistatin treatment reduced the wound healing rates of the cells on only the softer (0.4 and 24 kPa) substrates, consistent with the results in (89). Thus, crawling of cells at the wound edge and consequent wound healing on the softer substrates depends more on the transmission of contractile forces between cells. This mechanism is absent for isolated cells, which can explain the more pronounced reduction of speed of isolated cells on soft gels.

There are at least two possible explanations for our paradoxical observation that cells were unable to spread and migrate when isolated on the softest material but could nevertheless spread, generate traction when at the wound edge and crawl faster than isolated cells. One possibility is that cells at the wound edge are under contact inhibition of motility along their rear edges in contact with neighboring cells. This may allow the cell to focus its motile machinery (actin assembly, formation of adhesions, and actomyosin contraction) in order to generate a stronger leading edge in the direction devoid of cells (i.e. in the direction of wound closure). A second possibility is that the cells in the retracted monolayer collectively exert traction and strain the substrate at the wound edge. This strain locally stiffens the substrate which enables cells at the wound edge to crawl inward. This strain stiffening can possibly eliminate large deformations of the soft substrates that prevent motility of isolated cells (it is well known that isolated cells cannot crawl on soft substrates ((52-54, 86)and Table 1). The strain-stiffened substrate could thus enable cells at the wound edge to form stable adhesions and lamellipodia. This possibility is supported by our observation of radial strain due to retraction of the monolayer in the microwound experiments (Figure 5-6).

Our results are important because we show that wound healing is fundamentally different on soft materials. It is now well-appreciated that soft materials are better mimics of physiological microenvironments than hard materials. The relative insensitivity of collective cell migration to substrate rigidity raises the interesting possibility that cell-cell contacts may promote migration in soft physiological environments that do not otherwise support single cell motility.

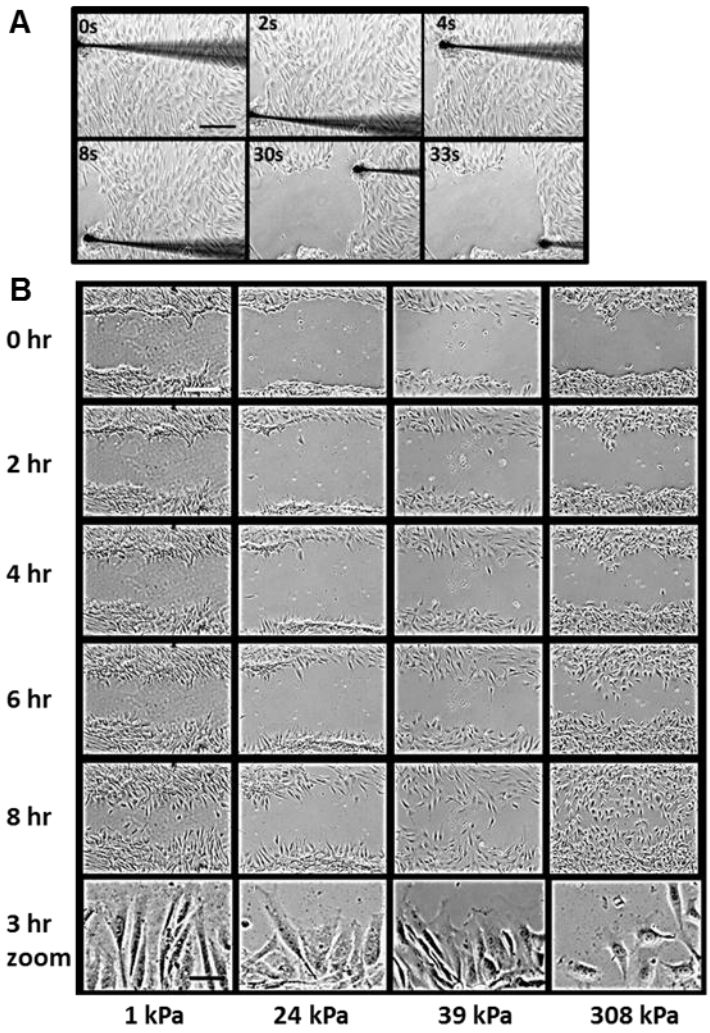

Figure 5-1. Substrate rigidity alters wound healing rates. A) Wounds were created on polyacrylamide substrates using a microinjection needle to remove cells without damaging the substrate. Scale bar =100 µm B) Wounds healing rates were higher on soft and rigid substrates but slowed on substrates with intermediate stiffness. On soft and intermediate substrates cells at the leading edge remain connected to each other unlike cells on the stiffest substrates which migrate more individually. Scale bar =100 µm, Zoom scale bar 20 µm

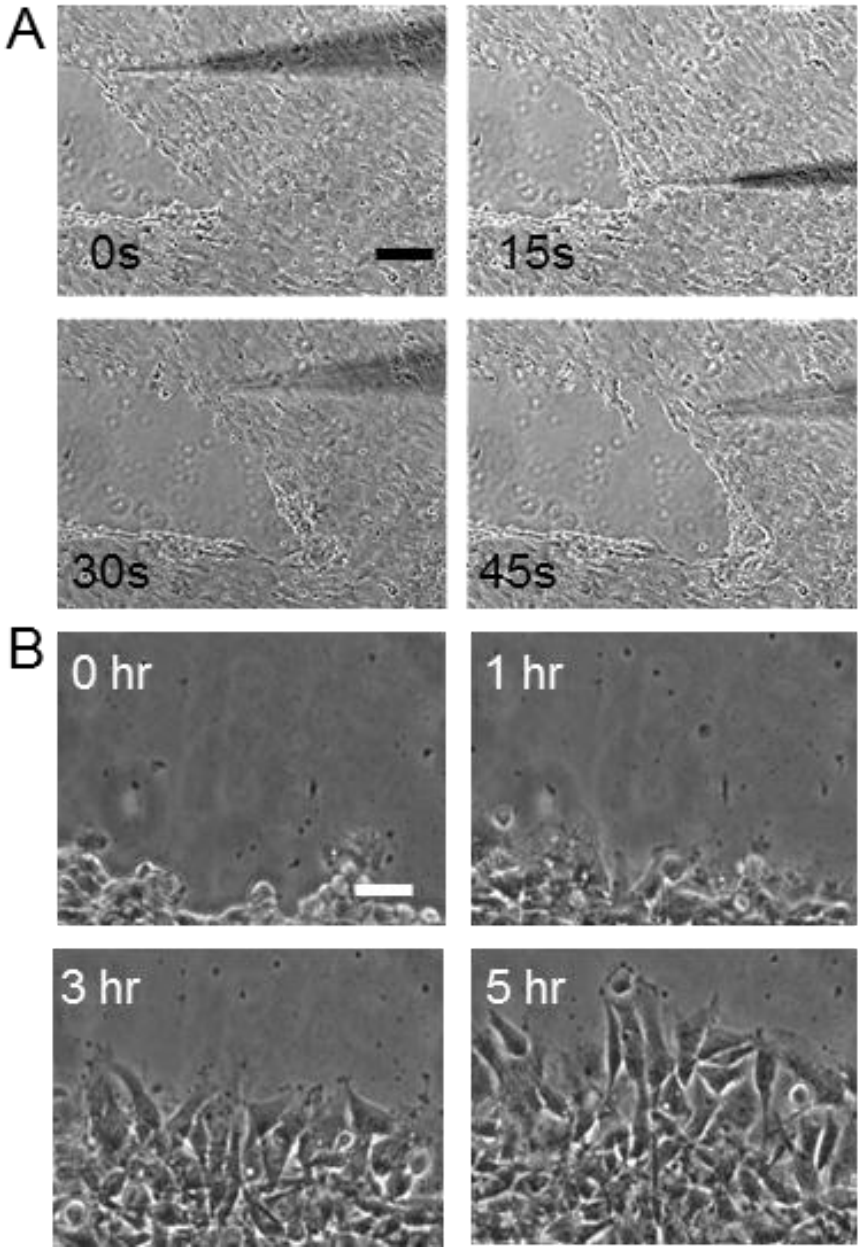

Figure 5-2**.** Micropipette wounding direction does not alter wound healing. A) Cell monolayers were wounded by moving the micropipette in a diagonal direction (as opposed to perpendicular) B) No differences in wound healing were seen.

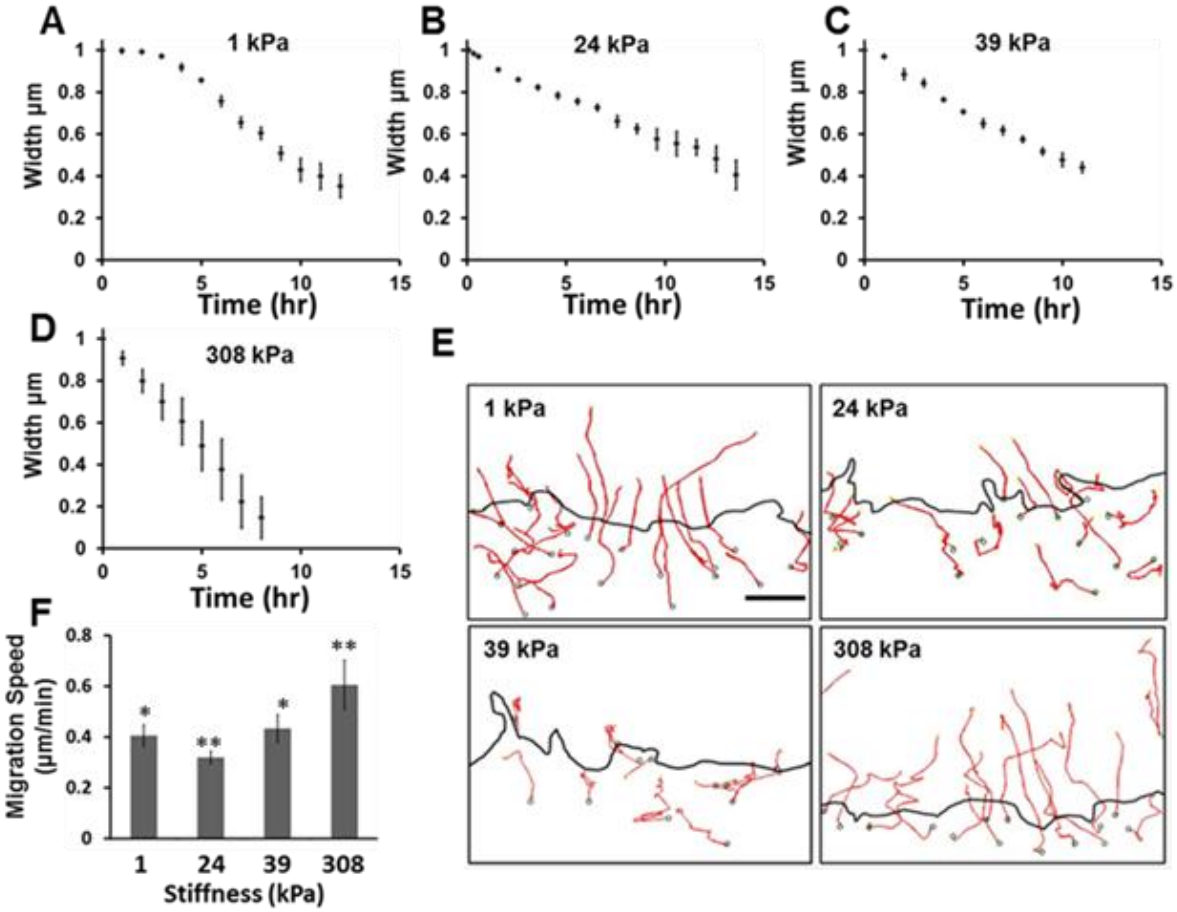

Figure 5-3. Quantification of wound healing profile. A-D) Cells on 1 kPa had an initial time lag not seen on more rigid substrates. E) Individual cell tracking reveals that cells on 0.4 kPa and 396 kPa took more direct routes into the wound the cells on the intermediate substrates. Scale bar =50 µm F) A biphasic profile was seen for wound healing rates as the substrate rigidity was increased from 0.4 kPa to 308 kPa,

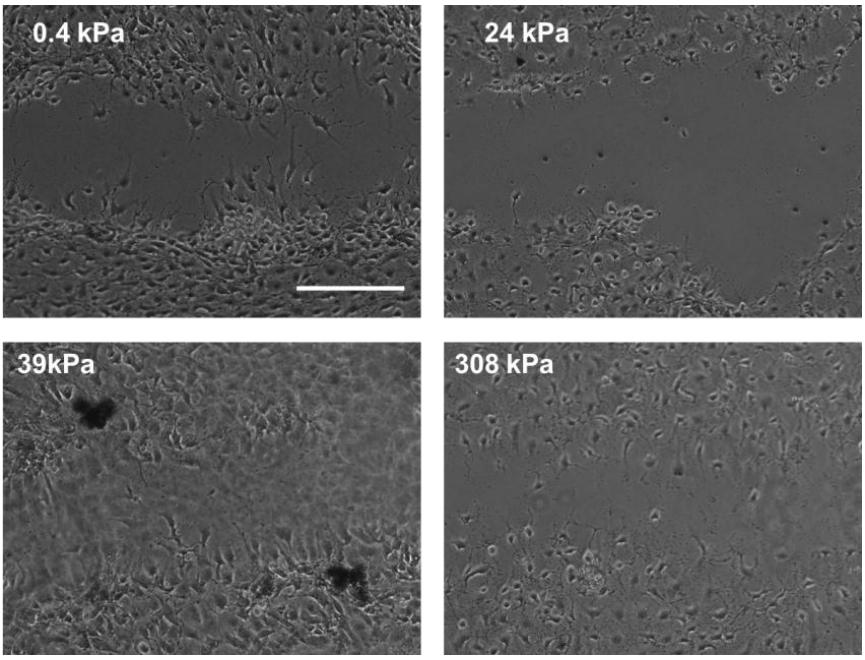

Figure 5-4. Myosin inhibition results dramatic change in cell morphology and decreases cell-cell contact. Cells treated with 50 μM blebbistatin immediately after wounding resulted in a change in cell shape on all substrate rigidities. Cells appeared to migrate more individually and cells on the leading edge broke away from the monolayer on all substrates.

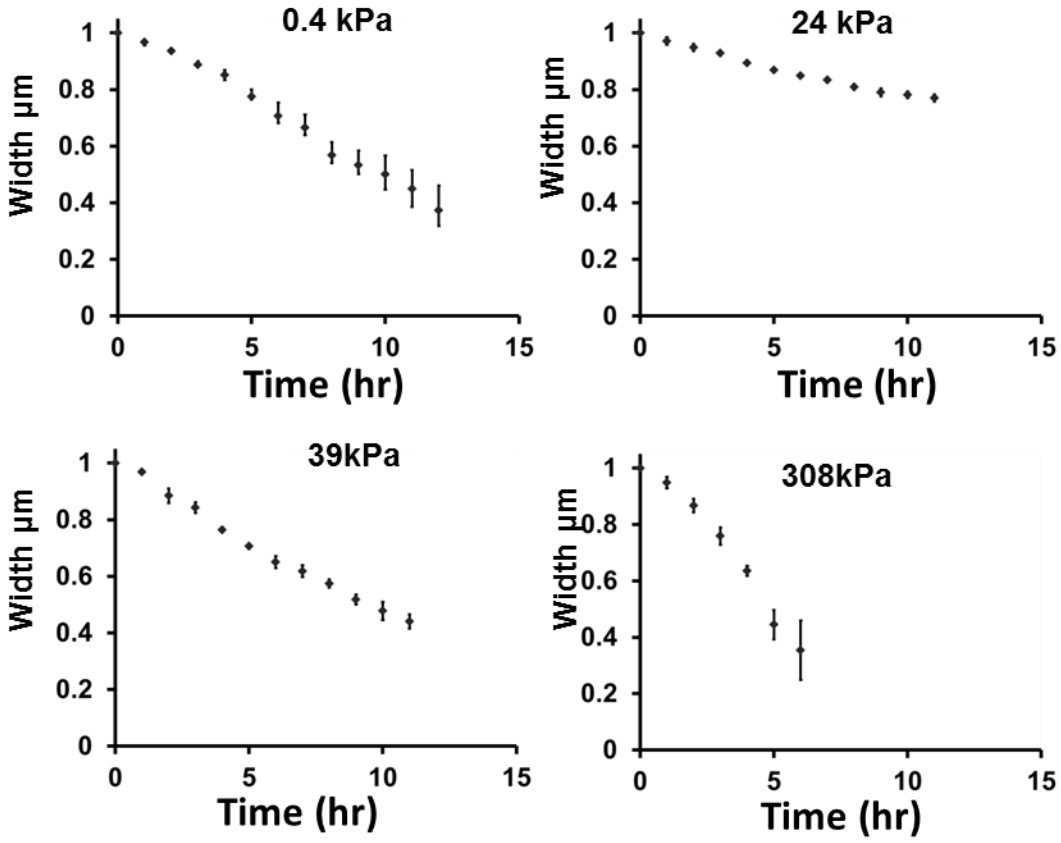

Figure 5-5. Myosin inhibition changes wound healing profiles. On 0.4 kPa the lag time previously seen in control cells was eliminated.

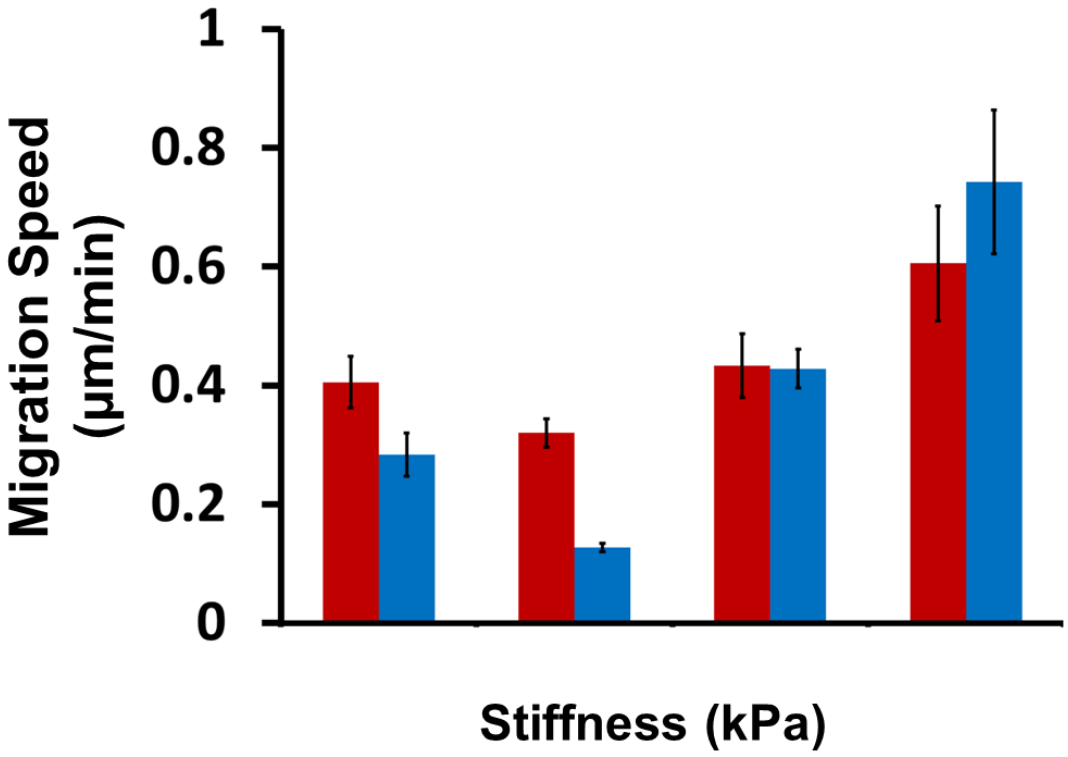

Figure 5-6. Myosin inhibition alters wound healing migration speed. Error bars are SEM.

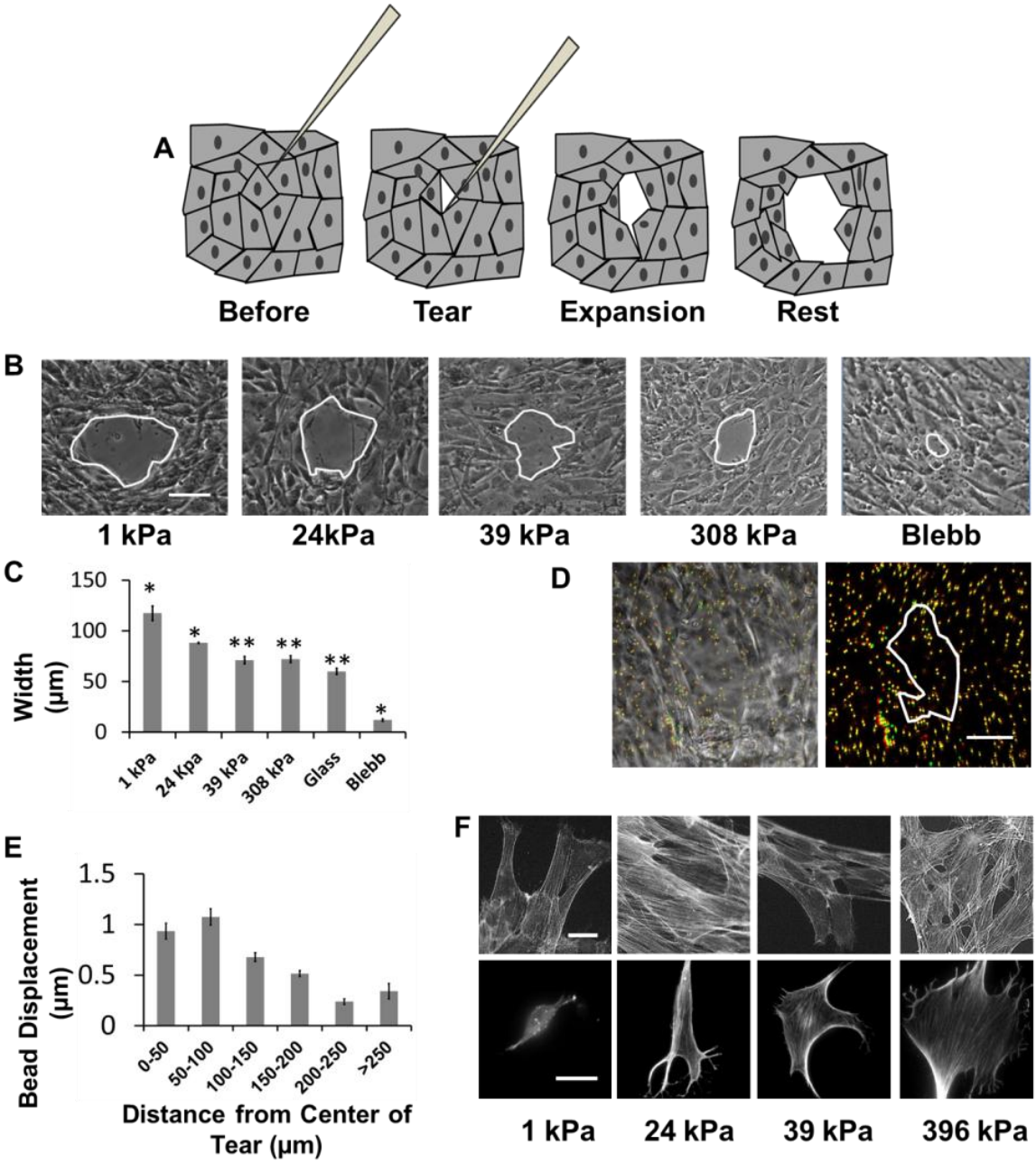

Figure 5-7. Initial wound retraction increases as substrates rigidity is decreased. A) Wounds were created by making contact with a nucleus within the monolayer with a microinjection pipette. The pipette was then translated 100-200 µm until the targeted cell was removed from the nucleus. B) Wounds retracted more as the softer substrate rigidity was decreased. Treatment with the myosin II inhibitor blebbistatin greatly hindered the retraction. C) Quantification of retraction width results in significantly different widths on substrates of different stiffness's. D) Bead tracking reveals that the gel relaxed beyond the edges of the expanded wound. E) Quantification of bead

displacement shows that most of the displacement occurred just past the wound edge. F) Stress fibers are clearly present on soft substrates in cells that are bound to other cells but are not present in individual cells on soft substrates

Table 5-1. Average migration rate of wound edge and individual cells.

Stiffness	1kpa	24.5 kPa	39 kPa	308 kPa
Single Cell Speed (μm/min)	0.18 ±0.02	0.76 ±0.22	0.89±0.11	1.17±0.13
Wound Healing Rate (μm/min)	0.21 ±0.04	0.16±0.02	0.89±0.05	0.31±0.10

CHAPTER 6
CONCLUSIONS

Summary of Findings

The LINC Complex Is Required For Normal Cell Function

Endothelial cell polarization and directional migration is required for angiogenesis. Polarization and motility requires not only local cytoskeletal remodeling but also the motion of intracellular organelles such as the nucleus. However, the physiological significance of nuclear positioning in the endothelial cell has remained largely unexplored. Here, we show that siRNA knockdown of nesprin-1, a protein present in the LINC complex (Linker of Nucleus to Cytoskeleton), abolished the reorientation of endothelial cells in response to cyclic strain. Confocal imaging revealed that the nuclear height is substantially increased in nesprin-1 depleted cells, similar to myosin inhibited cells. Nesprin-1 depletion increased the number of focal adhesions and substrate traction while decreasing the speed of cell migration; however, there was no detectable change in non-muscle myosin II activity in nesprin-1 deficient cells. Together, these results are consistent with a model in which the nucleus balances a portion of the actomyosin tension in the cell. In the absence of nesprin-1, actomyosin tension is balanced by the substrate, leading to abnormal adhesion, migration and cyclic strain induced reorientation

The Nucleus is In a Tug of War Between Actomyosin Pulling Forces in a Crawling Fibroblast

On cellular length scales, the nucleus is massive (~10-15 microns in diameter) and stiff relative to the cytoplasm. Motion of such a large object in the crowded intracellular space requires a significant expenditure of energy and represents a significant task for the motile cell. In Chapter 3, we show that the nucleus in a single, polarized crawling

NIH 3T3 fibroblast is pulled forward toward the leading edge. The pulling forces originate from actomyosin contraction between the leading edge and the nuclear surface; these forces are opposed by actomyosin pulling in the trailing edge. Microtubules serve to damp fluctuations in nuclear position, but are not required for directional nuclear motion. Disrupting nuclear-cytoskeletal linkage causes a disruption of forward nuclear motion and a decrease in the frequency of trailing edge detachment. Our results indicate that the nucleus is under net tension in a crawling cell due to a balance between actomyosin pulling from the front and back of the crawling cell.

A Novel Micropipette Aspiration Technique to Apply Forces to the Nucleus

We have developed a technique to exert measurable forces on the nucleus with a capillary under vacuum. This technique is capable detecting changes in nuclear-cytoskeletal coupling, has shown that nuclear translation deforms the surrounding actin cytoskeleton, and is precise enough to slightly perturb the location of nuclei of living cells. Combining this method with cytoskeleton altering drugs or treatments will allow the estimation of the contributions of intermediate, microfilament and actin cytoskeletons in restoring the nucleus to its central position. The flexibility of this technique will allow it to be of great use in future research on the nucleo-cytoskeleton force balance

The Control of Wound Healing by Mechanical Cues: Role of Substrate Rigidity

The function of adhesion-dependent cells is remarkably sensitive to the rigidity of the extracellular matrix. For example, the crawling of isolated NIH 3T3 fibroblasts is very different on soft substrates compared to rigid substrates. The effect of rigidity on collective cell migration is less clear owing to the lack of suitable methods for reliably measuring collective cell migration on soft gels. We modified the traditional scratch-

wound healing assay by using a micropipette to create wounds in fibroblast monolayers without damaging the underlying soft substrates. In contrast to single-cell speeds which were a strong function of rigidity, wound healing rates depended only modestly on the rigidity of the substrate. Wound healing rates were high on both soft and rigid substrates and low at intermediate rigidities. F-actin staining revealed that cells in confluent monolayers assembled stress fibers and had spread morphology even on soft substrates unlike their single cell counterparts. We developed a novel assay in which retraction in the monolayer was measured followed removal of a single cell. By tracking gel-embedded beads to quantify substrate relaxation, we found that cell-cell pulling forces dominated cell-substrate adhesion forces on soft materials consistent with the presence of stress fibers and flattened morphologies on soft substrates. We discuss contact inhibition at the wound edge and/or strain stiffening of the substrate as possible explanations for why wounds can heal on soft substrates. The relative insensitivity of collective cell migration to substrate rigidity raises the possibility that cell-cell contacts may promote migration in soft physiological environments that do not otherwise support single cell motility.

Future Work

Nuclear Stabilizing Forces

In chapter 4 we introduced a technique which makes it possible to apply external forces on the nucleus of a living cell. While all three cytoskeletal elements are connected to the nuclear surfaces, their relative contributions to the nuclear centering process are not yet known. Quantifying the nuclear centering forces in an experiment like in Figure 4-9 in cells with disrupted cytoskeletal elements (through drug treatments or siRNA knockdown) can allow the estimation of the relative contribution of individual

cytoskeletal elements to forces on the nuclear surface. Combining traction force microscopy with nuclear translation could feasibly be done by perturbing nuclei in cells which have been cultured soft substrates. Tracking beads in the substrate would reveal how forces on the nucleus are dispersed throughout the cell.

Nuclear Positioning in Monolayers

In collective cell migration cells mechanically communicate with each other over long distances (90). In figure 5-6 we observed an increase in wound retraction when “microwounds” were created on soft substrates. As cells on soft substrates are under considerable actomyosin tensile stresses from their neighboring cells, and since the nucleus is under actomyosin tension, it is possible that the nucleus balances cell-cell tensile forces. By balancing part of the cell-cell tension, the nucleus may play a key role in collective cell migration. Would the perturbation of the nucleus of a cell within a monolayer on a soft substrate alter the positioning of nuclei in surrounding cells? These questions could be answered by using the techniques described in chapter 4 and 5.

The Effects of Nuclear Tension on the Nuclear Pore Complex

The nuclear pore complex (NPC) connects the inner and outer nuclear membranes and is the only pathway for macromolecules to enter or exit the nucleus. Macromolecules with mass less then 40-70 kDa may diffuse across the nuclear envelope while larger macromolecules may only cross the nuclear pore through facilitated diffusion. Facilitated diffusion of proteins across the pore requires the presence of a nuclear localization signal or a nuclear export signal and is dependent on a RANGTP gradient. The NPC exists within the nuclear envelope and interacts with LINC complex proteins(91). HELA cells deficient in SUN1 have clustered NPC’s(91). Cell adhesion and the cytoskeleton are known to play a role in nuclear transport (92).

For example, MAP kinase nucleo-cytoplasmic distribution is differentially dependent on cell adhesion(93) and extracellular signal-regulated kinases are unable to localize to the nucleus in suspended cells (94) . Cyclic stretching of smooth muscle cells results in increased nuclear import(95).An intact microtubule network is necessary for optimal nuclear localization of tumor suppressor proteins Rb, P53 and PTHrP(96). Nuclear actin and myosin are able to alter nuclear pore porosity of dextrans in isolated nuclei(97). The f-actin network has also been shown to alter nuclear transport rates due to the impact of the f-actin cytoskeleton on the RAN-GTP/RAN-GDP gradient(98). Little is known about how the LINC complex proteins and the nuclear-cytoskeletal force balance influence nuclear transport.

One of the challenges in studying nuclear pore transport is that it is difficult to accurately estimate values of nuclear volume, cytoplasmic volume, nuclear envelope thickness, the number of nuclear pores in live cells. FRAP experiments could be performed simultaneously such that the ratio of the time constants can be measured. The resulting ratio eliminates the previous parameters and is equal to the ratio of the diffusivities of the probe. Using this technique in conjunction with current diffusion models the effect of acto-myosin forces on passive or facilitated nuclear transport could be investigated.

The Function of Nesprin-2

Our results in chapter 2 are that in the absence of nesprin-1, endothelial cells assemble more adhesions, exert greater traction on the surface, have increased nuclear heights and have decreased migration speeds. To explain these results we constructed a model in which the structure of the actin cytoskeleton was significantly altered resulting in less tension being exerted on the nucleus. However nesprin-2 also contains

an actin binding domain and was found to be present in our cell line. If nesprin-1 and nesprin-2's functions were redundant then we would not expect such drastic changes in cell behavior when only nesprin-1 was removed. Therefore it is likely that nesprin-2 interacts with the actin cytoskeleton in a unique manner. Using the techniques described in chapters 2 and 4 the function of nesprin-2 could be studied. These results would help to distinguish the functions of nesprin 1 and nesprin-2 which would lead to a greater understanding of how actomyosin forces are transmitted to the nucleus.

The Effects of 3D Cell Culture on Cell Behavior

All the experiments in this work have been conducted in a 2D environment with cells cultured on glass or soft substrates. While some cell types like endothelial cells do exist in flat monolayers, the majority of cell types exist in a 3D matrix in-vivo. Often behaviors observed in 2D in-vitro experiments are not seen in cells in-vivo(99). However nuclear shape has been shown to be changed by external forces in cells within tissues(100) .Cell migration rates in 3D culture are sensitive to the rigidity of the surrounding matrix (101, 102). Cells cultured in 3D have to manipulate through the structure and the nucleus must be able to be manipulated past impeding structures(55). Recently it has been shown that chromatin, which is partly organized through connections with the lamin network(103),must be compressed for cells to migrate through filters with diameters of 3-8μm (104, 105). The LINC complex may act as a mechanical linkage between the cytoskeleton and chromatin within the nucleus. Combining the techniques used in this work to alter nucleo-cytoskeleton force balance, such as siRNA knockdown of LINC complex proteins, with 3D-cell culture would allow us to study nuclear mechanics and cell migration in a more lifelike environment.

LIST OF REFERENCES

1. Huang, S., and D. E. Ingber. 1999. The structural and mechanical complexity of cell-growth control. Nat Cell Biol 1:E131-138.

2. Lauffenburger, D. A., and A. F. Horwitz. 1996. Cell migration: a physically integrated molecular process. Cell 84:359-369.

3. Ferrara, N., H. P. Gerber, and J. LeCouter. 2003. The biology of VEGF and its receptors. Nat Med 9:669-676.

4. Starr, D. A. 2009. A nuclear-envelope bridge positions nuclei and moves chromosomes. J Cell Sci 122:577-586.

5. Hale, C. M., A. L. Shrestha, S. B. Khatau, P. J. Stewart-Hutchinson, L. Hernandez, C. L. Stewart, D. Hodzic, and D. Wirtz. 2008. Dysfunctional connections between the nucleus and the actin and microtubule networks in laminopathic models. Biophys J 95:5462-5475.

6. Lammerding, J., P. C. Schulze, T. Takahashi, S. Kozlov, T. Sullivan, R. D. Kamm, C. L. Stewart, and R. T. Lee. 2004. Lamin A/C deficiency causes defective nuclear mechanics and mechanotransduction. J Clin Invest 113:370-378.

7. Lee, J. S., C. M. Hale, P. Panorchan, S. B. Khatau, J. P. George, Y. Tseng, C. L. Stewart, D. Hodzic, and D. Wirtz. 2007. Nuclear lamin A/C deficiency induces defects in cell mechanics, polarization, and migration. Biophys J 93:2542-2552.

8. Haque, F., D. J. Lloyd, D. T. Smallwood, C. L. Dent, C. M. Shanahan, A. M. Fry, R. C. Trembath, and S. Shackleton. 2006. SUN1 interacts with nuclear lamin A and cytoplasmic nesprins to provide a physical connection between the nuclear lamina and the cytoskeleton. Mol Cell Biol 26:3738-3751.

9. Worman, H. J., and G. G. Gundersen. 2006. Here come the SUNs: a nucleocytoskeletal missing link. Trends Cell Biol 16:67-69.

10. Padmakumar, V. C., T. Libotte, W. Lu, H. Zaim, S. Abraham, A. A. Noegel, J. Gotzmann, R. Foisner, and I. Karakesisoglou. 2005. The inner nuclear membrane protein Sun1 mediates the anchorage of Nesprin-2 to the nuclear envelope. J Cell Sci 118:3419-3430.

11. Starr, D. A., and M. Han. 2002. Role of ANC-1 in tethering nuclei to the actin cytoskeleton. Science 298:406-409.

12. Lammerding, J., J. Hsiao, P. C. Schulze, S. Kozlov, C. L. Stewart, and R. T. Lee. 2005. Abnormal nuclear shape and impaired mechanotransduction in emerin-deficient cells. J Cell Biol 170:781-791.

13. Zhang, Q., C. Bethmann, N. F. Worth, J. D. Davies, C. Wasner, A. Feuer, C. D. Ragnauth, Q. Yi, J. A. Mellad, D. T. Warren, M. A. Wheeler, J. A. Ellis, J. N. Skepper, M. Vorgerd, B. Schlotter-Weigel, P. L. Weissberg, R. G. Roberts, M. Wehnert, and C. M. Shanahan. 2007. Nesprin-1 and -2 are involved in the pathogenesis of Emery Dreifuss muscular dystrophy and are critical for nuclear envelope integrity. Hum Mol Genet 16:2816-2833.

14. Mislow, J. M., J. M. Holaska, M. S. Kim, K. K. Lee, M. Segura-Totten, K. L. Wilson, and E. M. McNally. 2002. Nesprin-1alpha self-associates and binds directly to emerin and lamin A in vitro. FEBS Lett 525:135-140.

15. Roux, K. J., M. L. Crisp, Q. Liu, D. Kim, S. Kozlov, C. L. Stewart, and B. Burke. 2009. Nesprin 4 is an outer nuclear membrane protein that can induce kinesin-mediated cell polarization. Proc Natl Acad Sci U S A 106:2194-2199.

16. Zhang, X., R. Xu, B. Zhu, X. Yang, X. Ding, S. Duan, T. Xu, Y. Zhuang, and M. Han. 2007. Syne-1 and Syne-2 play crucial roles in myonuclear anchorage and motor neuron innervation. Development 134:901-908.

17. Broers, J. L., E. A. Peeters, H. J. Kuijpers, J. Endert, C. V. Bouten, C. W. Oomens, F. P. Baaijens, and F. C. Ramaekers. 2004. Decreased mechanical stiffness in LMNA-/- cells is caused by defective nucleo-cytoskeletal integrity: implications for the development of laminopathies. Hum Mol Genet 13:2567-2580.

18. Stewart-Hutchinson, P. J., C. M. Hale, D. Wirtz, and D. Hodzic. 2008. Structural requirements for the assembly of LINC complexes and their function in cellular mechanical stiffness. Exp Cell Res 314:1892-1905.

19. Zhang, Q., C. Ragnauth, M. J. Greener, C. M. Shanahan, and R. G. Roberts. 2002. The nesprins are giant actin-binding proteins, orthologous to Drosophila melanogaster muscle protein MSP-300. Genomics 80:473-481.

20. Crisp, M., Q. Liu, K. Roux, J. B. Rattner, C. Shanahan, B. Burke, P. D. Stahl, and D. Hodzic. 2006. Coupling of the nucleus and cytoplasm: role of the LINC complex. In J Cell Biol. 41-53.

21. Zhang, Q., J. N. Skepper, F. Yang, J. D. Davies, L. Hegyi, R. G. Roberts, P. L. Weissberg, J. A. Ellis, and C. M. Shanahan. 2001. Nesprins: a novel family of spectrin-repeat-containing proteins that localize to the nuclear membrane in multiple tissues. J Cell Sci 114:4485-4498.

22. Dahl, K. N., A. J. Ribeiro, and J. Lammerding. 2008. Nuclear shape, mechanics, and mechanotransduction. Circ Res 102:1307-1318.

23. Starr, D. A. 2011. Watching nuclei move: Insights into how kinesin-1 and dynein function together. Bioarchitecture 1:9-13.

24. Friedl, P., K. Wolf, and J. Lammerding. 2011. Nuclear mechanics during cell migration. Curr Opin Cell Biol 23:55-64.

25. Levy, J. R., and E. L. Holzbaur. 2008. Dynein drives nuclear rotation during forward progression of motile fibroblasts. J Cell Sci 121:3187-3195.

26. Wu, J., K. C. Lee, R. B. Dickinson, and T. P. Lele. 2011. How dynein and microtubules rotate the nucleus. J Cell Physiol 226:2666-2674.

27. Tsai, J. W., K. H. Bremner, and R. B. Vallee. 2007. Dual subcellular roles for LIS1 and dynein in radial neuronal migration in live brain tissue. Nat Neurosci 10:970-979.

28. Folker, E. S., C. Ostlund, G. W. Luxton, H. J. Worman, and G. G. Gundersen. 2011. Lamin A variants that cause striated muscle disease are defective in anchoring transmembrane actin-associated nuclear lines for nuclear movement. Proc Natl Acad Sci U S A 108:131-136.

29. Luxton, G. W., E. R. Gomes, E. S. Folker, E. Vintinner, and G. G. Gundersen. 2010. Linear arrays of nuclear envelope proteins harness retrograde actin flow for nuclear movement. Science 329:956-959.

30. Gomes, E. R., S. Jani, and G. G. Gundersen. 2005. Nuclear movement regulated by Cdc42, MRCK, myosin, and actin flow establishes MTOC polarization in migrating cells. Cell 121:451-463.

31. Martini, F. J., and M. Valdeolmillos. 2010. Actomyosin contraction at the cell rear drives nuclear translocation in migrating cortical interneurons. J Neurosci 30:8660-8670.

32. Chancellor, T. J., J. Lee, C. K. Thodeti, and T. Lele. 2010. Actomyosin tension exerted on the nucleus through nesprin-1 connections influences endothelial cell adhesion, migration, and cyclic strain-induced reorientation. Biophys J 99:115-123.

33. Sims, J. R., S. Karp, and D. E. Ingber. 1992. Altering the cellular mechanical force balance results in integrated changes in cell, cytoskeletal and nuclear shape. J Cell Sci 103 (Pt 4):1215-1222.

34. Maniotis, A. J., C. S. Chen, and D. E. Ingber. 1997. Demonstration of mechanical connections between integrins, cytoskeletal filaments, and nucleoplasm that stabilize nuclear structure. Proc Natl Acad Sci U S A 94:849-854.

35. Buxboim, A., I. L. Ivanovska, and D. E. Discher. 2010. Matrix elasticity, cytoskeletal forces and physics of the nucleus: how deeply do cells 'feel' outside and in? J Cell Sci 123:297-308.

36. Wu, Y. I., D. Frey, O. I. Lungu, A. Jaehrig, I. Schlichting, B. Kuhlman, and K. M. Hahn. 2009. A genetically encoded photoactivatable Rac controls the motility of living cells. Nature 461:104-108.

37. Lammerding, J., and R. T. Lee. 2009. Mechanical properties of interphase nuclei probed by cellular strain application. Methods in Molecular Biology (Clifton, N.J.) 464:13-26.

38. Lammerding, J., K. N. Dahl, D. E. Discher, and R. D. Kamm. 2007. Nuclear Mechanics and Methods. In Cell Mechanics. W. Yu-Li, and E. D. Dennis, editors. Academic Press. 269-294.

39. de Vries, A. H., B. E. Krenn, R. van Driel, V. Subramaniam, and J. S. Kanger. 2007. Direct observation of nanomechanical properties of chromatin in living cells. Nano Lett 7:1424-1427.

40. Fabry, B., G. N. Maksym, J. P. Butler, M. Glogauer, D. Navajas, and J. J. Fredberg. 2001. Scaling the microrheology of living cells. Phys Rev Lett 87:148102.

41. de Vries, A. H. B., B. E. Krenn, R. van Driel, V. Subramaniam, and J. S. Kanger. 2007. Direct observation of nanomechanical properties of chromatin in living cells. Nano Letters 7:1424-1427.

42. Celedon, A., C. M. Hale, and D. Wirtz. 2011. Magnetic manipulation of nanorods in the nucleus of living cells. Biophysical Journal 101:1880-1886.

43. Kishino, A., and T. Yanagida. 1988. Force measurements by micromanipulation of a single actin filament by glass needles. Nature 334:74-76.

44. Felder, S., and E. L. Elson. 1990. Mechanics of fibroblast locomotion: quantitative analysis of forces and motions at the leading lamellas of fibroblasts. The Journal of cell biology 111:2513-2526.

45. Maniotis, A. J., C. S. Chen, and D. E. Ingber. 1997. Demonstration of mechanical connections between integrins, cytoskeletal filaments, and nucleoplasm that stabilize nuclear structure. Proceedings of the National Academy of Sciences of the United States of America 94:849-854.

46. Discher, D. E., P. Janmey, and Y. L. Wang. 2005. Tissue cells feel and respond to the stiffness of their substrate. Science 310:1139-1143.

47. Leipzig, N. D., and M. S. Shoichet. 2009. The effect of substrate stiffness on adult neural stem cell behavior. Biomaterials 30:6867-6878.

48. Flanagan, L. A., Y. E. Ju, B. Marg, M. Osterfield, and P. A. Janmey. 2002. Neurite branching on deformable substrates. Neuroreport 13:2411-2415.

49. Khatiwala, C. B., S. R. Peyton, and A. J. Putnam. 2006. Intrinsic mechanical properties of the extracellular matrix affect the behavior of pre-osteoblastic MC3T3-E1 cells. American journal of physiology. Cell physiology 290:C1640-1650.

50. Engler, A., L. Bacakova, C. Newman, A. Hategan, M. Griffin, and D. Discher. 2004. Substrate compliance versus ligand density in cell on gel responses. Biophys J 86:617-628.

51. Reilly, G. C., and A. J. Engler. 2010. Intrinsic extracellular matrix properties regulate stem cell differentiation. Journal of biomechanics 43:55-62.

52. Peyton, S. R., and A. J. Putnam. 2005. Extracellular matrix rigidity governs smooth muscle cell motility in a biphasic fashion. J Cell Physiol 204:198-209.

53. Stroka, K. M., and H. Aranda-Espinoza. 2009. Neutrophils display biphasic relationship between migration and substrate stiffness. Cell Motil Cytoskeleton 66:328-341.

54. Pelham, R. J., Jr., and Y. Wang. 1997. Cell locomotion and focal adhesions are regulated by substrate flexibility. Proc Natl Acad Sci U S A 94:13661-13665.

55. Zaman, M. H., L. M. Trapani, A. L. Sieminski, D. Mackellar, H. Gong, R. D. Kamm, A. Wells, D. A. Lauffenburger, and P. Matsudaira. 2006. Migration of tumor cells in 3D matrices is governed by matrix stiffness along with cell-matrix adhesion and proteolysis. Proc Natl Acad Sci U S A 103:10889-10894.

56. Kumar, S., and V. M. Weaver. 2009. Mechanics, malignancy, and metastasis: the force journey of a tumor cell. Cancer Metastasis Rev 28:113-127.

57. Hadjipanayi, E., V. Mudera, and R. A. Brown. 2009. Guiding cell migration in 3D: a collagen matrix with graded directional stiffness. Cell Motil Cytoskeleton 66:121-128.

58. Angelini, T. E., E. Hannezo, X. Trepat, M. Marquez, J. J. Fredberg, and D. A. Weitz. Glass-like dynamics of collective cell migration. Proc Natl Acad Sci U S A 108:4714-4719.

59. Xavier Trepat, M. R. W., Thomas E. Angelini, Emil Millet, David A. Weitz, James P. Butler, Jeffrey J. Fredberg. 2009. Physical forces during collective cell migration. Nature Physics 5:426 - 430.

60. Ganz, A., M. Lambert, A. Saez, P. Silberzan, A. Buguin, R. M. Mège, and B. Ladoux. 2006. Traction forces exerted through N-cadherin contacts. Biol Cell 98:721-730.

61. Rorth, P. 2009. Collective cell migration. Annual review of cell and developmental biology 25:407-429.

62. Herren, B., K. J. Garton, S. Coats, D. F. Bowen-Pope, R. Ross, and E. W. Raines. 2001. ADAM15 overexpression in NIH3T3 cells enhances cell-cell interactions. Exp Cell Res 271:152-160.

63. Magdalena, J., T. H. Millard, and L. M. Machesky. 2003. Microtubule involvement in NIH 3T3 Golgi and MTOC polarity establishment. J Cell Sci 116:743-756.

64. Cory, G. Scratch-wound assay. Methods Mol Biol 769:25-30.

65. Burke, B., and C. L. Stewart. 2002. Life at the edge: the nuclear envelope and human disease. Nat Rev Mol Cell Biol 3:575-585.

66. Mounkes, L. C., S. Kozlov, L. Hernandez, T. Sullivan, and C. L. Stewart. 2003. A progeroid syndrome in mice is caused by defects in A-type lamins. Nature 423:298-301.

67. Thodeti, C. K., B. Matthews, A. Ravi, A. Mammoto, K. Ghosh, A. L. Bracha, and D. E. Ingber. 2009. TRPV4 Channels Mediate Cyclic Strain-Induced Endothelial Cell Reorientation Through Integrin-to-Integrin Signaling. Circ Res.

68. Dickinson, R. B., and R. T. Tranquillo. 1993. A stochastic model for adhesion-mediated cell random motility and haptotaxis. J Math Biol 31:563-600.

69. Harms, B. D., G. M. Bassi, A. R. Horwitz, and D. A. Lauffenburger. 2005. Directional persistence of EGF-induced cell migration is associated with stabilization of lamellipodial protrusions. Biophys J 88:1479-1488.

70. Polte, T. R., G. S. Eichler, N. Wang, and D. E. Ingber. 2004. Extracellular matrix controls myosin light chain phosphorylation and cell contractility through modulation of cell shape and cytoskeletal prestress. Am J Physiol Cell Physiol 286:C518-528.

71. Tolic-Norrelykke, I. M., J. P. Butler, J. Chen, and N. Wang. 2002. Spatial and temporal traction response in human airway smooth muscle cells. Am J Physiol Cell Physiol 283:C1254-1266.

72. Mislow, J. M., M. S. Kim, D. B. Davis, and E. M. McNally. 2002. Myne-1, a spectrin repeat transmembrane protein of the myocyte inner nuclear membrane, interacts with lamin A/C. J Cell Sci 115:61-70.

73. Padmakumar, V. C., S. Abraham, S. Braune, A. A. Noegel, B. Tunggal, I. Karakesisoglou, and E. Korenbaum. 2004. Enaptin, a giant actin-binding protein, is an element of the nuclear membrane and the actin cytoskeleton. Exp Cell Res 295:330-339.

74. Hayakawa, K., N. Sato, and T. Obinata. 2001. Dynamic reorientation of cultured cells and stress fibers under mechanical stress from periodic stretching. Exp Cell Res 268:104-114.

75. Lele, T. P., J. Pendse, S. Kumar, M. Salanga, J. Karavitis, and D. E. Ingber. 2006. Mechanical forces alter zyxin unbinding kinetics within focal adhesions of living cells. J Cell Physiol 207:187-194.

76. Ghosh, K., C. K. Thodeti, A. C. Dudley, A. Mammoto, M. Klagsbrun, and D. E. Ingber. 2008. Tumor-derived endothelial cells exhibit aberrant Rho-mediated mechanosensing and abnormal angiogenesis in vitro. Proc Natl Acad Sci U S A 105:11305-11310.

77. Hu, S., J. Chen, J. P. Butler, and N. Wang. 2005. Prestress mediates force propagation into the nucleus. Biochem Biophys Res Commun 329:423-428.

78. Palecek, S. P., J. C. Loftus, M. H. Ginsberg, D. A. Lauffenburger, and A. F. Horwitz. 1997. Integrin-ligand binding properties govern cell migration speed through cell-substratum adhesiveness. Nature 385:537-540.

79. Burgess, B. T., J. L. Myles, and R. B. Dickinson. 2000. Quantitative analysis of adhesion-mediated cell migration in three-dimensional gels of RGD-grafted collagen. Ann Biomed Eng 28:110-118.

80. Libotte, T., H. Zaim, S. Abraham, V. C. Padmakumar, M. Schneider, W. Lu, M. Munck, C. Hutchison, M. Wehnert, B. Fahrenkrog, U. Sauder, U. Aebi, A. A. Noegel, and I. Karakesisoglou. 2005. Lamin A/C-dependent localization of Nesprin-2, a giant scaffolder at the nuclear envelope. Mol Biol Cell 16:3411-3424.

81. Lombardi, M. L., and J. Lammerding. Keeping the LINC: the importance of nucleocytoskeletal coupling in intracellular force transmission and cellular function. Biochem Soc Trans 39:1729-1734.

82. Morgan, J. T., E. R. Pfeiffer, T. L. Thirkill, P. Kumar, G. Peng, H. N. Fridolfsson, G. C. Douglas, D. A. Starr, and A. I. Barakat. Nesprin-3 regulates endothelial cell morphology, perinuclear cytoskeletal architecture, and flow-induced polarization. Mol Biol Cell 22:4324-4334.

83. Machacek, M., L. Hodgson, C. Welch, H. Elliott, O. Pertz, P. Nalbant, A. Abell, G. L. Johnson, K. M. Hahn, and G. Danuser. 2009. Coordination of Rho GTPase activities during cell protrusion. Nature 461:99-103.

84. Wang, X., L. He, Y. I. Wu, K. M. Hahn, and D. J. Montell. 2010. Light-mediated activation reveals a key role for Rac in collective guidance of cell movement in vivo. Nat Cell Biol 12:591-597.

85. Dupin, I., and S. Etienne-Manneville. 2011. Nuclear positioning: mechanisms and functions. Int J Biochem Cell Biol 43:1698-1707.

86. Lo, C. M., H. B. Wang, M. Dembo, and Y. L. Wang. 2000. Cell movement is guided by the rigidity of the substrate. Biophys J 79:144-152.

87. Angelini, T. E., E. Hannezo, X. Trepat, M. Marquez, J. J. Fredberg, and D. A. Weitz. 2011. Glass-like dynamics of collective cell migration. Proc Natl Acad Sci U S A 108:4714-4719.

88. Yeung, T., P. C. Georges, L. A. Flanagan, B. Marg, M. Ortiz, M. Funaki, N. Zahir, W. Ming, V. Weaver, and P. A. Janmey. 2005. Effects of substrate stiffness on cell morphology, cytoskeletal structure, and adhesion. Cell Motil Cytoskeleton 60:24-34.

89. Lo, C. M., D. B. Buxton, G. C. Chua, M. Dembo, R. S. Adelstein, and Y. L. Wang. 2004. Nonmuscle myosin IIb is involved in the guidance of fibroblast migration. Mol Biol Cell 15:982-989.

90. Angelini, T. E., E. Hannezo, X. Trepat, J. J. Fredberg, and D. A. Weitz. 2010. Cell migration driven by cooperative substrate deformation patterns. Phys Rev Lett 104:168104.

91. Liu, Q., N. Pante, T. Misteli, M. Elsagga, M. Crisp, D. Hodzic, B. Burke, and K. J. Roux. 2007. Functional association of Sun1 with nuclear pore complexes. J Cell Biol 178:785-798.

92. Aplin, A. E., and R. L. Juliano. 2001. Regulation of nucleocytoplasmic trafficking by cell adhesion receptors and the cytoskeleton. J Cell Biol 155:187-191.

93. Aplin, A. E., B. P. Hogan, J. Tomeu, and R. L. Juliano. 2002. Cell adhesion differentially regulates the nucleocytoplasmic distribution of active MAP kinases. J Cell Sci 115:2781-2790.

94. Aplin, A. E., S. A. Stewart, R. K. Assoian, and R. L. Juliano. 2001. Integrin-mediated adhesion regulates ERK nuclear translocation and phosphorylation of Elk-1. J Cell Biol 153:273-282.

95. Richard, M. N., J. F. Deniset, A. L. Kneesh, D. Blackwood, and G. N. Pierce. 2007. Mechanical stretching stimulates smooth muscle cell growth, nuclear protein import, and nuclear pore expression through mitogen-activated protein kinase activation. J Biol Chem 282:23081-23088.

96. Roth, D. M., G. W. Moseley, D. Glover, C. W. Pouton, and D. A. Jans. 2007. A microtubule-facilitated nuclear import pathway for cancer regulatory proteins. Traffic 8:673-686.

97. Schindler, M., and L. W. Jiang. 1986. Nuclear actin and myosin as control elements in nucleocytoplasmic transport. J Cell Biol 102:859-862.

98. Minakhina, S., R. Myers, M. Druzhinina, and R. Steward. 2005. Crosstalk between the actin cytoskeleton and Ran-mediated nuclear transport. BMC Cell Biol 6:32.

99. Haycock, J. W. 2011. 3D cell culture: a review of current approaches and techniques. Methods Mol Biol 695:1-15.

100. Langevin, H. M., K. N. Storch, R. R. Snapp, N. A. Bouffard, G. J. Badger, A. K. Howe, and D. J. Taatjes. 2010. Tissue stretch induces nuclear remodeling in connective tissue fibroblasts. Histochem Cell Biol 133:405-415.

101. Ehrbar, M., A. Sala, P. Lienemann, A. Ranga, K. Mosiewicz, A. Bittermann, S. C. Rizzi, F. E. Weber, and M. P. Lutolf. 2011. Elucidating the role of matrix stiffness in 3D cell migration and remodeling. Biophys J 100:284-293.

102. Zaman, M. H., P. Matsudaira, and D. A. Lauffenburger. 2007. Understanding effects of matrix protease and matrix organization on directional persistence and translational speed in three-dimensional cell migration. Ann Biomed Eng 35:91-100.

103. Shimi, T., K. Pfleghaar, S. Kojima, C. G. Pack, I. Solovei, A. E. Goldman, S. A. Adam, D. K. Shumaker, M. Kinjo, T. Cremer, and R. D. Goldman. 2008. The A- and B-type nuclear lamin networks: microdomains involved in chromatin organization and transcription. Genes Dev 22:3409-3421.

104. Gerlitz, G., and M. Bustin. 2010. Efficient cell migration requires global chromatin condensation. J Cell Sci 123:2207-2217.

105. Gerlitz, G., and M. Bustin. 2011. The role of chromatin structure in cell migration. Trends Cell Biol 21:6-11.

BIOGRAPHICAL SKETCH

T. J. Chancellor was born in Wichita Falls, TX in 1983 to Tom and Karen Chancellor. After graduating from Wichita Falls Hirschi High school in 2001 he enrolled in the University of Oklahoma. While at the University of Oklahoma he conducted his first research under the guidance of Dr.Dimitrios Papavassiliou In 2005 he received a Bachelor of Science degree in chemical engineering. He began his graduate studies at the Department of Chemical Engineering at the University of Florida in 2006. At the University of Florida he joined Dr. Tanmay Lele's research group and was one of the first 2 students to work in the lab. His research focused on the nuclear force balance between the nucleus and the cytoskeleton. He earned his Doctor of Philosophy in chemical engineering from the University of Florida in 2012.